Polytechnic Institute of New York
MICROWAVE RESEARCH INSTITUTE

POLY-MRI-1428-83
March 1983

FINAL REPORT

on

A MORPHOLOGICAL STUDY OF WAVES IN THE THERMOSPHERE

by

Stanley H. Gross

Prepared for

NATIONAL AERONAUTICS AND SPACE ADMINSTRATION

Grant No. NSG-5284

(NASA-CR-170189) A MOPHOLOGICAL STUDY OF WAVES IN THE THERMOSPHERE Final Report, 1 Jul. 1978 - 31 Dec. 1982 (Polytechnic Inst. of New York, Brooklyn.) 127 p HC A07/MF A01 CSCL 04A G3/46

N83-22871
THRU
N83-22873
Unclas
03301

TABLE OF CONTENTS

Introduction

This is a final report for the AE Guest Investigator Program, NASA Grant No. NSG5284, which started July 1, 1978 and ended December 31, 1982. The research has been under the guidance of Dr. Stanley H. Gross of the Electrical Engineering and Computer Science Department of the Polytechnic Institute of New York as Principal Investigator and Dr. Carl A. Reber of the Goddard Space Flight Center as Co-investigator.

During the course of the program, Atmosphere Explorer (AE) data (AE-C and AE-E) were studied to determine whether coherent wave structures were present and to establish their characteristics. These data included density, temperature and wind measurements of neutrals, and density and temperature measurements of plasma. Power and cross spectra have been calculated from the fluctuation data for these various geophysical parameters. Both UA and GU data files have been employed. Computations were made both at the Goddard Space Flight Center and the Polytechnic Institute of New York. It was established that coherent wave-like fluctuations are present in all the neutral and ionization parameters observed by the satellites, that broad spectra are just about always present extending from 10's km to 1000's km in wavelength in about six years of observations. The broad spectra follow power law types of distributions with spectral indices different for each parameter. They show that individual neutral species are coupled and that plasma is coupled to neutrals. There is also a suggestion of flattening of the spectra at the longest wavelengths. A statistical study was started to relate these properties to geophysical aspects of importance, such as magnetic activity, time of day, season, latitude band, etc. This study was not completed.

Efforts to find correlative ground based measurements for the flight paths of the orbits have been limited and mostly unsuccessful. Some ground measurements have been obtained from France of total electron content and from the Chatanika radar. These have been partially studied and remain to be completed.

Theoretical models with localized line sources have been developed. Numerical calculations have been made for various species in two fluid

models. Theoretical cross spectra have been computed for comparison with the spectra of measured data. More work is required to improve the calculation of cross spectra of the measured data and to model the data to obtain possible wave characteristics. However, successful computation of cross correlation functions have enable the determination of transfer functions between geophysical parameter responses. The theoretical models provide insight into the nature of wave properties, relationships to sources and guidance for interpreting numerical studies and measured data. They also serve as test problems for elaborate computer programs that are used in models too complex for theoretical analysis.

It was also found that there may be interesting fluctuations of neutral parameters where there are "bubbles" in the measured equatorial electron density. Furthermore, localized heating at low latitudes over restricted longitude bands was found for a number of cases during magnetic storms. These findings need further investigation.

Some of the data imply the presence of quasi-stationary wave structures on a global scale. This is concluded from attempts to analyze the data with conventional gravity wave theory and from comparison of AE-E and AE-C fluctuations and spectra.

Further work is desirable in terms of (1) completion of the statistical study of AE-C and AE-E data for levels of fluctuations, spectral properties in relation to latitude ranges, time of day, season, magnetic activity and other geophysical aspects; (2) the programming of cross spectral computations and modeling to interpret the results and to determine wave characteristics; (3) the study of French total electron content measurements in relation to data from AE-C overflights; (4) the further search for corroborative ground based data for comparison with AE measurements; (5) the extension of theoretical modeling and numerical modeling to guide the interpretation of the data and to relate data to source characteristics; (6) the study of the special low latitude heating events to relate to the mechanisms whereby energy is transported in the thermosphere; (7) the study of "bubbles" and their possible relationship to fluctuations in densities, temperature and winds of neutral species;

(8) the further study of waves to determine whether a major component is quasi-stationary, as implied by some of the data.

1. The Program

The program was arranged mainly in three phases: These were:

1. The analysis of Atmosphere Explorer (AE) data (AE-C and AE-E) to determine whether coherent wave structures are present and their characteristics.
2. Theoretical studies of waves emitted by sources in media of two or more species with particular emphasis on the spectral region of gravity waves for comparison with measured data.
3. A search for corroborative measurements by ground facilities near the tracks of the AE satellites.

The ground facilities provide temporal data, whereas the satellite provides spatial data. Direction of arrival information may also be provided by the former.

The first two tasks were carried out essentially in parallel. The third task was carried out as opportunity permitted. These tasks were carried out in the main, but, as typical in research, more work is suggested to accomplish more fully the original goals. The work, however, led to the presentation of material at various meetings of the American Geophysical Union, URSI, and at Atmosphere Explorer team meetings. Results were presented by Dr. Gross at the NATO/AGARD meeting in Naples, Italy, in October 1980. These results were published in the proceedings of that meeting. A copy of the paper is attached. Material has been prepared for publication in the Journal of Geophysical Research, a copy of which is attached as Report No. POLY-MRI-1427-83 entitled, "Large Scale Waves in the Thermosphere Observed by the AE-C Satellite," and another report, POLY-MRI-1426-83, has been written covering a major portion of the data analysis. This latter report is also attached and is entitled, "Gravity Waves in the Thermosphere Observed by the AE Satellites." A number of papers will be forthcoming from this report. A number of other efforts will result in additional material to be submitted for publication when manuscripts are completed.

A great deal of effort was expended on the second task. Both analytical and numerical techniques were used. They represent new contributions to the field, consisting of two fluid models with energy sources. Two approaches were used, a theoretical analysis and a numerical analysis. The theoretical analysis was to provide insight into the nature of the wave solutions and to provide a simpler problem to check the computer methods which are intended for more complex problems. Further work is required for both. The theoretical analysis requires a statement of final equations in terms of known functions that can be numerically computed. The main features of these formulas can be computed and studied to gain physical insight. This work will be submitted for publication once completed.

The numerical analysis of the first version that has been treated is nearly complete. It differs from the theoretical analysis by incorporating physical temperature profiles, mean mass variation with altitude and more exact formulation, features too difficult to treat analytically. Nevertheless, some further calculations are needed for other models and for checking with known solutions from the analytical work. It is hoped that this work may be completed on receiving additional support.

The third task has been mainly one of frustration. It was found that incoherent backscatter facilities were not operating during particular times of good satellite observations. These stations included Arecibo, Jicamarca, Millstone Hill, and St. Santin. Ionosonde stations provide data that are more difficult to use in a comparison with satellite data, though a trio of stations were recently setup by Dr. Millet Morgan of Dartmouth College to detect gravity waves. Unfortunately, these were not functioning during most of the period for the AE data. It is possible that later AE data (1980, for example) may be used with the Dartmouth data. This is an area for consideration in a new program. Ground measurement data were found as a result of contacts with Dr. Francois Bertin of CNET in Paris, France. Measurements were made in France of total electron content along a line to a synchronous satellite. These were made for several months on the ground in Brittany in 1976 by Dr. H. Sizun of CNET. There were overflights of AE-C during this

period. The French data were obtained early in 1981 and analyzed, but the comparison remains to be accomplished. The unavailability of the Sigma 9 has held up some of this analysis. It can be done on another computer if a new program is funded. Contacts were also made early in 1981 with Drs. R. Vondrak and O. de la Beaujardiere of SRI with respect to the Chatanika radar data. Some Chatanika data were provided at times of overpasses. These data are near the auroral source region, and it is important to identify wave disturbances, their nature and characteristics in this region. Time did not permit further effort here as well, and work remains for the future. Other efforts might be fruitful; for example, Kwajalein radar data may be useful for comparisons with AE-E data. A search for coordinated ground and space measurements may bear other fruit.

There were other discoveries as a result of this work. For example, there is a suggestion that at times of so-called "bubbles" in the equatorial region, neutral densities and temperatures fluctuate. This requires more investigation. Further, the popular belief that gravity waves seed "bubble" phenomena needs clearer demonstration. Studies of AE data may provide such evidence. This area is again one for future work. Localized heating events at restricted longitude bands at low latitudes during magnetically active times were also noted in AE-E data. This discovery led to the realization that comparisons for the same time of AE-C and AE-E data and with ground based measurements, measurements by other satellites may lead to clearer demonstrations of the nature of energy transport from high to low latitudes, much more than the observation of TID's. This too is an area for continued work. Examples of the "bubble connection" and the heating event are given in Section 2. The work done on fluctuations, spectra and cross correlations, as well as comparisons of AE-E and AE-C data, suggests that much of the large scale wave structure seen by the satellites are what can be called "quasi-stationary"; that is, waves excited by auroral sources which propagate at about 250 km reflect on themselves at the anti-podal point. In essence, they are natural spherical modes. There are implications here as to loss mechanisms. Further, it is likely that they

are generated at F region heights, though this is not certain, from particles associated with diffuse aurora, and so may relate to magnetospheric processes, though, again, this is not certain. Section 3 is a summary of papers presented at meetings of scientific societies and papers prepared for publication.

2. Bubble Phenomena and Localized Heating

Figure 1 is an example of AE-E data for April 28, 1977. It shows the variations of densities in the upper graph against time in seconds (UT) of oxygen, nitrogen, helium, argon and the electrons. The middle graph shows the variations of the neutral temperature and a small portion of the ion temperature. The temperature of the MSIS model (Hedin et al. 1977) is also shown. The lowest graph is for neutral winds of nitrogen in the cross-track direction which is mostly in the north-south direction. The data are based on 15 second samples and the time span shown is for one orbit. Other scales along the abscissa are for magnetic latitude (MLAT), dip angle, local solar time (LST), longitude (LONG), latitude (LAT), and altitude (ALT). This day was a relatively quiet day magnetically. The mean A_p index and sum of k_p indices are shown along with the 10.7 flux. Six vertical, dashed lines are shown in the figure. Four of these, those to the left, are at the times of sudden drops in the electron density, at the so-called "bubble" features. One sees at these times suggestions of corresponding changes in the neutral temperature and the wind. Corresponding fluctuations in the neutral densities are too small in the figure to be useful.

One may gain a better sense of the fluctuations of the neutral densities from Figure 2. These are graphs of the fluctuations of all the data of Figure 3, except for the ion temperature which are too sparse. All are computed by the filtering techniques described in the attached papers. All, except the wind, are normalized to their background trends. The bubbles may be observed in the electron density fluctuations where there are large negative excursions. Five of eight vertical, dashed lines shown in the figure are at the bubbles. Counting from the left, these are the third to the seventh line. All except one correspond to the lines in Figure 1. The extra line was missed there, but became clearer from

the fluctuations. There seem to be perturbations in the neutral densities, as well as the temperature and wind, at these times, not necessarily in phase, but associated.

The evidence in Figures 1 and 2 are not conclusive. Much further study is needed, particularly of higher resolution data.

An example of an unusual heating event at equatorial latitudes in a restricted longitude range is shown in Figure 3. The day is May 3, 1977. It is quite active magnetically. The three hour k_p indices are shown. The previous day was even more active and corresponding graphs appeared like those in Figure 3. This figure contains information on density and temperature variations as in Figure 1, but there are no wind data and there are much more ion temperature data. The event is seen to occur centered at the dashed, vertical line on the left in the figure. Note the decrease in densities of O, He and the electrons, and the increase in N_2 and A. Note the significant increases in both the ion temperature and the neutral (N_2) temperature. The spread of the event is from about a longitude of 130° west to about 60° west. The corresponding magnetic latitude spread is from about 16° through 28° to about 25° north. These changes are only explainable as due to localized heating, as borne out by the temperature variations. Ordinarily, at equatorial latitudes during magnetic storms, no particular feature is observed as a function of longitude. Only a general warming is apparent (Mayr and Hedin, 1977). However, Trinks et al. (1975) from ESR04 data and Trinks et al. (1976) from ESR04 and AEROS-A data have suggested similar events though these satellites were in highly inclined, elliptical orbits. Other such events have been found in the AE-E data. An investigation was started of AE-C data for these days, data from other satellites and some ground stations. It is not clear whether the heating is due to a low latitude heating phenomena as has been suggested by some, or by a "tongue" of precipitation, waves or winds in a restricted longitude range extending well down in latitude from the northern auroral region. These matters deserve further study.

3. Papers Presented and Prepared for Publication

Gross, S. H. and C. A. Reber (1979), "Wave Structure in the Neutral Species Observed by Atmospheric Explorer Satellites," Paper SA-29, Spring Meeting of the American Geophysical Union, Washington, D. C., May 28-June 1, EOS 60.

Gross, S. H., C. A. Reber and F. Huang (1979), "Large Scale Waves in the Ionosphere Observed by the AE Satellites," Session H-1, Paper 5, National Radio Science Meeting, November 5-8, Boulder, Colorado.

Gross, S. H. (1980), "Model Analysis of Large Scale Wave Structure as Observed by AE Satellites," Paper SA 100, Spring Meeting of The American Geophysical Union, May 22-27, Toronto, Canada, EOS 61, 322-323.

Gross, S. H., C. A. Reber and F. Huang (1980), "Large Scale Waves in the Ionosphere Observed by the AE Satellites," AGARD Meeting, Pozzuoli, Italy, October 21-27, in AGARD Conference Proceedings No. 295, The Physical Basis of the Ionosphere in the Solar-Terrestrial System, 27th Meeting of the Electromagnetic Wave Propagation Panel (attached).

Huang, F., C. A. Reber and S. H. Gross (1980), "Large Scale Waves in the Atmosphere and Ionosphere Observed by the AE Satellites," paper SA 101, Spring Meeting of The American Geophysical Union, May 22-27, Toronto, Canada, EOS 61, 323.

Gross, S. H., C. A. Reber and F. Huang (1981), "Large Scale Structures Observed in the Thermosphere," paper SA-26, Spring Meeting of The American Geophysical Union, May 25-29, Baltimore, Maryland.

Gross, S. H., C. A. Reber and F. Huang (1981), "Large Scale Waves in the Ionosphere at Equatorial Latitudes," XXth General Assembly of URSI, August 11-18, Washington, D. C.

Gross, S. H., C. A. Reber and F. Huang (1982), "Gravity Waves in the Thermosphere Observed by the AE Satellites," POLY-MRI-1426-83, revised September 1982, to be submitted to J. Geophs. Res.

Gross, S. H. (1983), "Large Scale Gravity Waves and Quasi-Stationary Structures," paper submitted to AGU for Spring 1983 Meeting in Baltimore, Maryland.

Gross, S. H., C. A. Reber and F. Huang (1983), "Large Scale Waves in the Thermosphere Observed by the AE-C Satellite," Report No. POLY-MRI-1426-83, Polytechnic Institute of New York, March 1983.

REFERENCES

Hedin, A. E., J. E. Salah. J. V. Evans, C. A. Reber, G. P. Newton, N. W. Spencer, D. C. Kayer, D. Alcayde, P. Bauer, L. Coggerand, J. P. McClure (1977), "A Global Thermospheric Model Based on Mass Spectrometer and Incoherent Scatter Data," MSIS 1. N_2 density and temperature. J. Geophys. Res. 82, 2139-2147.

Mayr, H. G. and A. E. Hedin (1977), "Significance of Large-Scale Circulation in Magnetic Storm Characteristics with Application to AE-C Neutral Composition Data," J. Geophys. Res. 82, 1227-1234.

Trinks, H., S. Chandra and N. W. Spencer (1976), "A Two-Satellite Study of the Neutral Atmosphere Response to a Major Geomagnetic Storm," J. Geophys. Res. 81, 5013-5017.

AGARD

ADVISORY GROUP FOR AEROSPACE RESEARCH & DEVELOPMENT

7 RUE ANCELLE, 92200 NEUILLY SUR SEINE, FRANCE

Paper Reprinted from
Conference Proceedings No. 295

THE PHYSICAL BASIS OF THE IONOSPHERE IN THE SOLAR-TERRESTRIAL SYSTEM

NORTH ATLANTIC TREATY ORGANIZATION

LARGE-SCALE WAVES IN THE IONOSPHERE OBSERVED BY THE AE SATELLITES

S.H. Gross
Polytechnic Institute of New York
Farmingdale, New York 11735, U.S.A.

C.A. Reber
NASA, Goddard Space Flight Center
Greenbelt, Maryland 20771, U.S.A.

F. Huang
Computer Sciences Corp.
Silver Spring, Maryland 20910, U.S.A.

ABSTRACT

We report here on efforts utilizing Atmospheric Explorer (AE) satellite data to establish whether coherent waves in the gravity wave range are present in both neutral and ionized media in the thermosphere. AE-C data in particular are shown (altitude 250km, circular orbit inclined 68°). Data consists of in situ argon, helium, nitrogen and oxygen densities, plasma density and ion and electron temperatures. Filtering provides the fluctuation signals for each which are spectrum analyzed for power and cross spectra. The observed frequencies are essentially proportional to the spatial wavenumbers along the satellite track. Scale sizes range from thousands to tens of kilometers.

Modeling efforts to determine the temporal characteristics, direction of propagation and other wave parameters from the spectra were made with little success. Unfortunately, efforts to find near simultaneous ground measurements to corroborate wave characteristics have been fruitless so far. On reviewing the data it was found that turbulence-like structure over the full range of wavelengths is present with different spectral indices for each measured density and temperature. These appear to be consistent in all data studied to date. Wave packets are present superimposed on top of this turbulence structure in all data channels, (densities and temperatures), many of which exhibit excellent correlation with each other.

1. INTRODUCTION

Since the hypothesis of Martyn (1950) 30 years ago, it has been generally accepted that many, if not all traveling ionospheric disturbances (TID's) originate from gravity waves in the neutral atmosphere. Ions are presumed to be dragged by the neutrals, and in this way exhibit the wave characteristics of the neutrals, but with constraints due to the earth's magnetic field. In spite of many measurements of meteor trails, rocket experiments and radar neutral scattering experiments, there has been almost no direct evidence to confirm this postulate from ground measurements, because of the difficulty of remotely measuring the neutral medium in the upper atmosphere. The wide acceptance resulted from indirect evidence, such as the measured velocity, scale lengths, periods and the direction of phase propagation (Hines, 1960).

Direct evidence is more likely in space, since spacecraft provide a suitable platform for making observations of both neutrals and ionization. Yet the simultaneous observations of both media has only become available in more recent years so that published results are few. Two examples are Dyson et al (1970) who use Explorer 32 data and Reber et al (1975) using Atmosphere Explorer C (AE-C) data. In the first reference the fluctuation in the total neutral density is compared with the fluctuation in the electron density. In the second, two examples are given; one compares the fluctuations in the densities of argon, nitrogen and helium, and the other compares the fluctuations in the densities of argon, nitrogen and the ions and the fluctuation in the electron temperature. Both examples were for elliptic orbits for which the altitude changes rapidly. These limited cases depend on visual examination of the records to convince oneself that correlated motion exists.

Nevertheless, it is apparent in the examples of the latter paper that the fluctuations of helium are quite different from those of nitrogen or argon in that helium appears at times to be about 180° out of phase with the other two gases. Also, the amplitudes are different with the amplitude of argon about twice that of N_2 and that of helium about half that of N_2. This behavior has been found to be consistent with the theory of gravity waves involving more than one species for thermospheric conditions (Gross and Eun, 1976 and 1978a; Dudis and Reber, 1977; Del Genio et al, 1979).

A more recent example involving just neutrals (Hoegy et al, 1979) utilized AE-E data. The interpretation and analysis was more sophisticated than a visual treatment. In that work a wave is identified and all wave characteristics are derived. However, the theory of their modeling is not fully explained. Further examples for neutrals were given by the authors of this paper at various meetings of the American Geophysical Union and URSI (Gross and Reber, 1979; Gross et al, 1979; Huang et al, 1980) based on AE-C data. Some of these results will be presented in this paper along with newer material.

We have been studying data from many orbits of the AE-C satellites, those that are near circular and at an altitude of about 250 km. Circular orbits were chosen to eliminate the effects of altitude variations on the observed fluctuations. There is evidence of correlation in the fluctuations of all neutral species and ionization in every case examined. Since the satellite moves very rapidly (~ 7.8 km/sec) through the medium, the measurements essentially provide the spatial distribution of the measured quantities. The variations exhibit scale lengths typical of gravity waves and are presumed to be such waves. Both large scale (thousands of kilometers) and smaller scale (hundreds of kilometers) waves are observed. The scales of the waves are determined by spectral analysis using power spectra and cross spectra derived by the

maximum entropy method (Ulryck and Bishop, 1975). Generally, the stronger spectra are for the larger scale waves.

The AE satellites provide in situ measurements of the density and drift velocity of argon, helium, nitrogen and oxygen as measured by the Neutral Atmospheric Composition Experiment (NACE); neutral temperature for these species from the Neutral Atmospheric Temperature Experiment (NATE); plasma density and ion temperature by means of the Retarding Potential Analyzer (RPA) experiment; plasma density and electron temperature by means of the Cylindrical Electron Probe, as well as other experiments (Dalgarno et al, 1973). Many of these measurements are essentially simultaneous, making direct comparison of the measured properties and their fluctuations meaningful. Data utilized are available in two different sample intervals: 15 second averaged data from the so-called "UA" files and approximately 1.5 second samples from the so-called "GU" files.

Our goal was to determine whether observed wave structures are auroral in origin, so we emphasized AE-C circular orbit data because that satellite is in a high inclination (~ 68°) orbit. Though AE-E has yielded much data, its low inclination orbit is more suitable for non-auroral-connected events, which are of interest as well.

2. EXAMPLES OF DATA AND SPECTRA

Examples shown in this paper are illustrative. They are taken from data measured during two orbits of AE-C, orbit 5133 on January 20, 1975, and orbit 5359 on February 3, 1975. In both cases the altitude was approximately 250 km. Data for complete orbits are shown based upon 15 second averaged data samples, as well as the higher data rate 1.5 second samples for the study of regions in each of the hemispheres.

Complete orbit data are shown in Figure 1. This figure is a composite made up of the time variation in orbit of a number of data channels for orbit 5133, consisting of nitrogen particle density, electron density and ion and electron temperatures. Universal time in seconds is along the abscissa and ranges from 28000 to 34000. The ordinates for all the channels are logarithmic. Fluctuations are evident in all cases, but correlations between these fluctuations is not clear from this record. (Vertical lines in the N_2 and N_e (CEP) graphs are due to spurious computer effects.)

One obtains the fluctuations by extracting the low frequency or background content from the data shown in Figure 1. This is done by passing the data through a lowpass filter and subtracting its output from the original data. Such filtering is readily done digitally. We utilize the relative fluctuation rather than the fluctuation. The relative fluctuation is obtained by dividing the fluctuation by the background, the output of the lowpass filter as a function of the time in orbit. Figure 2 shows the relative density fluctuations for the complete orbit 5359 for nitrogen, argon, helium and the ionization. The figure also provides the fluctuation in the electron and ion temperatures. In contrast with the variation in total quantities in Figure 1, the fluctuations in Figure 2 exhibit, on visual examination, some degree of correlation.

Stronger evidence of correlation may be observed in the power spectra for these same data channels, not shown here. These are plots against the Doppler frequency in Hz along the abscissa. Since the satellite moves so much faster than the phase velocity of a wave, this Doppler spectrum is essentially $kv\cos\theta$, where k is the wave number, v is the satellite velocity and θ is the angle between the wave normal and the satellite path. Therefore, for fixed v it represents the component of the spatial distribution as given by $k\cos\theta$. Such spectra are calculated at evenly spaced frequencies by the computer and shown as lines. There are many common lines in the spectra of the various data channels, particularly for the stronger lines. Strong lines are found for the Doppler range from about 0.003 Hz to about 0.008 Hz. For a satellite velocity of 7.8 km/sec this frequency range corresponds to a horizontal wavelength range of about 2600 km to 975 km., assuming the satellite track and wavenormal are coincident. Since θ may not be zero, the actual wavelength range may be smaller. Apparently such long wavelength waves are present on a worldwide (full orbit) scale. There are also common spectra in the hundreds of kilometer range, though of much smaller intensity.

The shorter wavelengths (hundreds of km) are much more apparent in the spectra of 1.5 second data samples. An example of power spectra for orbit 5133 for the northern latitude range 55° to 0° is shown in Figure 3. The Nyquist frequency is 1/3 Hz, and the strongest lines are evident from about .025Hz to about .040 Hz, corresponding to horizontal wavelengths of about 300 km down to about 200 km. Smaller scale structure are also evident.

Further evidence for correlation of the various data channels for orbit 5133 in the same latitude region (55° to 0°) is shown in Figure 4. Here the co- and quadrature spectra are shown for each data channel relative to nitrogen. (The power spectrum of a data channel x(t) of total sample time T is $C_{xx}(f) = 1/T|X(f)|^2$, where X(f) is the Fourier transform and f is the frequency. The cross spectrum between two data channels x(t) and y(t) for total data samples of time T is given by $C_{xy}(f) = X^*(f)Y(f)/T$, where X(f) and Y(f) are the Fourier transforms of x and y and the asterisk means complex conjugate. The real part of C_{xy} is the co-spectra, and the imaginary part is the quadrature spectra (Jenkins and Watts, 1961).) It is evident from the strong lines of these spectra that the various channels are not in phase, phaseshift being given by the arctangent of the ratio of the quadrature spectrum to the co-spectrum for the same Doppler frequency.

The amplitude and phase spectra are derivable from the co- and quadrature spectra, the first by taking the square root of the sum of the squares of the two spectra and the second as explained above to obtain the phaseshift. These spectra are of use in modeling the wave perturbations and their characteristics. By dividing the amplitude spectrum by the power spectrum of nitrogen at each of the major cross-spectral frequencies, the amplitude of the relative response of the particular geophysical parameter analyzed (density of neutrals or plasma, or temperature) to that of nitrogen is obtained; that is, $|Y(f)/X(f)|$, if x is the nitrogen fluctuation and y is the particular parameter of interest. Of course, this division only makes sense if we are dealing with a coherent wave. The phase spectrum of a channel provides the phase response relative to that of nitrogen. For the most significant frequencies, one may deduce the missing characteristics of the wave by appropriate modeling using the relative phase and amplitude responses of

the various channels. The Doppler frequency only provides the spatial wavelength along the orbital track. It is not necessarily the horizontal wavelength of the wave. Thus, by modeling one, in principle, is able to deduce the wave's temporal frequency, horizontal wavelength, direction of travel relative to the orbital path, the velocity of propagation and the vertical wavelength. A knowledge of these parameters together with the wave amplitudes is of great importance, since it would permit some deductions of the energy and momentum transported by the waves.

Bands of strong frequencies are common. Modeling of such adjacent lines should provide redundant information as though all are from a common source. However, it is a characteristic of the maximum entropy method (Ulry and Bishop, 1975) to cause spreading of these bands and to introduce uncertainty as to their structure. As a consequence one should not take each line as exact. Instead, the average over several lines may be preferable. More work in spectral data analysis in this regard is needed.

Data were analyzed using the modeling techniques as described below. The techniques were only applied to neutrals, because the theory of modeling the ionization requires further study incorporating the magnetic field.

3. FIXED LAYER MODELING ANALYSIS

A full scheme of modeling wave solutions should include localized sources, multiple constituents and at least an altitude varying background atmosphere. In addition, winds and horizontal non-uniformity may play important roles. A problem of this complexity has not as yet been solved. However, parts of it have been treated. In the literature solutions have been given for two constituent atmospheres with vertical non-uniformity in density (Del Genio et al, 1979), and for vertical non-uniform density and temperature and mean mass and height dependent collision frequencies (Gross and Eun, 1976, 1978a and b). Solutions have also been given for two constituents with all these non-uniformities and localized sources (Gross, 1980). None of these solutions exhibit the degree of variation present in the measured data. Gross (19[illegible]) has shown that the spectra derived in the theoretical problem for two species is quite smooth and slowly varying with wavelength and temporal frequency. It is not clear then whether the degree of variation exhibited in spectra as in Figure 4 is due to the stochastic nature of the source or to propagation effects caused by variations in the medium.

Modeling was attempted using a locally homogeneous medium about the satellite's altitude to avoid these difficulties. We call this method the fixed layer analysis. In this analysis one assumes a gravity wave moving through an atmosphere with given background characteristics at an altitude of 250 km: temperature, temperature vertical gradient, mean mass, density for each constituent and collision frequencies between species. These values are obtained either from the measured data or else from models of the atmosphere for the particular time of year, location, solar cycle year, etc. The MSIS models (Hedin et al, 1977a and b) were used for this purpose. Densities were obtained by averaging over the measured data for the portion of orbit being modeled. Mean mass was also obtained from the average densities or else from the MSIS models. An atmosphere of more than two species is treated with two fluid theory by taking one (atomic oxygen), or a combination (atomic oxygen and molecular nitrogen), as a major species and each of the others (helium, argon), in turn, as minor. The gravity wave's characteristics are determined by the major constituent, and the response of helium or argon is relatable to that of the main species from the two fluid theory (Gross and Eun, 1976; Dudis and Reber, 1977; or Gross, 1980, for example). When the main constituent is a mixture of atomic oxygen and nitrogen, the same two fluid theory provides the eigenvalues appropriate to the gravity wave-like solutions for this mixture as well.

Thus, for orbit 5359 at southern mid-latitudes one obtains the complex relative responses of argon to nitrogen and of helium to nitrogen, as explained in the discussion on the cross spectra, for each Doppler frequency. These relative responses consist of amplitude and phase information as shown in Figures 5 and 6, respectively. Here the Doppler frequency is plotted as a harmonic number rather than frequency, since the latter is discrete. The fundamental is 1.3021 mHz. The lines in these figures are for the most significant responses, all others being weaker, noisy or uncertain due to possible noise.

With these relative responses for each Doppler Frequency, one has sufficient information for a model, neglecting wind effects and assuming horizontal uniformity, to find the corresponding wave period, horizontal wavelength, direction relative to the orbital path and the vertical wavelength. The method of defining the wave consists of scanning an appropriate range of wave periods and horizontal wavelengths to find that wave which comes closest to matching the argon and helium relative responses. A minimum mean square error based on the in phase and quadrature components of the responses was used as the criteria; that is, the differences between the calculated and the measured in phase and quadrature components were squared and summed for both argon and helium, and the sum was minimized. There are two solutions for each frequency, one for an upgoing wave, the second for a downgoing wave. Table I exhibits the wave solutions for the data of Figures 5 and 6 for phase-wise downgoing waves. Wave solutions for 15 Doppler frequencies, shown as harmonic numbers, are given. These frequencies are adjacent to each other, and one would expect waves of similar characteristics. Instead, the table shows a complete scatter in the periods and horizontal wavelengths, (shown as λ_x). Furthermore, one cannot determine the wave direction relative to the satellite path, θ, for most cases, since the best solutions give $\cos\theta > 1$. The measured and calculated amplitudes for the argon/nitrogen and helium/nitrogen responses, shown as A/N_2 and He/N_2 in the table, are considerably different. The fit is poor; the errors are comparable to the measured values. Similar results are obtained for phase-wise upgoing waves, for the other parts of the same orbit and for other orbits. If one averages adjacent lines to compensate for the peculiarities of the maximum entropy method and models the resulting values, similar results are obtained averaging three at a time, four at a time, etc. Varying the temperature or the collision frequencies by $\pm$ 10% yields no improvement.

Thus, the modeling attempts were unsuccessful. The medium may be far too complex for the assumptions. Data for thousands of kilometers must be used to analyze waves of several hundred kilometers wavelength. Undoubtedly, winds, wind shears and horizontal non-uniformity are not inconsequential over such distances. Further, the greater the distance from the source, the more is the change in wave characteristics (Chimonas and Hines, 1970). To model all these effects requires information not readily available, and, even if available, difficult to incorporate. We cannot rule out noise in the data, as well.

When we started this program we were optimistic that we could determine the characteristics of the waves from the satellite measurements because of the number of simultaneously measured quantities. These negative results, however, lead us to believe that it is essential to correlate spacecraft and ground measurements to find all the characteristics of the waves, temporal and spatial. Unfortunately, to date we have not been able to find suitable ground experiments functioning during a satellite pass over the station when events occurred.

Another approach has been to review the data in a different fashion. This has led to the discovery of new, possibly important, characteristics that had not originally been appreciated, nor possibly known at all before, as far as these authors can determine. Though these new results are preliminary, they may hopefully lead to a much better understanding of the mechanisms at work and their relationships to important geophysical aspects, such as magnetic storms, solar cycle variations, season, etc. These findings will now be explained.

4. LARGE SCALE WAVE DISTRIBUTIONS AND TURBULENCE

By a very simple process, that is, by replotting the spectral data shown in Figures 3 or 4 on a log-log graph, an unappreciated feature became evident. In this paper we show this only for the power spectra. All are for the northern latitude range 55° to 0° of orbit 5133. We see similar features in other parts of the same orbit and for other orbits.

The power spectra of N_2, O and electron density n_e are plotted versus the harmonic frequency number in Figure 7 through 9. They are shown as dots on the graphs. Those below about harmonic number 20 are in the lowpass filter range and should be ignored; the fluctuations of interest are those from harmonic number 20 and up. Harmonic number 20 corresponds to a wavelength of 300 km along the orbital path. Also shown on each graph is a best logarithmic straight line fit. Such a fit is expressible as An^{-a}, where A is an amplitude constant, n is the harmonic number and a is the spectral index characterizing the wave number decay rate. The fits for Figures 7 - 9 are based on the spectrum from n = 25 to n = 100. The deviation of the spectra in these figures is, except for some discrete values of n, relatively small. The values of a for these three fits are -5.3719 for nitrogen, -3.14128 for atomic oxygen and -2.1401 for the electron density. Curiously, the ratio of the value of a for nitrogen to that for oxygen is very close to the ratio of their molecular weights. Not enough data have been analyzed to establish whether this is real or a coincidence.

Do the fits in Figures 7 - 9 imply a turbulence-like spectrum for these large scale waves? The graphs are really wave number plots, and as such they are reminiscent of eddy distributions (Monin and Yaglom, 1971), but for much larger scale lengths. It is also possible that such spectra are representative of a stochastic source and therefore not turbulence. It may originate from non-linear interactions in the region in and about the source. In any event, it is believed that strong non-linear interactions must be involved, whether turbulence or source derived.

Plots similar to those of Figures 7 through 9 were made for helium and the electron temperature. These are not shown here. The fit for helium for the spectrum between n = 25 and n = 100, as in Figures 7 - 9, has the exponent a = -0.1645. This line yields a power spectral density almost independent of wavenumber, like white noise, and corroborates a noise-like distribution evident in data, particularly beyond n = 50. If a fit is made between n = 25 and n = 50, one obtains a second line with an exponent a = -1.45. A close examination of the data shows that there is a decreasing spectrum in this range of n. Apparently at shorter wavelengths noise dominates over the decreasing spectrum suggested by the second fit. This latter fit is probably not very accurate due to the influence of noise. Though not shown here as well, the fluctuation vs. time data for helium in this portion of the orbit, unlike that in Figure 2 for helium, appears quite noisy, implying that the NACE instrument was limited by the noise level in this measurement of helium. Nitrogen and oxygen are more abundant, so that noise does not appear to be a problem. The electron density measurements are from another instrument, the cylindrical electron probe.

The spectrum for the electron temperature is even noisier than that of helium. Two fits are also suggested. One is for n = 25 to n = 50 for which the exponent is positive and small (a = 0.342), as is expected for white noise. The other fit is for n = 25 to n = 40. This fit was computed because there seems to be a decreasing spectrum in the range. Its exponent is a = -2.31. What is interesting is that the elimination of just 10 frequencies from n = 41 to n = 50 produces this change. In contrast, the computation of fits for ranges other than n = 25 to 100 for nitrogen, oxygen and the electron density causes minor modification of their exponents. As for helium, the correct fit for the electron temperature spectrum is uncertain. At best, one can only conclude there is some hint of a decreasing spectrum that becomes overwhelmed by noise as the scale size decreases. As far as these authors know, such an electron temperature spectrum is the first of its kind ever deduced in natural plasma. Unfortunately, room does not permit its inclusion.

Over the range n = 25 to n = 50 there appear to be significant departures in the various spectra from their straight line fit at or near particular values of n. These departures or deviations may imply a wave system sitting on a turbulence-like spectrum. The features are made evident by plotting the difference, or residuals, vs. n on linear plots. Figure 10 shows these differences for nitrogen, oxygen and the electron density. The match of the peaks in these differences, between those of nitrogen and oxygen, is excellent, and that for the electron density is quite good. We find this match even though the maximum entropy method tends to broaden any peaks. The first large peak in all three of the residuals is at a wavelength along the orbit of about 272 km. The second peak (missing in the electron density spectrum) is at about 240 km. The third, fourth and fifth peaks are at about 190km, 150km, and 133 km, respectively. Though speculative, this group could be indicative of a wave packet moving through the medium.

The deviations for helium and the electron temperature are shown in Figure 11, based upon the n = 25 to 50 fit for helium and the n = 25 to 40 fit for the electron temperature. Though there is some degree of overlap with the spectra in Figure 10, the wide excursions are not surprising in view of the noisiness of the data for these two channels. These spectra are not considered too reliable.

5. CONCLUSIONS

The negative results that were obtained in attempting to model the fluctuations in the neutrals as gravity waves is not surprising in view of the complexity of the wave structure seen in Figures 7 to 11. Apparently, non-linear processes, probably associated with strong stochastic sources in the auroral region, and possibly from meteorological sources, are at work producing a turbulence-like spectrum in the gravity wave range stretching from wavelengths of many hundreds of kilometers down to the smallest scales observable before noise dominates, on the order of tens of kilometers. Work with complete orbit data also suggests that the turbulence-like structure extends to waves of thousand of kilometers in wavelength. The exponents of the spectra for each of the neutral constituents, the plasma and electron temperature are of different values in the limited examples given here and the few others that have been investigated. Why this is the case is not clear, but might arise from non-linear cascading processes and loss mechanisms associated with diffusion. There is much theory to be investigated here. It is not clear how or if these waves are propagating. Are the waves stationary, are they propagating in all directions or from the sources outwards? The deviations of Figures 10 and 11 suggest that wave packets are propagating on top of turbulence. It is conceivable that such wave packets would be observed as a traveling ionospheric disturbance on the ground.

A most interesting future investigation will consist of the statistical study of these characteristics and how they may relate to geophysical aspects, such as the year in the solar cycle, seasonal effects, magnetic storms, solar sector boundary crossings, etc. There is also a need to study similar characteristics in the equatorial region, as is possible with AE-E data, for relationships to the equatorial electrojet and meteorological events.

ORIGINAL PAGE IS
OF POOR QUALITY

REFERENCES

CHIMONAS, G. and C.O. Hines (1970), Atmospheric Gravity Waves Launched by Auroral Currents, Planet. Sp.Sci.18, 565-582.

DALGARNO, A., W.B. Hanson, N.W. Spencer, E.R. Schmerling (1973), The Atmospheric Explorer Mission, Radio Science 8, 263-266.

DEL GENIO, A.D., G.Schubert, J.M.Strauss (1979), Characteristics of Acoustic-Gravity Waves in a Diffusively Separated Atmosphere. J.Geophys. Res. 84, 1865-1879.

DUDIS, J.J. and C.A.Reber (1977), Composition Effects in Thermospheric Gravity Waves, Geophys. Res. Lett. 3, 727-730.

DYSON, P.L., G.P. Newton and L.H.Brace (1970), In Situ Measurements of Neutral and Electron Density Wave Structure from the Explorer 32 Satellite. J.Geophys. Res. 75, 3200-3210.

GROSS, S.H. (1980), Model Analysis of Large Scale Wave Structure as Observed by AE Satellites, paper SA100, Spring Meeting of the American Geophysical Union, May 22-27, Toronto, Canada, EOS 61, 322-323.

GROSS,S.H. and H.Eun (1976), Traveling Neutral Disturbances. GRL 3, 257-260.
(1978a), Traveling Neutral Disburbances and Minor Constituent Particle Mass. J.Atm.Terr.Phys.40, 183-193.
(1978b), Relative Phase and Amplitude Response to Gravity Waves of Minor Species in the Thermosphere. Geophys., Astrophys. Fl.Dyn. 11, 131-140.

GROSS, S.H. and C.A.Reber (1979), Wave Structure in the Neutral Species Observed by Atmospheric Explorer Satellites, paper SA-29, Spring Meeting of the American Geophysical Union, Washington, D.C., May 28 - June 1, EOS 60, 331-332.

GROSS, S.H., C.A. Reber and F.Huang (1979), Large Scale Waves in the Ionosphere Observed by the AE Satellites, Session H-1, paper 5, National Radio Science Meeting, 5-8 November, Boulder, Colorado.

HEDIN, A.E., J.E.Salah, J.V.Evans, C.A.Reber, G.P.Newton, N.W.Spencer, D.C.Kayser, D.Alcaydé, P.Bauer, L.Cogger and J.P.McClure (1977a), A Global Thermospheric Model Based on Mass Spectrometer and Incoherent Scatter Data. MSIS 1. N_2 Density and Temperature. J.Geophys. Res. 82, 2139-2147.

HEDIN, A.E., C.A.Reber, G.P.Newton, N.W.Spencer, H.C.Brinton and H.G.Mayr (1977b), A Global Thermospheric Model Based on Mass Spectrometer and Incoherent Scatter Data, MSIS 2. Composition. J.Geophys. Res.82, 2138-2156.

HINES, C.O. (1960), Internal Atmospheric Gravity Waves at Ionospheric Heights, Can. J.Phys. 38, 1441-1481.

HOEGY, W.R., P.Dyson, L.E.Wharton and N.Spencer (1979), Neutral Atmospheric Waves, GRL 6, 187-190.

HUANG, F., C.A.Reber and S.H.Gross (1980), Large Scale Waves in the Atmosphere and Ionosphere Observed by the AE Satellites. Paper SA101, Spring Meeting of the American Geophysical Union, May 22-27, Toronto, Canada, EOS 61, 323.

JENKINS, G.M. and D.G.Watts (1968), Spectral Analysis and Its Applications. Holden-Day, San Francisco, California, pp.210, 216-222, 341-348.

MARTYN, D.F. (1950), Cellular Atmospheric Waves in the Ionosphere and Troposphere. Proc. Roy. Soc. A201, 216-234.

MONIN, A.S. and A.M.Yaglom (1971), Statistical Fluid Mechanics: Mechanics of Turbulence. Vol. 2. The MIT Press, Cambridge, Mass., p.201.

REBER, C.A., A.E.Hedin, D.T.Pelz, N.E.Potter and L.H.Brace (1975), Phase and Amplitude Relationships of Wave Structure Observed in the Lower Thermosphere. J.Geophys. Res. 80, 4576-4580.

ULRYCK, T.J. and T.N.Bishop (1975), Maximum Entropy Spectral Analysis and Autoregressive Decomposition. Rev. Geophys. Sp.Phys. 13, 183-200.

TABLE I

FIXED LAYER ANALYSIS

250 km Southern Mid-Latitudes
AE-C Orbit 5359
Downgoing Phasewise Wave

Harmonic Number	Period min	λ_x km	θ	Measured		Calculated	
				$\lvert A/N_2 \rvert$	$\lvert He/N_2 \rvert$	$\lvert A/N_2 \rvert$	$\lvert He/N_2 \rvert$
16	106	2600	x	6.0	12.0	2.9	6.7
17	625	1200	x	1.6	2.3	3.8	1.0
18	286	5400	x	3.8	9.0	10.9	10.4
19	10	120	67°	1.1	18.2	8.7	25.7
20	628	13000	x	2.1	5.8	5.9	7.2
21	84	1100	x	1.2	12.4	4.8	8.8
22	18	170	50°	9.1	24.3	18.8	8.6
23	11	88	70°	6.7	13.5	14.2	7.8
24	11	60	76°	5.0	4.5	2.1	3.3
25	200	1460	x	8.6	12.2	7.8	10.5
26	10	315	x	3.5	16.9	2.1	24.5
27	57	1190	x	2.6	18.8	7.9	25.3
28	70	1570	x	2.8	15.1	7.1	21.7
29	188	5400	x	3.0	8.6	6.4	12.7
30	10	38	72°	13.1	12.3	1.3	5.2

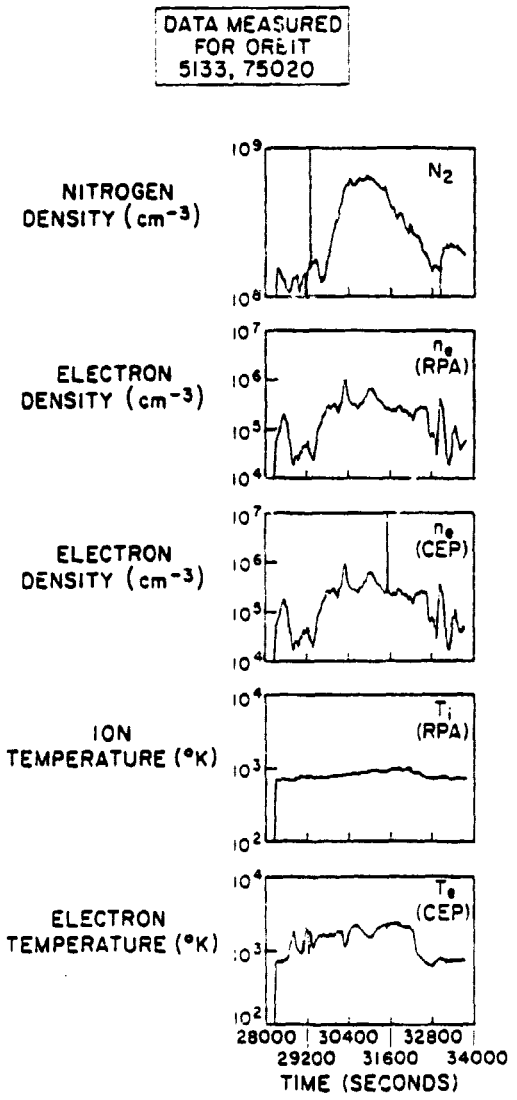

Figure 1 Densities and temperatures for one entire orbit, orbit 5133.

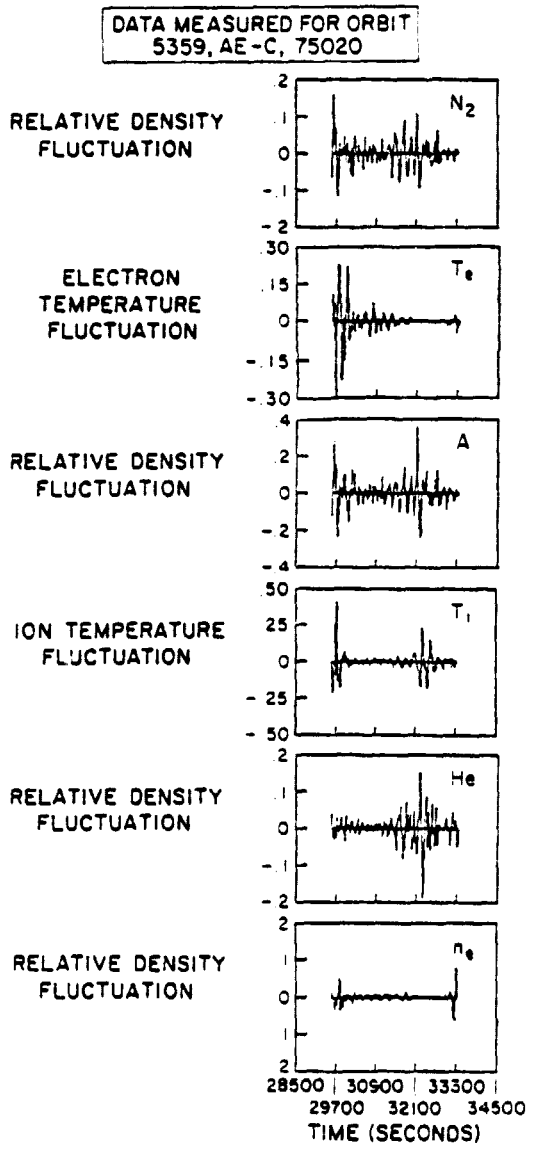

Figure 2 Relative fluctuations of densities and temperatures for orbit 5359.

5133 MEM/GU 29800

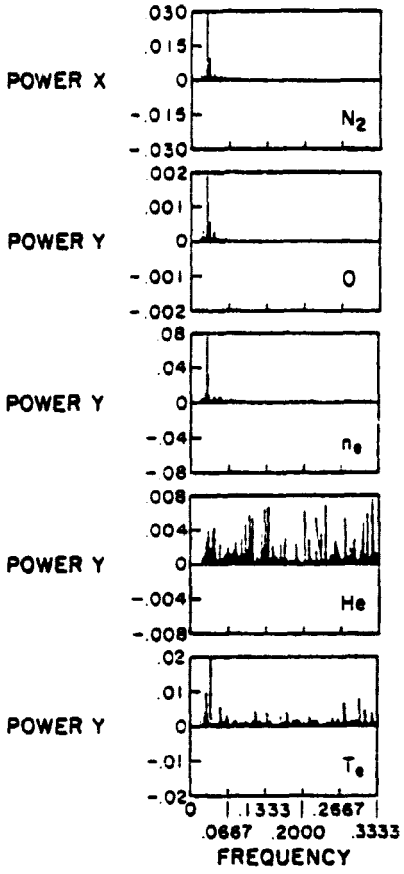

Figure 3 Power spectra for a part of orbit 5133, 55° to 0° latitude.

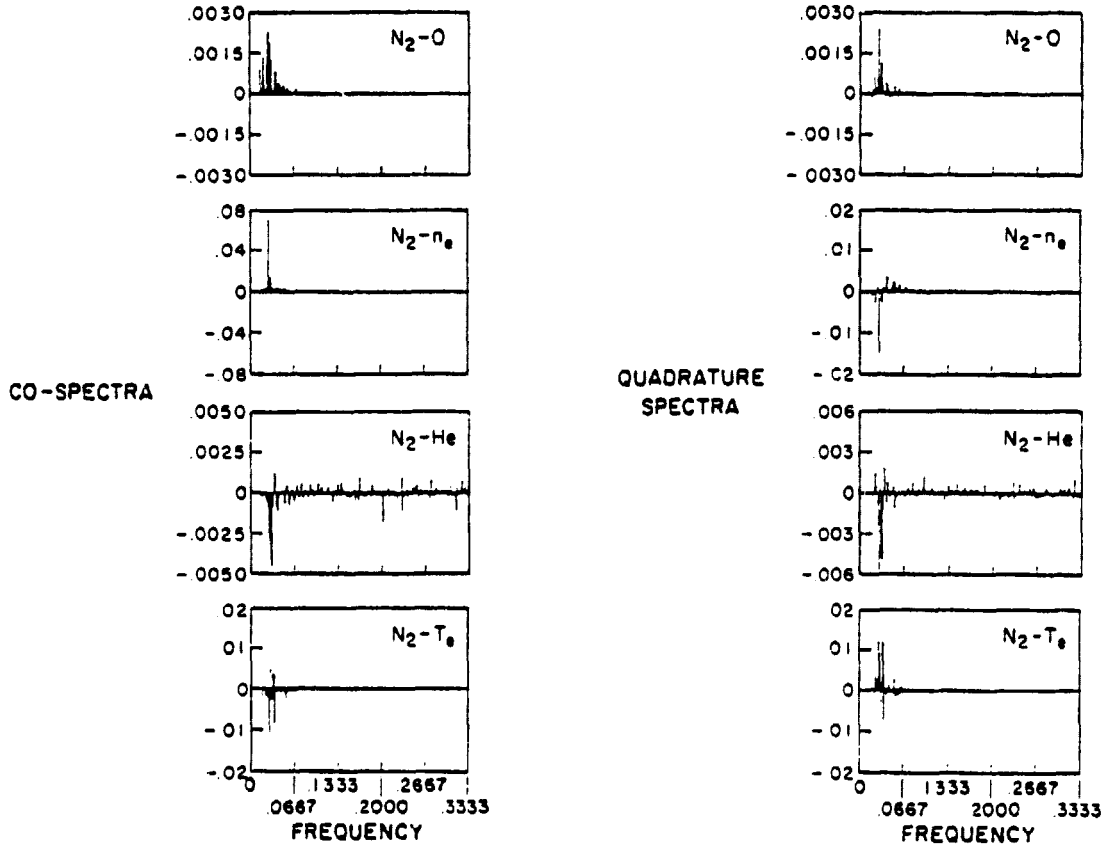

Figure 4 Co- and quadrature spectra for the data channels of Figure 3 relative to nitrogen.

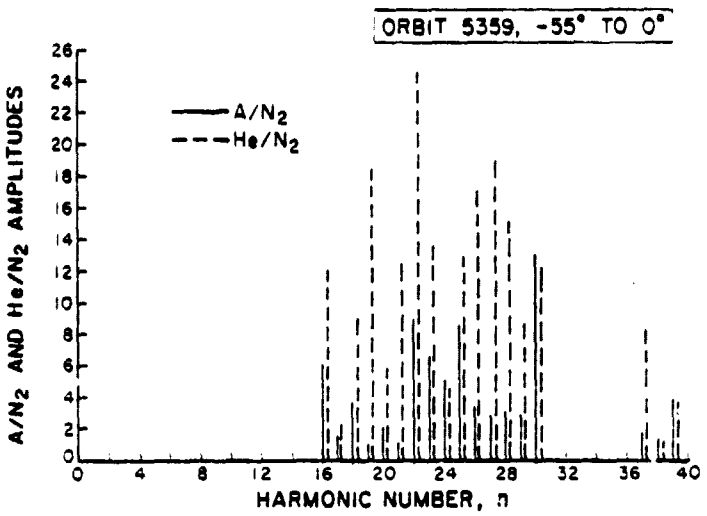

Figure 5 Amplitude ratios of argon to nitrogen and helium to nitrogen for significant lines of the cross spectra, orbit 5359, southern mid-latitudes.

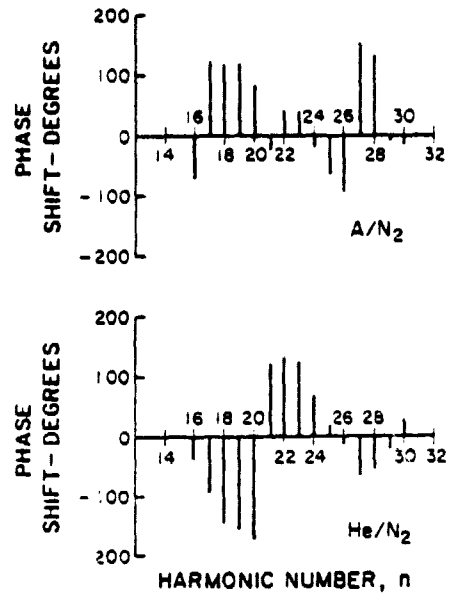

Figure 6 Phase spectra associated with the amplitude spectra of Figure 5.

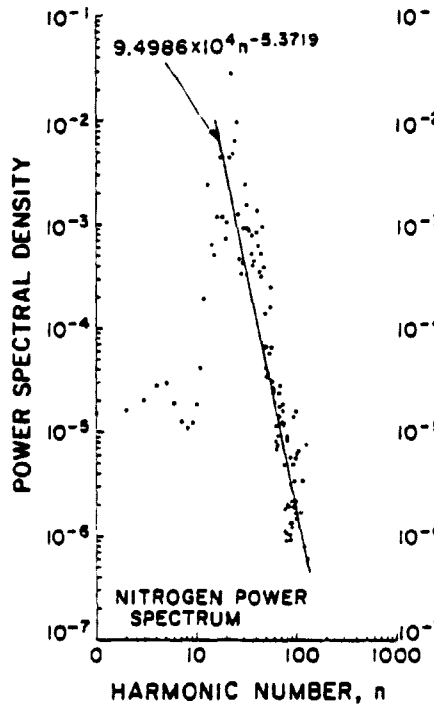

Figure 7 Power spectrum of nitrogen vs. the harmonic number n for data of Figure 3. Best fit line based on the spectra from n = 25 to 100 is shown.

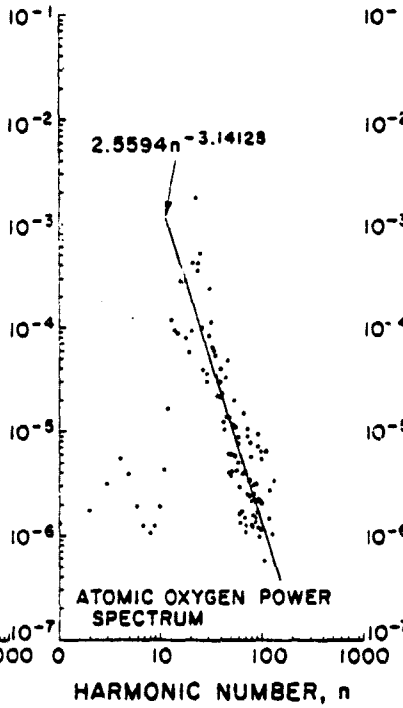

Figure 8 The same as Figure 7 but for atomic oxygen.

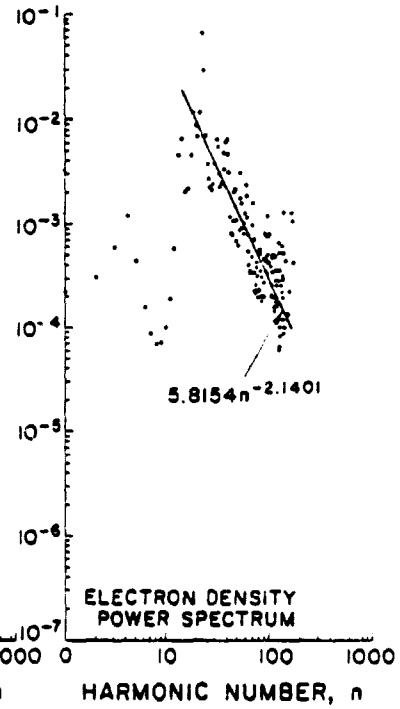

Figure 9 The same as Figure 7 but for the electron density.

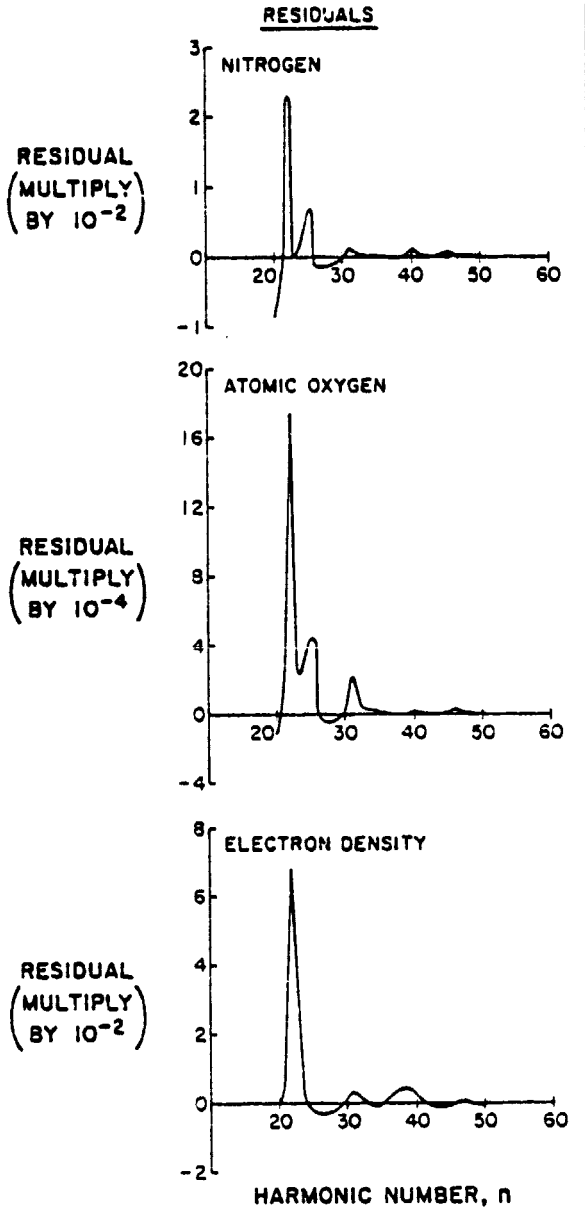

Figure 10 Plots of residuals of spectra in Figure 7 - 9 in the range n = 20 to n = 50.

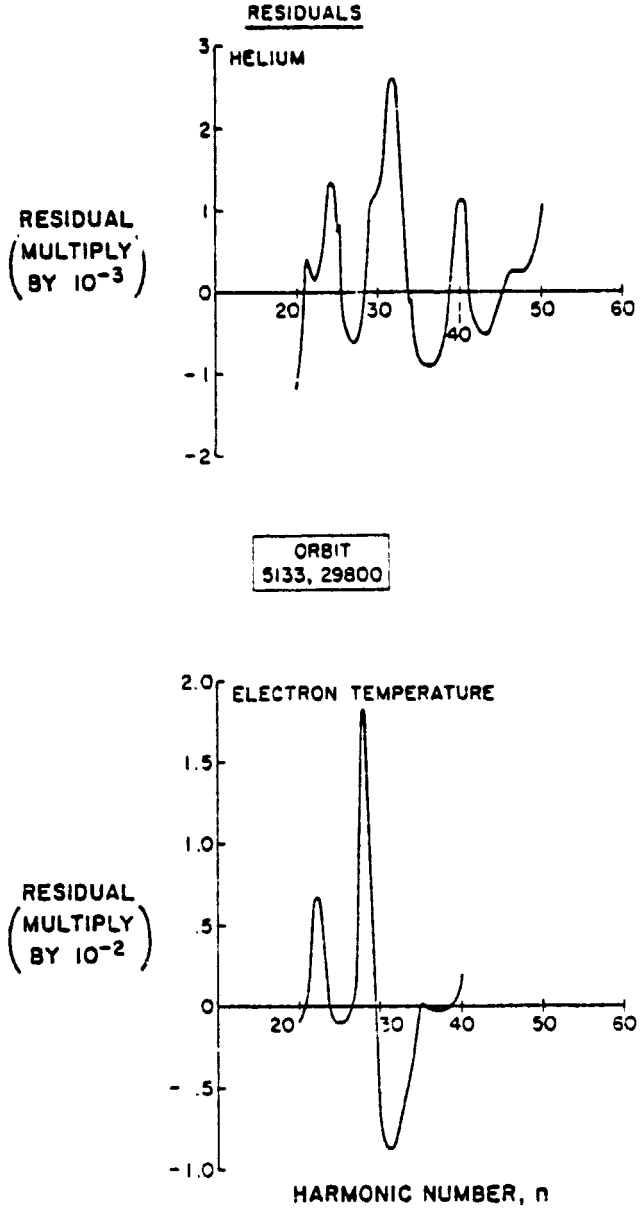

Figure 11 The same as Figure 10 but for helium and the electron temperature.

POLY-MRI-1426-82
July 1981
Revised September 1982

GRAVITY WAVES IN THE THERMOSPHERE OBSERVED BY THE AE SATELLITES

by

S. H. Gross
Polytechnic Institute of New York
Microwave Research Institute
Farmingdale, New York 11735

C. A. Reber
National Aeronautics and Space Administration
Goddard Space Flight Center
Greenbelt, Maryland 20771

F. Huang
Computer Sciences Corporation
Silver Spring, Maryland 20910

Prepared for

NATIONAL AERONAUTICS AND SPACE ADMINISTRATION

Grant No. NSG-5284

Abstract

Atmosphere Explorer (AE) satellite data were used to investigate the spectral characteristics of wave-like structure observed in the neutral and ionized components of the thermosphere. Power spectral analysis derived by the maximum entropy method indicate the existence of a broad spectrum of scale sizes for the fluctuations ranging from tens to thousands of kilometers. A new discovery is a power law decrease of power with decreasing wavelength, much like a turbulence structure, though not necessarily turbulence, which is generally observed in all data examined. Waves that may be gravity waves are observed in the species and other parameters studied. These appear superposed on top of the turbulence-like structure. Correlation of many waves in the spectra of the various parameters, including neutral and plasma parameters, is quite evident, demonstrating strong coupling between the constituents of the medium. A typical example is shown which illustrates these features.

Introduction

The direct observation of large scale waves both in neutral and ionized media in the thermosphere has been made possible by the measurements of the Atmosphere Explorer (AE) satellites. These satellites provide in situ measurements of the density of argon, helium, nitrogen, and oxygen, the temperature and drift velocities of nitrogen or oxygen, plasma density, ion and electron temperatures, as well as other measurements (Dalgarno et al., 1973; Pelz, et al., 1973; Nier et al., 1973; Spencer, et al., 1973; Brace et al., 1973; Hanson et al., 1973). Many of these measurements are essentially simultaneous, making direct comparison possible. Data from a number of orbits of the AE-C satellite have been studied, focusing on those that are near circular at an altitude of about 250 km. Circular orbits eliminate the effects of altitude variations on observed fluctuations. The AE-C orbit is inclined $\approx 68^{\circ}$.

There is evidence of correlation in the fluctuations of all neutral species and ionization in every case examined, implying the existence of wave like structures, and supporting previous, more limited examples based just on visual examination of the measured data (Reber et al (1975) using AE-C data; Dyson et al (1970) using Explorer 32), and analytically treated examples (Hoegy et al 1979). Since the satellite moves very rapidly (~ 7.8 km/sec) , the measurements essentially provide the spatial distribution of the measured quantities. The scales of the waves are determined from spectral analysis using power spectra derived by the maximum entropy method, MEM (Ulryck and Bishop, 1975). Scale lengths are observed from 10's to 1000's of kilometers.

Data and Spectra

One typical example of AE-C data is shown in Figure 1. These data are approximately 1.5 second samples, plotted vs time over a time interval of 750 seconds. They are from orbit 5133 on January 20, 1975 for a portion of the orbit in the northern hemisphere from about 10° to 54° latitude. Altitude varies from about 244 km to 252 km, and the local time ranges from 1100 to 1300 hours. Magnetic and solar activities at the time were relatively quiet. The indices were $A_p = 7$, $K_p = 2$, AE = 114, and the 10.7 cm solar flux $F_{10.7} = 77$. Shown are the densities of oxygen, nitrogen, helium and the electrons and the electron temperature plotted against time in seconds (UT). The ordinate scales for the densities are logarithmic.

Some fluctuations are evident in the geophysical parameters in Figure 1. With the exception of nitrogen and oxygen, and possibly the electron density, any relationship between these fluctuations is not clear from the figure. Relationships become more evident on separating the fluctuations from the data. This is done by extracting their background, or low frequency content using a low pass digital filter. Its output is subtracted from the data to obtain the fluctuations. Since the scale of the fluctuations varies with the parrameters, comparisons between parameters are best made by normalizing the fluctuations. This is done by dividing the fluctuations by the output of the low pass filter. The normalized fluctuations (designated $\Delta n/n$ for densities, or $\Delta T/T$ for temperature) for each of the parameters in Figure 1 are shown in Figure 2.

The filter used is a Hamming non-recursive filter including Lanczos sigma factors (Hamming, 1977). Its order is 60. It passes all frequencies below 0.01 Hz, equivalent to 780 km wavelength. The attenuation of the filter at 0.01 Hz is 0.5. Less than 1% of the power is passed at 0.02 Hz and far less for higher frequencies. Finer details of its transfer function are not given here.

The power spectra for each of the fluctuations in Figure 2 are shown in Figure 3. These are plots of power spectral density as a function of frequency as observed by a moving satellite (analogous to a Doppler frequency). About 380 fluctuation samples for each parameter are used after filtering to obtain the spectra by means of the MEM with an order equal to 100 and using the Burg algorithm. This order was selected after study of the effects of the MEM order on spectra and by comparing with FFT spectra and spectra derived by other means. The details are not given here. The spectra are shown at evenly spaced frequencies in the figure, making them have the artificial appearance of line spectra. The frequency range shown extends out to the Nyquist frequency, 1/3 Hz. A wavelength scale is shown below the frequency scale. This scale corresponds to the equivalent wavelength of a wave standing along the satellite track and is obtained by dividing the satellite velocity, 7.8 km/sec, by the corresponding frequency. A wave of given wavelength traveling at an angle to the satellite track would appear to have a longer wavelength along the track.

More features of the spectra are brought out by plotting on log-log

graphs. Figure 4 shows the power spectra of oxygen, nitrogen and electron density replotted in this fashion. The crosses are at frequencies that are multiples of 1.302 mHz, which corresponds to the time period, 768 seconds, of 512 samples spaced 1.5 seconds apart. The frequencies shown are mostly above the filter range, so that these spectra represent the high frequency content of the fluctuations. The corresponding wavelengths of the spectra shown there are from about 545 km to about 40 km. Shown on each graph are straight lines which represent least squares power law fits. These fits are based on the spectra above the filter range (for wavelengths below 374 km). The exponents, or spectral indices, differ for all three species shown: -5.38 for nitrogen, -3.51 for oxygen, and -2.25 for the electron density.

The spectra of helium and the electron temperature were not included in Figure 4 because of their noisy appearance. They exhibit many of the features of white noise, particularly at higher frequencies. Nevertheless, their lower frequency spectra have some features in common with those of oxygen, nitrogen and the electron density, in spite of the noise, as may be seen in figure 3, but the details are not given here.

Discussion

One observes in Figure 1 relatively smooth variation in the densities of N_2 and O and rather irregular, or noisy, variations in the density of He. The noisiness of the He data is well brought out by the appearance of its fluctuations, in contrast with those of N_2 and O, as shown in Figure 2. It is also seen in the broad, white-noise-like spectrum of He, in contrast with the narrower band spectra of N_2 and O, as seen in Figure 3. Nevertheless, the lowest frequency peaks in the He spectrum are about the same as those of N_2 and O and one can associate some of the fluctuations of He in Figure 2 with those of N_2 and O. They appear out of phase.

The variation of the electron density in Figure 1 also exhibits fluctuations along with large scale changes, of which the largest, at about 30250sec (UT), is apparently associated with the equatorial anomaly. There are also sections of the data that exhibit fluctuations much like those of N_2 and O. The relative fluctuations of the plasma density in Figure 2 appear to be a bit noisy, yet somewhat like those of N_2 and O, as may be seen in that figur . Figure 3 shows that the power spectrum of the electron density is also limited in width, similar to N_2 and O.

Considerable variation in the electron temperature is also apparent in Figure 1. Rapid, noise-like fluctuations are evident, as well as a large scale change at about 30250 sec (UT) that is associated with the anomaly. Its fluctuations, as seen in Figure 2, also appear noisy, though perhaps not as much as that of He. One can associate some of the fluctuations with those of

N_2 and O. Its power spetrum in Figure 3 is also broad, like white noise, though somewhat reduced at higher frequencies. The lower frequency peaks are about the same as those of N_2 and O.

The fluctuations of O, N_2, and the electron density exhibit wave-like structures, as seen in Figure 2. N_2 and O fluctuations are quite similar, though of different magnitude. One observes structure with a number of periods, but there is an outstanding periodicity roughly of the order of 35 seconds, or about 270 kilometers on converting to the corresponding path length along the satellite track. The level of the N_2 fluctuations averages about 3% with some fluctuations reaching peaks of as much as 7 to 8%. The O fluctuations average about 1% with some peaks equal to about 3%. These fluctuations are not particularly intense, though, the example is typical and adequate for illustration here. The electron density fluctuations are larger than those of N_2 and O, averaging about 8% with some peaks reaching 13%. The noise-like fluctuations of He and the electron temperature both average on the order of 5%. A close examination of the fluctuations of N_2, O and the electron density shows very small phase shifts between their various wavelets with the electron density leading by about 20 seconds.

The power spectra in Figure 3 of N_2, O and the electron density exhibit peaks at about the same frequencies, or wavelengths, corroborating the similarities in the structure of their fluctuations. The first spectral peaks are at frequencies on the order of 0.01 Hz, within the low pass filter band and therefore attenuated. Their wavelengths are on the order of 800km. A

larger second peak, a still larger third peak and a much smaller fourth peak are evident in all three spectra. These are at wavelengths of roughly 430, 270 and 195 km respectively. The 270 km wavelength corresponds to the 35 second periodicity seen in the fluctuation data. It is believed that all these peaks are due to gravity waves, though it is not clear if they are propagating, and, if so, with what velocity, direction and temporal frequency. Such wave characteristics are more easily determined in conjunction with ground measurements which, unfortunately, were not available during passes of the satellite over such facilities. It may be possible to obtain this information from cross spectra (Hoegy et al., 1979), but difficulties with the MEM algorithm for obtaining such spectra has precluded their use for the purposes of this paper (Gross et al., 1980).

The log-log presentations of the power spectra of N_2, O and the electron density in Figure 4 indicates that these fluctuations consist of broad spectra. The power law fits illustrate that the power in each specie decreases with increasing frequency, or decreasing wavelength. The decrease of power with frequency is greatest for nitrogen, less for oxygen and least for the electron density. We believe that part of the power law - like variation is due to the sources. Why the rates for each are different is unknown. If these spectra arise from the same sources, as seems likely, it is conceivable that the differences arise from the propagation characteristics of the medium. Such power law distributions are also reminiscent of eddies or turbulence (Monin and Yaglom, 1971), though of much larger scale lengths,

leading to the description "turbulence-like". However, not enough information is available to establish whether or not turbulence is involved. It is possible, for example, to obtain similar spectra from simple perturbations. Since coherence tends to narrow spectra, the breadth of the spectra may merely be indicative of non-coherent sources.

Peaks are evident in the discrete spectra in Figure 4. Those corresponding to wavelengths greater than 100 km are listed in the table below. All figures are in kilometers.

Nitrogen	Oxygen	Electron Density
428	400-428	428
272	272	260
193	193	193
162	162	150
136	133	---
111	111	111

Though the values are to three figures, these peaks approximate the wavelengths of the waves along the satellite track. This is due to the use of discrete frequencies and because of offsets arising from the MEM. The longest wavelength is in the filtered range and therefore somewhat attenuated. All others are unattenuated. The first three correspond to peaks clearly seen in Figure 3. The match between these various wavelengths for the three species

is excellent, particularly for nitrogn and oxygen. (Though not given, the corresponding peaks of He and the electron temperature also match well.) Those of the electron density are either the same or close, with the exception of a missing (or possibly indistinct) peak at about 130 km. These spectra provide evidence that common wave systems are affecting all three species, and probably the other parameters as well. Also, this example clearly demonstrates the coupled behavior of the ionosphere and neutral atmosphere. Though expected, such evidence is generally sparse. It is likely that the waves in the ionization result from wave motion of the neutrals. All these waves may be medium scale gravity waves, as described by Georges (1968). They appear to be superposed on the turbulence-like spectra of each of the species.

More than one source may be needed to produce the medium scale waves; for example, one source for each wave. Each source would excite its own wave characterized by its own structural size. Multiple sources may occur typically during intense meteorological activity. On the other hand, if the waves emanate from one source they might represent different structural features of the source. Regardless of the nature of the sources, waves of these scales are likely to be local, since waves of wavelengths of only several hundred kilometers or less would be well attenuated, if they propagated from distant sources.

The spectra shown here are just for one example from AE-C. We find similar spectra for other parts of the same orbit and for other orbits in all

the data we have analyzed. The length of the data samples in Figure 1 is 750 seconds. This is about the time interval (representing about 6000 kilometers) required to study waves for specific latitude belts of geophysical significance, such as mid-, high and equatorial. Scale lengths on the order of tens to hundreds of kilometers are found. When longer time samples are analyzed, the scale sizes are larger. Full orbit data provide similar spectra, but sizes to thousands of kilometers are obtained still characterized by power law fits and peaking at individual frequencies as in Figure 4. Such spectra, however, represent a mix of "local" phenomena as well as worldwide large scale phenomena. A broad, power law-type spectrum with waves superposed, a new discovery for waves of these scales, is apparently omnipresent as far as we can tell from the data analyzed.

The nature of the spectra described here are also corroborated by another experiment. Total electron content was measured between two spacecrafts during the Apollo-Soyuz Test Program by the differential doppler technique (Estes and Grossi, 1980; Weiffenbach et al., 1977). These measurements exhibit power spectra with similar features with the measured data processed directly by the MEM without filtering (Gross et al., 1981). It is also interesting that Dyson et al (1974) found similar structures in AE-C electron density measurements.

The complexity of wave structures is further exhibited by the broad frequency spectrum found by Titheridge (1971) from ground temporal measurements of total electron content.

The material shown here provides further insight into the nature of waves in the upper atmosphere as observed by satellites. The data of the AE satellites, both AE-C and AE-E, are rich with such evidence. Much more work is needed in analyzing these data to establish the characteristics of these waves, particularly gravity waves, their function in transporting and distributing energy and momentum, and their properties in terms of geophysical parameters, such as solar and magnetic activity, season and time of day.

Acknowledgement: These authors thank K. Coakley of Computer Sciences Corporation for his aid in calculating some of the material in this paper.

Brace, L. H., R. F. Theis and A. Dalgarno (1973), The Cylindircal Electronstatic Probes for Atmosphere Explorer-C, -D, and -E, Radio Science, 8, 341-348.

Dalgarno, A., W. D. Hanson, N. W. Spencer, E. R. Schmerling (1973), The Atmosphere Explorer Mission, Radio Science, 8, 263-266.

Dyson, P. L., G. P. Newton, and L. H. Brace (1970), In Situ Measurements of Neutral and Electron Density Wave Structure from the Explorer 32 Satellite. J. Geophys. Res., 75. 3200-3210.

Dyson, P. L., J. P. McClure, and W. B. Hanson (1974), In Situ Measurements of the Spectral Characteristics of F Region Ionospheric Irregularities, J. Geophys. Res., 79, 1497-1502.

Estes, R. D. and M. D. Grossi (1980), Observations of Short Wavelength (λ < 300 km) Ionospheric Irregularities by a Satellite-to-Satellite Doppler Tracking Link, submitted for publication.

Georges, T. M. (1968), HF Doppler Studies of Traveling Ionospheric Disturbances, J. Atmos. Terr Phys., 30, 735-746.

Gross, S. H., C. Friedman and M. Grossi (1981), Wavelike Ionospheric Structure Observed by a Satellite to Satellite Doppler Tracking Link, in preparation.

Gross, S. H., C. A. Reber, F. Huang (1980), Large Scale Waves in the Ionosphere Observed by the AE Satellites, AGARD Meeting, 27th Symposium of the Electromagnetic Wave Propagation Panel, 28-31 October, Pozzuoli, Italy.

Hamming R. W. (1977), Digital Filters, Prentice Hall, Inc., Englewood Cliffs, N.J., pp. 95-104.

Hanson, W. B., D. R. Zuccaro, C. R. Lippincott and S. Sanatani (1973), The Retarding-Potential Analyzer on Atmosphere Explorer. Radio Science, 8, 333-339.

Hoegy, W. R., P. Dyson, L.E. Wharton and N. Spencer (1979), Neutral Atmospheric Waves, GRL, 6, 187-190.

Monin, A. S. and A. M. Yaglom (1971), Statistical Fluid Mechanics: Mechanics of Turbulence, Vol. 2. The MIT Press, Cambridge, MA, page 201.

Nier, A. O., W. E. Potter, D. R. Hickman, and K. Mauersberger (1973), The Open-Source Neutral-Mass Spectrometer on Atmosphere Explorer -C, -D, and -E. Radio Science, 8, 271-276.

Pelz, D. T., C. A. Reber, A. E. Hedin, and G. R. Carignan (1973), A Neutral-Atmosphere Composition Experiment for the Atmosphere Explorer -C, -D, and -E, Radio Science, 8, 277-285.

Reber, C. A., A. E. Hedin, D. T. Pelz, N. E. Potter, and L. H. Brace (1975) Phase and Amplitude Relationships of Wave Structure Observed in the Lower Thermosphere, J. Geophys. Res., 80, 4576-4580.

Spencer, N. W., H. B. Niemann and G. R. Carignan (1973), The Neutral-Atmosphere Temperature Instrument, Radio Science, 8, 287-296.

Titheridge, J. E. (1971), The Spectrum of Electron Content Fluctuations in the Ionosphere, Planet. Space Sci., 19, 1593-1608.

Ulryck, T. J. and T. N. Bishop (1975), Maximum Entropy Spectral Analysis and

Autoregressive Decomposition, Rev. Geophys. Sp. Phys., 13, 183-200.

Weiffenbach, G. C., M. C. Grossi, P. W. Shores (1977), Doppler Tracking Experiment MA-089, in Summary Science Report, Apollo-Soyuz Test Project, Volume 1, pp. 137-175.

Figure Captions

Figure 1. Densities of nitrogen, oxygen, helium and the electrons and the electron temperature vs time in seconds, altitude and latitude from January 20, 1975 Atmosphere Explorer C Orbit 5133. Neutral density measurements are from Neutral Atmosphere Temperature Experiment (NATE), and electron density and temperature from Cylindrical Electrostatic Probe (CEP).

Figure 2. Relative fluctuations in the densities, $\Delta n/n$, of nitrogen, oxygen, helium and electrons, in electron temperature, $\Delta T/T$, vs time in seconds for data in Figure 1.

Figure 3. Discrete power spectra of relative fluctuations in Figure 2 vs frequency in mHz for the entire range to 333 mHz, the Nyquist frequency, and vs wavelength in kilometers.

Figure 4. Discrete power spectra of Figure 3 from 14.3 mHz to 195 mHz replotted with logarithmic axes for nitrogen, oxygen and electron densities vs frequency and wavelength, spaced logarithmically. Power law fits are shown in the form $f^{-\alpha}$, where f is the frequency, based on spectra between 20.8 mHz and 130.2 mHz.

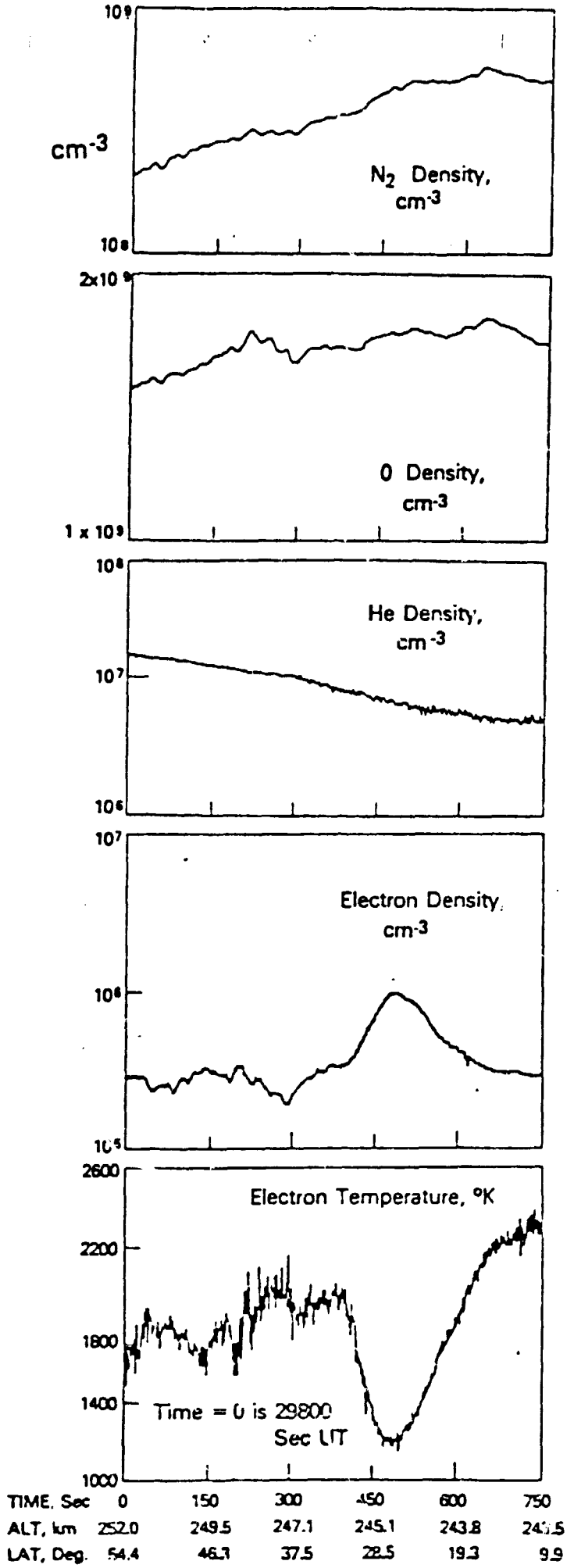

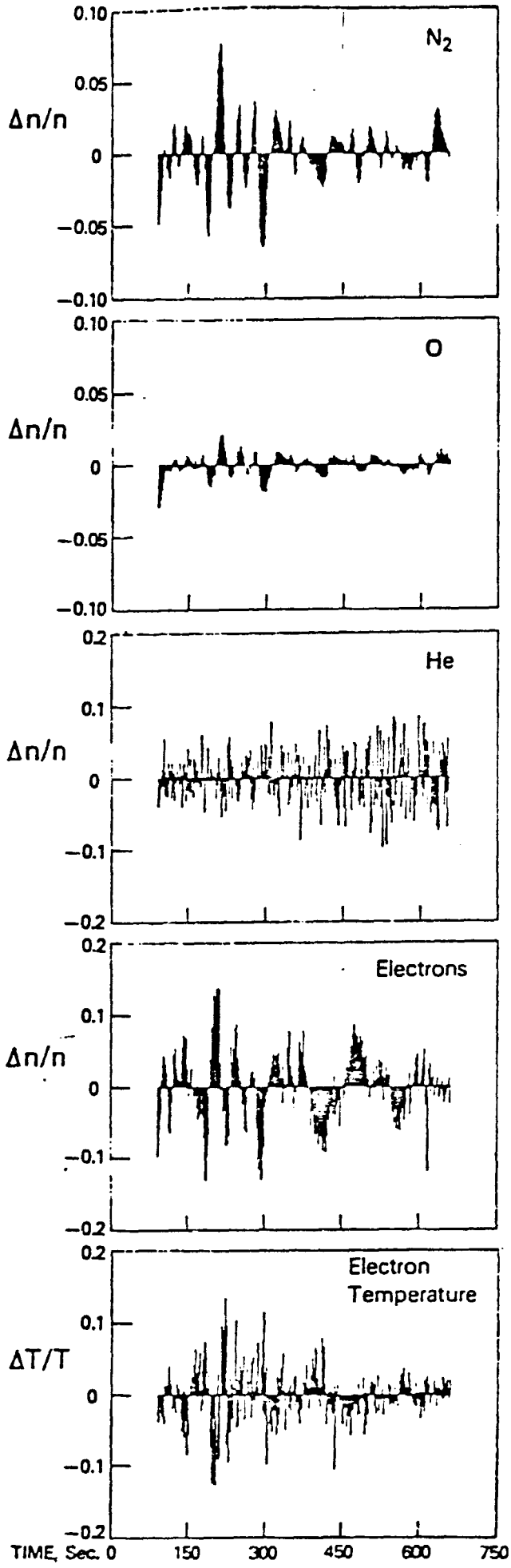

Time = 0 is 29800 Sec. UT

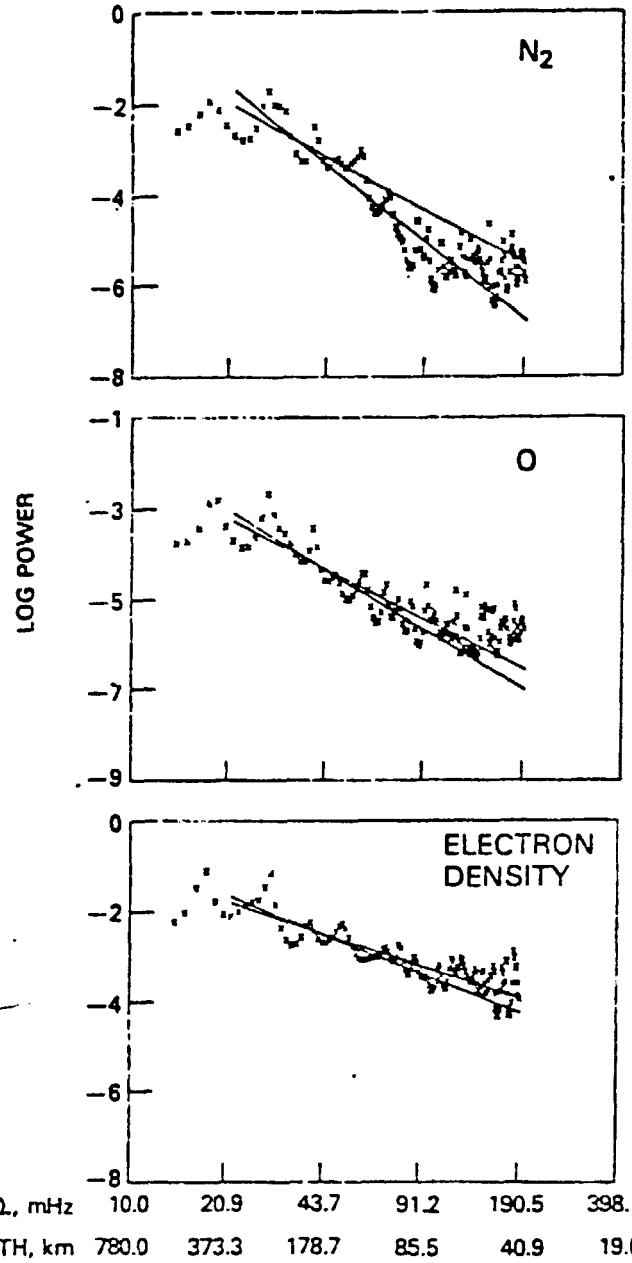

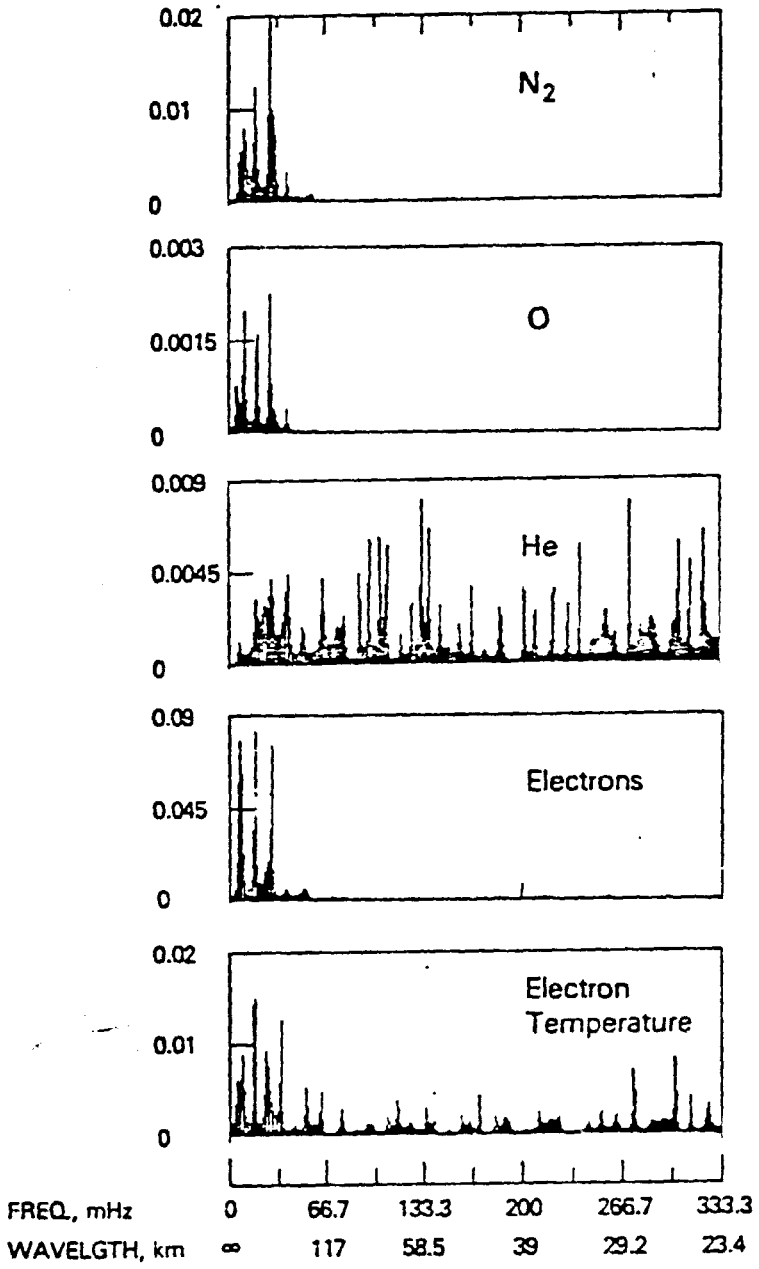

POLY-MRI-1427-83
February 1983

LARGE SCALE WAVES IN THE THERMOSPHERE OBSERVED BY THE AE-C SATELLITE

by

S. H. Gross
Polytechnic Institute of New York
Microwave Research Institute
Farmingdale, New York 11735

C. A. Reber
National Aeronautics and Space Administration
Goddard Space Flight Center
Greenbelt, Maryland 20771

F. T. Huang
Computer Sciences Corporation
Silver Spring, Maryland 20910

TECHNICAL REPORT

Prepared for

NATIONAL AERONAUTICS AND SPACE ADMINISTRATION
Grant No. NSG-5284

TABLE OF CONTENTS

Large Scale Waves in the Thermosphere Observed by the AE-C Satellite

S.H.Gross

Polytechnic Institute of New York, Farmingdale, NY 11735

C.A.Reber

NASA, Goddard Space Flight Center, Greenbelt, MD 20771

F.T.Huang

Computer Sciences Corporation, Silver Spring, MD 20910

ABSTRACT

Atmospheric Explorer C (AE-C) data are analyzed to study wavelike perturbations in the thermosphere at an altitude of about 260 km. The data are from a large portion of an orbit on January 20, 1975. The examples shown are typical of many other orbits of satellites AE-C and AE-E. Four geophysical parameters are analyzed. These are nitrogen and oxygen densities, electron density and ion temperature as measured by three different instruments on board AE-C.

The data are processed by normalizing them to their average values and their fluctuations are obtained by passing the normalized data through a high pass filter. These fluctuations exhibit strong periodicities that persist throughout the records, regardless of the filter cutoff frequency. The fluctuations are cross correlated by direct comparison, by comparison of their spectral content as obtained by the MEM and fft, and by computing cross correlation functions.

The ratio of the fluctuations and their relative phase shifts are treated as the magnitude and phase shift of a transfer function between the responses of all parameters relative to the response of the oxygen density. These transfer functions are used in a plane wave modeling study to deduce all wave characteristics. It was not

possible to account for the wave characteristics, suggesting that the fluctuations may be a mixture of standing and traveling waves.

It is found that there are large scale structures in all four parameters with horizontal scale sizes ranging from about 4000 km to about 400 km. Both ionization and neutrals are driven by these waves. Ionization, including even the ion temperature, is coupled to the neutrals for most waves. The coupling and wave system persists over large global distances and in both hemispheres.

The spectra for all parameters contain peaks at wavelengths that are confirmed by the periods of the fluctuations and decrease with decreasing wavelength with a power law type of variation. The 'spectral index', or exponent of the power law, for the four parameters differ, though those of oxygen and nitrogen are close in value. Comparison of the spectral peaks show that many waves are common to all parameters.

1. Introduction

Wave-like perturbations of constituents in the thermosphere are detected by measurements of the ionosphere by ground facilities and by instrumentation on board satellites measuring both neutral and ionospheric parameters. Perturbations of ionization are known as traveling ionospheric disturbances (TID's) (Hines,1974; Georges,1968; Yeh and Liu,1974). A number of reports of large scale TID's (from hundreds to thousands of km) have shown that they propagate from high latitude regions during auroral substorms (Thome, 1968; Davis and da Rosa,1969; Testud et al,1975). These waves are believed to be caused by heat and momentum input into the atmosphere in the auroral zones from particle precipition and Joule heating (Vickrey et al,1982; Wickwar et al, 1975). Their origins have been reviewed by Hunsucker (1982). Studies have also been made of these waves in association with magnetic storms by Richmond and Matsushita (1975), Mayr and Volland (1973 and 1974), Testud et al (1975), Roble et al (1978), Richmond (1979) and Prolss (1982).

Medium scale TID's (from tens to hundreds of km) are also observed, but their sources have not been well identified, though it is believed that meteorological phenomena may produce most of them. Larsen et al (1982) have associated thunderstorms with these waves. Mastrantonio et al (1976) have also associated these waves with jet streams in the atmosphere, and Bertin et al (1977) have detected waves

related to the jet stream.

The characteristics of all these TID's are found to be generally in accordance with gravity wave theory (Hines,1974). It is believed that the neutrals are perturbed by gravity waves as a result of localized sources of heating and momentum, and the neutrals, in turn, drive the ionization by collisions to produce these TID's. Gravity waves are believed to be associated with Spread F in the ionosphere and ionospheric bubbles in the equatorial region, affecting communications with synchronous sattelites (Anderson et al, 1982; Kelley et al, 1981). Anderson et al (1982) also pose another mechanism for generation of gravity waves in the thermosphere in the equatorial zone.

Gravity wave theory is concerned with two types of waves called gravity waves and acoustic-gravity waves. Acoustic-gravity waves make up the upper frequency branch and gravity waves the lower frequency branch of the hydrodynamical system in which both gravity (buoyancy) and compressibility act as restoring forces. The upper branch becomes identical to ordinary sound waves in the audio frequency range, but at its lowest frequencies such waves are called 'infrasonic waves'. This branch has a lower cutoff frequency called the 'acoustic cutoff frequency', and there is a cutoff region below this frequency, which separates the two branches. The lower end of the cutoff band, which is the upper limit of the gravity wave branch, is called the 'buoyancy frequency'. The cutoff band is determined by the temperature and its vertical gradient and by the mean molecular mass of the medium, so that it varies somewhat with altitude. The cutoff band is relatively narrow, and periods within it range from about several minutes at low altitudes to from 10 to 15 minutes at higher altitudes, depending on temperature. The periods of gravity waves then range from the period of the buoyancy frequency to many hours, whereas those of acoustic-gravity waves range from the acoustic cutoff period to periods of seconds and less. In the gravity wave branch, long period waves usually have large horizontal wavelengths and shorter periods smaller wavelengths (Hunsucker, 1982).

Though fluctuations in ionization in the thermosphere have been measured both on the ground and by satellite borne instrumentation, the detection of wave-like perturbations of neutral constituents in the thermosphere depends mostly on access by rockets and satellites. Radar is used only up to an altitude of about 100 km. Satellite borne experiments have detected wave-like perturbations, both in total neutral density and temperature; for example, ESRO 4 (Prolss and Von Zahn, 1974 a and b; Trinks and Mayr, 1976), OGO 6 (Reber and Hedin, 1974; Taeusch et al, 1971), AEROS-A (Chandra and Spencer, 1975 and 1976; Trinks et al, 1976), AE-C (Reber et al, 1975; Potter et al, 1976). The density variation of

individual species, namely nitrogen, oxygen, helium and argon, have also been measured on board ESRO 4, AEROS-A and AE-C. Vertical velocity variations of these species have also been measured by AE-E.

Until the advent of satellites there has been little confirmation that wavelike perturbations in both the neutrals and ionization are correlated. Visual examination of data measured on board Explorer 32 (Dyson et al, 1970 and 1974) and AE-C (Reber et al, 1975) provided some support for such correlation. Some additional evidence were provided by Hoegy et al (1979) employing some analytical modeling. Gross et al (1980 and 1981), found still more evidence on the basis of visual comparisons of spectra and fluctuations.

Here we report on a study of some AE-C data to examine these wavelike perturbations in greater detail using various data processing techniques. Since instrumentation on board AE-C make in situ measurements of many parameters nearly simultaneously, it is possible to cross correlate their fluctuations to seek their common properties and to show the degree to which they are truly correlated. AE-C measurements are made of neutral densities, electron density and temperature, and ion temperature, as well as many other parameters. Here we use nitrogen and oxygen densities as determined by the Neutral Atmosphere Temperature Instrument (Spencer et al, 1973), electron density from the Cylindrical Electrostatic Probe experiment (Brace et al, 1973) and ion temperature from the Retarding Potential Analyzer experiment (Hanson et al, 1973). The satellite was in a near circular orbit at an altitude of about 260 km while measuring the data treated here. The orbit was inclined 68°.

The satellite's velocity in orbit is about 7.8 km/sec. The waves of interest have group velocities of the order of the acoustic velocity or less, about 800 m/sec in the thermosphere. Since the satellite velocity is so much greater than the wave velocity, the in situ measurements are essentially a snapshot of the distribution of the measured parameters at the altitude of the satellite at a particular time. Thus, wavelike variations in the measured time series are really spatial variations. One observes the horizontal wavelength for a circular orbit and not the wave period, though the terms frequency and periodicity will be used often interchangeably with horizontal wavelength. Frequency in this case relates to the time series of the in situ data. The true period or true frequency of a wave will be distinguished from the period or frequency of the in situ data by calling the former the 'temporal' period or 'temporal' frequency.

The best method to obtain temporal characteristics of the disturbances is to utilize data measured by a ground facility, such as an incoherent scatter radar or Doppler

ionospheric sounder, during a pass of the satellite. Then, from the satellite and ground measured data one can determine both spatial and temporal characteristics, check the dispersion relationship and determine the amount of energy and momentum that they transport.

Unfortunately, very few satellite passes over ground facilities have been reported where data are available from both for the same time, suitable for wave analysis. Even when ground stations are operating, they may not be in the proper mode for determining the desired parameters. Prearranged measurements may not be successful too because of a lack of interesting events.

In the absence of such corroborative experiments, one may try to take advantage of the simultaneous measurements of many parameters by AE-C instrumentation to extract the temporal characteristics. This would be possible if the measured phase and amplitude relationships between the responses of individual parameters could be modeled. The simplest models are plane wave models. However, more complex modeling may be necessary; for example, a spherical model incorporating a dipole magnetic field. Here, we have attempted the simplest, just plane wave modeling, and the results are reported.

Satellite data for a full orbit were used. The data are typical of many orbits, and the results of the study are typical of results in analyzing other orbits of AE-C and also AE-E. The particular data set shown here was chosen to exemplify the results. The orbit is 5133 on January 20, 1975. The magnetic field index K_p during the day was no greater than 3+. Since the in situ data were only for one altitude, vertical profiles can only be surmised by using modeling techniques. The data were available as 15 second samples. They come from the so-called AE-C 'Unified Abstract' (UA) files.

The remainder of the body of this paper is as follows. Section 2. describes the data that were analyzed, the satellite orbit and geophysical conditions. Section 3. describes the techniques of data processing that were used to study the data. Section 4. contains results from studies of some statistical properties, such as auto- and cross correlation. Section 5. presents an attempt to model the responses of the geophysical parameters that were measured. Finally, the results of the study are discussed in Section 6.

2. Data Analyzed

Figure 1 is a graph of the densities of atomic oxygen, molecular nitrogen, helium and the electrons vs time in seconds UT for AE-C orbit 5133. The ordinate scale is logarithmic. Density is in particles per cm^3. The highest curve is for oxygen, followed in decreasing density by nitrogen, helium and the electrons. Abscissa scales also include altitude, latitude, longitude, local time, and the magnetic field L shell parameter (McIlwain,1961). The altitude of the orbit is in the range 260 km ± 13 km. 15 second samples are plotted in the figure. They are so close that a continuous line appears in almost all cases; parts of the electron density curve show individual points where changes are large. The nitrogen and helium curves are coded with small crosses, so that they are heavy in appearance. Each curve contains 360 samples. One may note small intervals where there are data drop-outs in the individual curves. These occur simultaneously for the neutral gas densities, since these parameters are measured by the same instrument. Fluctuations are apparent in all these densities, though some of the variations in the electron density are quite large and not necessarily connected with wave phenomena. For example, on close examination one can see the so-called equatorial anomaly (Hanson and Moffett, 1966; Baxter and Kendall,1968), as well as rapid variations in the auroral regions.

Figure 2 is a graph of the electron and ion temperatures for the same period of time as in Figure 1. Altitude, longitude, L shell radius and geomagnetic inclination angle, in addition to time, are shown as abscissa scales. Fluctuations in both temperatures are quite evident, though those of the electron temperature are considerably greater. The electron temperature is more than twice the ion temperature over most of the time span. There is a small interval of time at about 32298.8 seconds UT where the ion temperature appears double valued. A fluctuation between two values is actually occuring here, but the back and forth variation is obliterated by the + symbol used to code the trace. The ion temperature is higher in the southern hemisphere, which is for the interval from 30952.5 seconds UT to 32298.8 seconds UT, than it is in the northern hemisphere for the interval from 28260.0 seconds UT to about 30700.0 seconds UT. The large rise in the electron temperature within the first time interval is associated with the southern auroral zone and appears broader and more intense than for the corresponding parts of the trajectory in the northern hemisphere.

A Mercator plot of the orbit is shown in Figure 3. The times in seconds UT given on the abscissa scale of Figure 1 are shown in the plot at about the position of the satellite in its orbit at these times. The direction of the satellite in its orbit is shown by the arrows. The data starts at

28260.0 seconds UT in the center with the satellite headed north over the eastern coast of the United States on the right side of the map. The orbit crosses over the northern auroral region to Europe and Asia reaching the right edge of the map at 60° east longitude and about 40° north latitude. The trajectory transfers over to the extreme left edge of the map where it is shown heading south. In the southern hemisphere it is over the Indian and Pacific Oceans and passes close to Antartica in the southern auroral zone. The path turns north and the data stream and orbit both end in the center of the map just west of Mexico at 33645 seconds UT.

A polar plot of the orbit in geomagnetic coordinates is shown in Figure 4. The path is shown as a thin line in the northern hemisphere and heavy in the southern hemisphere. The pole is the magnetic pole of the equivalent dipole field. The path shown is what would be observed looking down over this pole if the earth were transparent. The position at selected times in seconds UT in the orbit are shown and may be related to various features evident in Figures 1 and 2. Local times may be obtained from Figure 1.

Magnetic and solar activity at the time were relatively quiet. The 3 hour planetary indices (Akasofu and Chapman, 1972) were a_p=7, k_p=2, and the AE index (Davis and Suguira, 1966) was 114. The solar 10.7 cm flux, $F_{10.7}$ was 77.

3. Data Processing

Only the densities of oxygen, nitrogen, and the electrons and the ion temperature were processed to study their fluctuations, spectra and statistical correlations. This group of geophysical quantities will be referred to in places as the 'parameters'. Much of the data for helium and the electron temperature were considered too noisy for further study; some of these data are useful, but for much smaller time intervals. Though fluctuations of the parameters studied are evident in Figures 1 and 2, any relationship between these fluctuations is not clear. They become clearer, however, on separating the fluctuations from the data. This separation was done by filtering the data, as will be explained below.

Prior to filtering, it was necessary to close up any data gaps; they are barely evident in Figure 1. This was done by fitting with a cubic spline interpolation scheme (Forsythe et al., 1977). Data samples are then available for every interval throughout the entire time record.

3.1 Data Normalization

It was also necessary to normalize all data to be able

to compare different geophysical parameters. This had to be done prior to filtering. Normalizing could be done in two ways. In the first, the data are normalized to the average value of the entire run of data. In the second, the data are normalized to the slowly varying component obtained by passing the data through a suitable lowpass filter. This latter process introduces some contamination at lower frequencies and spreads any spectral feature at higher frequencies. Otherwise, there does not appear to be any difference between the spectra of data when processed in these two ways. The first method of normalizing was chosen to avoid any complications, and is presented here.

Plots of normalized densities of oxygen, nitrogen and electrons and of the normalized ion temperature are shown in Figures 5 through 8, respectively. These are linear plots vs time in seconds UT. The entire group of data for each parameter are shown. Since each instrument was turned on at slightly different times, there are small differences in the initial times in Figures 7 and 8 from those of Figures 5 and 6. All the records shown end at the same time. The fluctuations are far more evident in these figures than in Figures 1 and 2. One can even see some similar features in the curves of oxygen and nitrogen, which become more apparent on superposing their graphs. Similar associations seem unlikely for the graphs of the electron density and ion temperature.

3.2 Filtering

The fluctuations are extracted from the normalized data by passing the latter through a highpass digital filter. The filters employed are based on a design given by Hamming (1977). It is a nonrecursive filter which includes a Lanczos window to reduce ripples and minimize the Gibb's phenomenon. The filter is described by its order and cutoff frequency. Figure 9 is the transfer function of a typical filter. Its order and cutoff frequency are 40 and 0.003 Hz, respectively. The frequency scale in the figure is logarithmic and normalized to the sampling time, 15 seconds, so that 0.003Hz corresponds to 0.045 on that scale. The value of the Nyquist frequency on the same scale is 0.5, the last point on the abscissa axis. The value of the transfer function at the cutoff frequency is 0.5. Since the order is the number of weighted in-sequence samples that are summed to obtain the filter output, this many data are lost at the beginning and end of the record. Therefore, it is desirable to use the lowest order consistent with a reasonable steepness at the cutoff transition. The selection of a filter order is a compromise between the number of data points available at the filter output and the suppression of frequency components in the cutoff region. Thus, an order of 40 was found satisfactory based on trial and error and

judgment of the quality of the power spectra of the output of the filter. All filters referred to, hereafter, are of this order. The original 360 data samples are reduced to 282 samples at the filter output, which is adequate to provide 256 data samples, a power of two, as needed by the Fast Fourier Transform.

The choice of cutoff frequency is based on the emphasis given to the various frequency components in the signal. For too low a cutoff frequency (0.001Hz and less), the transition at cutoff is inadequate to keep out strong low frequency components without significant increases in the order. Furthermore, the filter cutoff must be selected so as to eliminate the fundamental frequency which has a period equal to the entire time interval of the data record, and, for safety, at least those frequencies up to the fifth harmonic of this fundamental. This part of the spectrum contains much power, but is of questionable validity because of the finite size of the data record. If not filtered, it would impair processing of the higher frequencies components of the spectrum. Because all data were found to decrease in almost a power law fashion with frequency, the lowest frequencies in the pass band are emphasized. Several different cutoff frequencies were used to take advantage of this feature, as will be explained.

There was concern that spurious frequencies may be introduced by the Gibb's phenomenon as a result of the filter cutoff. Figure 10 demonstrates that such effects are insignificant. Three curves are shown in the figure plotted against time. The upper curve is the same as the nitrogen density curve in Figure 1. The middle curve is the output of a highpass filter with a cutoff frequency of 0.001Hz. The bottom curve is the same, but for a cutoff frequency of 0.003 Hz. The curves have been lined up so that their abscissas in seconds UT match. Note the very excellent alignment of perturbations in the original data with the fluctuations in the outputs of the two filters. No spurious frequency components are detectable in the outputs of the filters.

3.3 Fluctuations

The fluctuations may be clearly observed at the output of a high pass filter. Figures 11 through 13 are plots of fluctuations vs time for a high pass filter of 0.003 Hz cutoff frequency. 0.003 Hz corresponds to a period of 333.3 seconds, or a horizontal wavelength of 2600 km. The fluctuation data used to plot Figures 11 to 13 are normalized to their maximum values, so they that may be graphed between ordinates of -1.0 to 1.0. Each of the figures contains plots of the fluctuations of two parameters to study their correlation and relative phase. The fluctuation of oxygen, the major constituent, is used as the standard for

comparison in all three figures. Figure 11 compares oxygen and nitrogen density fluctuations. Figure 12 compares oxygen density and ion temperature fluctuations, and Figure 13 those of oxygen and electron densities. In all three figures the fluctuation of oxygen is shown as a solid line, and the other parameter as a dotted line. In Figure 13 the dots are so close in many places as to make the line solid. Nevertheless, the trace can be discerned. Oscillations are quite clear in all three figures. Dominant periods are evident, adding constructively in some places and destructively elsewheres. It is also quite clear in all three figures that there are correlations between the fluctuations. That between nitrogen and oxygen densities is most outstanding. Oxygen density and the ion temperature in Figure 12 appear anticorrelated. The electron density and oxygen fluctuations in Figure 13 are certainly correlated with respect to the time durations of the individual oscillations.

However, the electron density fluctuations are at first close to being in phase with those of oxygen, but from about 30585.0 seconds UT to about 32235.0 seconds UT they are nearly out of phase. The electron density fluctuations appear relatively small in most places in this time interval, when normalized to the scale -1,1. The region of the equatorial anomaly is centered just about 30585.0, so that the satellite is passing from the northern to the southern hemisphere here. It seems that the electron density fluctuations from this filter, 0.003 Hz, do not relate to oxygen in the same way in both hemispheres.

It is clear from the figures that the periods of the oscillations are about the same for all the parameters, even the electron density, and that more than one periodicity may be present. Measuring the spacing between several peaks for all parameters, one finds periods of the order of 140 seconds and 250 seconds, corresponding to about 1090 km and 1950 km, respectively, for a satellite velocity of 7.8 km/sec. The shorter period wave is outstanding at time 29760 seconds UT, whereas the longer period is readily observable in the fluctuations at about 30585 seconds UT and later. One may still observe the shorter period in features throughout.

Maximum and root mean square values of the fluctuations are listed in Table I for oxygen, nitrogen, ion temperature and electron density for the 0.003 Hz filter. The rms fluctuations of nitrogen is about twice that of oxygen, whereas the rms fluctuations of the ion temperature is slightly greater than that of oxygen. The rms and peak fluctuations of the electron density are more than ten times that of oxygen, even though they appear small in Figure 13 due to their being normalized to a scale of -1 to 1. Whereas the rms electron density fluctuations relative to the background density is about 20%, that of the neutral

TABLE I

Peak and Root Mean Square Fluctuations

Filter Order = 40, Filter Cutoff Frequency = 0.003 Hz

Parameter	Peak Value	RMS Value	Ratio Peak/RMS
Oxygen Density	.0525	.0159	3.3
Nitrogen Density	.107	.0338	3.2
Ion Temperature	..0728	.0182	4.0
Electron Density	1.255	.203	6.2

TABLE II

Peak and Root Mean Square Fluctuations

Filter Order = 40, Filter Cutoff Frequency = 0.006 Hz

Parameter	Peak Value	RMS Value	Ratio Peak/RMS
Oxygen Density	.0428	.00926	4.6
Nitrogen Density	.0756	.0194	3.9
Ion Temperature	.0809	.0150	5.4
Electron Density	.468	.0867	5.4

densities and ion temperature are only a few percent at most. Such large relative deviations of the electron density are well known from observations of TID's (Thome, 1968). The ratio of peak to rms values range from 3 to 6 for the four parameters.

The location of the satellite in geomagnetic coordinates is also of interest relative to the graphs of Figures 11 to 13. The key times in the plots are shown in the trajectory in Figure 4. It can be seen that the large oscillations of nitrogen and oxygen in Figure 11 start when the satellite is close to the probable position of the auroral oval and continue to and past the geomagnetic equator at 30585 seconds UT into the southern hemisphere. Oscillations are smaller in the southern mid-latitude zone, but pick up again as the satellite enters the region of the southern auroral zone between 31410 seconds UT and 32235 seconds UT. The ion temperature in Figure 12 behaves about the same way, but appears to have the strongest fluctuations in the auroral zone. The electron density fluctuations in Figure 13 appear fairly uniform starting from 29760 seconds UT across the northern and southern regions. There are some strong peaks on the northern side of the geomagnetic equator, which is associated with the equatorial anomaly that may be clearly seen as the first of the two outstanding peaks near the middle of Figure 7. The southern part of the equatorial anomaly, the second and smaller peak in Figure 7, does not produce as large an excursion in Figure 13. It appears that the oscillations of the fluctuations obtained with the 0.003 Hz filter are associated more with northern hemispheric activity than is the case in the southern hemisphere, except for the hotter southern auroral zone (see Figure 2).

Figures 14 to 16 are the same as Figures 11 to 13, except that the filter cutoff frequency is increased to 0.006 Hz (167 seconds period or 1300 km horizontal wavelength). Correlation in the fluctuations in all three figures is quite apparent. Even the electron density fluctuations in Figure 16 correlate better throughout, in contrast with Figure 13; much more of the record is close to being in phase with the oxygen fluctuations, though phase shifts are a little larger in the equatorial region and the southern hemisphere. Nitrogen and oxygen appear to be in phase in Figure 14, and the ion temperature in Figure 15 is shifted somewhat away from anti-correlation. In all figures there is a dominant fluctuation. In contrast with Figures 11 to 13, the dominant oscillation in Figures 14 to 16 persists more clearly throughout much of the time span and appears to be on the order of the 140 seconds oscillation noted for Figures 11 to 13. This persistence is quite remarkable. Variations in amplitude also appear which imply the presence of waves of other periods, or horizontal wavelengths, that are beating against each other.

Peak and rms values for the fluctuations of Figures 14 to 16 are given in Table II. Note that the values are smaller than those of Table I. The rms values for nitrogen and oxygen are smaller by about the same amount. The ion temperature fluctuations have not changed very much. The rms electron density fluctuations have decreased more than any of the other parameters. These changes result from the nature of the spectra which is found to decrease with wavelength; that is, there is more energy in the longer wavelengths, as will be shown in the next section.

Figure 14 to 16 may also be analyzed with regard to the position of the satellite. Much the same can be stated with respect to nitrogen and oxygen in Figure 14 as was stated for Figure 11. The comments relative to ion temperaature fluctuations in Figure 12 still pertain with regard to Figure 15, and the same is true for the electron density fluctuations in Figures 13 and 16. Activity in the two hemispheres for scale sizes as indicated in Figures 14 to 16 appear to be the same as for the larger scale sizes of Figures 11 to 13.

3.4 Spectral Analysis

Power spectra of the fluctuations are estimated using the Maximum Entropy Method (MEM) (Ulryck and Bishop, 1975) because of the finite size of the data sample and because of the lack of knowledge of data outside the time interval. The Fast Fourier Transform (fft) is also employed to help in selecting the order of the MEM and to judge its spectrum. Comparison with the periods of the fluctuations is necessary, as well, to insure that the MEM order and spectrum are consistent.

Attempts were made to use the Akaike, or final prediction error (fpe), criterion to select the MEM order (Ulryck and Bishop, 1975). Figure 17 is a plot of the fpe vs. the MEM order for nitrogen fluctuations for a 0.0015 Hz filter. One chooses as the order the value that minimizes the fpe. Unfortunately, the minimum is too broad and shallow to be useful for this purpose. The fpe is found to be similar for all other cases, so that the selection of MEM order is based on comparison with the periods of the fluctuations and with fft spectra.

All spectra and fluctuations shown in this section are for nitrogen, and they are obtained with various filters. The spectra for oxygen density, ion temperature and electron density fluctuations are similar and need not be shown. In all cases a set of 256 fluctuation data are processed, all for the same time interval.

An example of fluctuations is shown in Figure 18 which

is for a high pass filter with a cutoff of 0.0015 Hz. The ordinate is scaled for the actual magnitude of the fluctuations in contrast with the plots of Figure 11 through 16. The periods, though not exactly constant, are quite evident and are found to be about 500 seconds for one set of fluctuations and 250 seconds for another. These times correspond to horizontal wavelengths of about 3900 km and 1950 km, respectively. Figure 19 is a plot of the fft spectrum of the fluctuations in Figure 18. The abscissa scales are the frequency in millihertz (mHz) and the wavelength in km. The frequency scale extends from 0 to the Nyquist frequency for 15 seconds data samples, 0.0333 Hz. Spectral peaks are labeled by numbers that represent harmonics of the fundamental frequency which has a period equal to the total time span of the 256 samples in Figure 18, namely, 3825 seconds. These peaks are at harmonic numbers 4, 8, 10 and 16. The peak at harmonic number 4 is ignored as too low, since it may be affected by the finite data sample. The peaks at harmonics 8 and 16 correspond to periods of 478 and 239 seconds, or wavelengths of 3729 and 1865 km, respectively. These waves confirm the periods evident in Figure 18. The peak at harmonic 10 may be real, or it may be the result of the variations in the 500 second period in Figure 18. Since the computed spectrum is at discrete frequencies, the broadening associated with this variation may appear as a nearby additional, but false peak.

One must select an order for the MEM. If too low, significant spectral features may be submerged. If too great, spurious features may arise. It is difficult to judge what order to use. The fpe in Figure 17 is not very helpful. A value anywhere from 4 to 16 appears to produce a shallow fpe minimum. For an order of 15 (not shown here) the MEM spectrum misses the waves of harmonic number 8 and 16 entirely. Only one peak arises at harmonic 11. Increasing the order to 20 results in a spectrum with the desired peaks. This spectrum is shown in Figure 20. The two largest are for harmonics 8 and 16. Another much smaller peak appears at harmonic numbers 30, and still smaller peaks are suggested at harmonic numbers 42 and 60. A logarithmic plot of the spectrum is shown in Figure 21 which is for frequencies from the 8th harmonic to the Nyquist frequency. The third abscissa scale in the figure gives the harmonic numbers. The peaks at the higher frequencies, or shorter wavelengths, can be seen in this plot. Note the power law fall off with frequency. The straight line is a least square fit to the spectrum. The slope of the line on a log-log plot is -3.1, which means a power law with frequency varying as $f^{-3.1}$ over at least a 16,5 :1 frequency range.

By passing the normalized data through high pass filters of higher cutoff frequencies which filter out the lower, more powerful parts of the spectrum, one can get a better sense of the higher frequencies or shorter wavelength

components in the data. Figure 22 is a plot of the MEM spectrum of order equal to 20 for nitrogen using a filter with a cutoff of 0.003 Hz. There is one dominant peak at about harmonics 15 to 16. The cutoff is sufficient to eliminate the peak at harmonic 8 observed in Figure 20, since 0.003 Hz corresponds to a non-integral harmonic of 11.5. This cutoff is too low to highlight waves of wavelength shorter than that of harmonic 16. A filter with a cutoff of 0.006 Hz will do this by eliminating the peak at harmonic 16. Figure 23 is a plot of the fluctuations at the output of this filter. Careful measurements of the periods between peaks there give periods of about 170 seconds, 127 seconds and 106 seconds with about a ± 5% error. These correspond to harmonic numbers 23, 30, and 36 with harmonic number errors of ±1 at 23 to ±2 at 36. Only one of these components are evident in Figure 21, that for harmonic 30. This component is the more persistent periodicity in Figure 23. The corresponding MEM spectrum of order 20 of the fluctuations in Figure 23 is shown in Figure 24, where we observe a strong peak at harmonic 31 and a weaker peak at harmonic 25. The latter confirms the longer period in Figure 23. The period for harmonic number 36 is not seen in this spectrum. On increasing the order of the MEM to 35 with a filter cutoff of 0.0015, one obtains the logarithmic spectrum shown in Figure 25. Here we find peaks close to all expected periods based on analysis of Figures 18 and 23. The corresponding fft spectrum (not shown here) has peaks at the desired values as well.

On increasing the cutoff frequency further, we obtain fluctuations for nitrogen shown in Figure 26 which is for a filter cutoff of 0.0095 Hz. Careful scaling, with account taken of measurement accuracy, suggests periods for harmonic numbers 34 to 38, 39 to 43, and 57 to 63. Peaks at, within, or close to these values are exhibited in the spectrum of Figure 25. The fft spectrum (not shown here) has many more peaks for this case, some of which may be extraneous. Fluctuations for a filter with a cutoff of 0.013 is shown in Figure 27. The periodic wave there, with error accounted for, is in the harmonic range 60 to 66. This wave may account for the peak at harmonic number 63 in Figure 25. The fft spectrum for this case, not shown here, exhibits many peaks that must be extraneous.

Since most of the waves suggested by the nitrogen density fluctuations appear to be exhibited in the MEM spectrum for the order 35, this order and spectrum are taken as adequate for the purpose here. Similar tests with different filters, as used with nitrogen density data, were employed with the other parameters. These tests confirmed the use of an MEM order of 35 for these parameters. Thus, this order is used to obtain the MEM power spectra for the fluctuations of all of the parameters after passing their data through a high pass filter with a cutoff frequency of 0.0015 Hz. A

comparison against harmonic numbers of peak frequencies for these parameters is given in Table IIIa. The horizontal wavelengths corresponding to the oxygen spectral peaks are also given in the table. The power law exponents for the least square straight line fits to the logarithmic spectra are given in Table IIIb.

The MEM tends to broaden spectral peaks. Nevertheless, Table IIIa indicates spectral agreement for as many as three or four parameters for a number of wavelengths, 1865 km, 1193 km, 962 km, 523-533 km and 466 km. In addition, oxygen and nitrogen spectra correspond for 3729 km. The ion temperature may also have the same feature at this wavelength, though its value is somewhat off. The ion temperature and oxygen have features at 728 km, but nitrogen and the electron density spectra both peak at a smaller wavelength in the range 678-693 km. Similar features also appear possible for shorter wavelengths at 409 km and less. Still shorter wavelength spectra may be limited by noise.

From the numbers in Table IIIa, it appears that the spectra of neutral densities correspond for many wavelengths from the order of 4000 km to hundreds of kilometers. Correspondence of ionization with neutral spectral features over many thousands of kilometers may not really occur, since plasma is subject to many other physical processes, particular those involving electric fields that do not affect neutrals. Nevertheless, the spectral feature at 1865 km is present in the electron density spectrum as well as those of the neutral densities and the ion temperature. Since the ion temperature is coupled to the neutral temperature at an altitude of 260 km, it would not be surprising to find that the ion temperature spectrum has features at very long wavelengths like those of the neutral gases.

The power law type of decrease with spatial frequency, or with decreasing wavelength, is present in all parameters. The exponents are different, as shown in Table IIIb, though those of oxygen and nitrogen are close in value. The ion temperature spectral decay rate is smallest, whereas that for the electron density is faster than oxygen and nitrogen. Such power law decreases may arise from the sources as well as the medium, but may also be related to turbulence generating processes. The reason for the different exponents is far from clear and requires further study. These characteristics are in agreement with ideas of Van Zandt (1982).

4. Statistical Aspects

Statistical investigations here include only computation of autocorrelation and cross correlation functions and an autoregressive (AR) analysis (Jenkins and Watts, 1968). These quantities and functions require stationary statistics. Furthermore, the MEM technique requires at least

TABLE III

Possible Spectral Harmonics for 256 Data Samples

Oxygen Density	Nitrogen Density	Ion Temperature	Electron - Density	Horizontal Wavelength (km)
			6	
8	8	7		3729
16	16	16	16	1865
25	24-25	26-27	24	1193
31	31	31	32-33	962
-	37	-	-	-
41	43-44	41	43-44	728
56-57	56	56	55	523-533
64	63	64	63-64	466
73	73	71	71	409
82	83	81		364
90	90	92	88	332
		Power Law Exponents		
-339	-3.09	-2.15	-3.85	

quasi-stationarity to be meaningful.

Since the number of data samples are limited, tests for stationarity were not attempted. A qualitative evaluation was used instead. For one, fluctuation signals, as in Figure 11, were visually examined to determine whether the nature of the signal was maintained throughout the record. The persistent character of the records in Figures 11 to 16 suggest some degree of stationarity.

Typical ensemble samples were computed using an autoregressive analysis to check further for stationarity. If a sample has characteristics similar to those of the actual fluctuation signal, the autoregressive process was judged to be satisfactory and an indication of stationarity. This indeed was found to be the case for the four parameters that were studied. Other data not shown here for helium, a parameter that was not analyzed, were deemed quite noisy and poor for analysis. AR models for these data were vastly different from the actual fluctuations, so that the helium data were judged unsuitable for a stationary process.

Figure 11 exhibits both the nitrogen and oxygen fluctation signals. Figures 28 and 29 are AR models of order 20 for oxygen and nitrogen, respectively. Autocorrelation coefficients needed to compute the model are based on data passed through a 0.003 Hz filter. Note the similarity in the oscillatory character of the models to the actual fluctuations in Figure 11. The spacing between peaks in tnat figure appear narrower than those of Figures 28 and 29, but this is due to the smaller time interval in the abscissa scale in those figures. Figure 11 is 300 seconds longer in time than Figures 28 and 29. The AR model for each neutral gas is but one ensemble sample. Since the process is controlled by a noise source, a whole ensemble class may be generated. It is found that the characteristics persist, from which we conclude that the data are at least quasi-stationary. The same is found for the ion temperature and the electron density.

Figures 30 and 31 are the autocorrelation functions of the oxygen and nitrogen fluctuations shown in Figure 11, respectively. The oscillatory nature of these graphs are quite evident. The plots are against time lag intervals, where one lag represents 15 seconds. The oscillations persist out to at least 80 lags in both cases. Further, the oscillations in these two graphs are quite similar. The periodicity is almost the same. Also, other frequencies must be present to account for the nature of the variation with the time lag. The separation between the peak at zero lag and the next peak is scaled to be 267 seconds and 247 seconds for oxygen and nitrogen, respectively. These times agree with the periods in Figure 11 and the spectral peak in Figure 22. Small differences may arise from beats due to

other wave components.

The cross correlation function (CCF) between the fluctuations of two parameters is useful to obtain a sense of the degree of correlation and the phase shift between the parameters; that is, the phase angle of the transfer function between the responses for the latter. Oxygen density fluctuations are used for this purpose to compare with the fluctuations of the other three parameters obtained using the same filter. Oxygen is chosen for comparison, since it is the main neutral constituent. Figures 32 and 33 are cross correlation functions plotted vs. 15 second lags for oxygen and nitrogen density fluctuations obtained with filters of cutoff frequencies of 0.003 Hz and 0.006 Hz, respectively. Note the oscillatory behavior in both figures. Note too that the peak values of the CCF is quite adequate for correlation in both cases, being just more than 0.7 for the 0.003Hz filter and about 0.69 for the 0.006 Hz filter. The phase shift is nearly zero; there appears to be a slight phase angle with nitrogen leading (to the left of zero lag) for both filters. The best that can be determined is that the lead is about 1/2 a lag interval, about 7.5 seconds. The oscillatory behavior persists on both sides of zero to longer lags than shown. The spacing between peaks in Figure 32 on either side of the large peak near zero lag is 16 1/2 lags. Thus, the dominant period is 247.5 seconds which corresponds to an on-track horizontal wavelength of 1931 km for the fluctuations from the 0.003 Hz filter. This period agrees with the corresponding values from the autocorrelation functions in Figures 30 and 31, the spectrum in Figure 22 and the estimated period in Figure 11. The dominant period for the 0.006 Hz filter in Figure 33 is 8 1/2 lags, or 127.5 seconds, which corresponds to a horizontal wavelength of 995 km. This period and wavelength are roughly in accord with the spectrum in Figure 24 for nitrogen, the harmonic 31 listed in Table IIIa and the periods of the fluctuations in Figure 14. The 1/2 lag interval phase lead corresponds to a leading phase angle of 11^{o} for the 0.003 Hz filter and 21^{o} for the 0.006 HZ filter. The peak CCF becomes even larger for fluctuations of nitrogen and oxygen from filters of cutoff frequencies as high as 0.013 Hz. Oscillatory behavior of the CCF persists with periods that are shorter than for filters of lower cutoff frequencies.

The CCF for oxygen density and ion temperature fluctuations show some correlation but not as strong as that between nitrogen and oxygen. That for a 0.003 Hz filter is shown in Figure 34. This CCF is quite irregular in contrast with that for Figures 32 and 33. Note that the peak is negative with a value of -0.38, implying anti-correlation. The period cannot be determined from Figure 34. Figure 35 is a plot of the CCF for oxygen and ion temperature fluctuations from a 0.006 Hz filter. There are more oscillations than in

Figure 34; particularly on the leading side, and the peak is nearly anti-correlated with a value of -0.41. The negative peak leads by somewhat less than 1 lag interval. The plot suggests the presence of more than one wave with resultant interference. Such interference would produce an error in scaling the dominant period, as well as the phase shift. The spacing of peaks on the lead side is 10 lag intervals, whereas that on the other side is 7 lag intervals. The mean of 8 1/2, if meaningful, agrees with that for oxygen and nitrogen in Figure 33. The maximum negative peak at -1 lag on the leading side in Figure 35 corresponds to a lagging phase angle of -138^{o} for a period of 8 1/2 lags, whereas the phase angle would be -159^{o} for a maximum negative peak at a -1/2 lag interval. Thus, the phase shift appears to lie between the two values, -138^{o} and -159^{o}. The CCF peak reaches -0.49 for a filter cutoff of 0.008 Hz (not shown here), where anti-correlation persists. The cutoff for this last filter corresponds to what would be a non-integral harmonic value of 30.6, or a horizontal wavelength of 975 km. Thereafter, at still higher filter cutoffs the CCF between oxygen and ion tempe ature becomes smaller, but the correlation to nitrogen remains stronger, reaching -0.46 at a filter cutoff of 0.010 Hz. This suggests the possibioity that, for the shorter wavelengths, the ion temperature is coupled to the nitrogen density more than the oxygen density.

Though the degree of cross correlation of ion temperature and oxygen is not large, anti-correlation stands out, and for wavelengths of 1000 km and less a periodicity is evident in the cross correlation function. This periodicity relates to that between nitrogen and oxygen and suggests that the cross correlation of the ion temperature is significant though the peak values are less than 0.5.

Figure 36 is a plot of the CCF of oxygen and electron density fluctuations for a 0.003 Hz filter. Though the peaks are not large, an oscillatory variation is quite evident. In addition, there appears to be interference which may be from another wave that makes it difficult to determine the true peak near zero lag. The lag seperation between peaks for negative lag intervals is about 17 which is close to the 16 1/2 found for nitrogen and oxygen for the same filter. The separation between the other peaks is much smaller. The changes in the phase shift of the fluctuations, as described in Section 3.3 relative to Figure 13, may be the reason for these difficulties and the poor magnitude of the peak CCF.

Figure 37 is the CCF of the electron density and oxygen for a filter with a cutoff of 0.006 Hz. Much more oscillatory behavior is evident. The largest peak is well to the right of the peak near zero lag. This suggests interference between wave components. The peak at zero lag is 0.39, whereas the peak to its right is 0.45. The interval between

the peaks about zero lag is 9 1/2 lags which is one lag larger than that found in Figure 33 for nitrogen and oxygen. The discrepancy may arise from interference.. Nevertheless, the cyclic variation suggests better cross correlation than indicated by the magnitudes of the peaks.

Since neither the ion temperature nor the electron density CCF has peak magnitudes of 0.5 or more, they would not be expected to correlate well with each other, as their own CCF does indicate, though not shown here.

There is a small phase lead for the CCF of Figure 37 of about 1/2 lag. This would correspond to a phase lead of the electron density fluctuations relative to the oxygen fluctuations of 21°. No reliable phase shift may be obtained from Figure 36 for the 0.003 Hz filter. As the filter frequency becomes larger, the cross correlation of electron density and oxygen density is found to become poorer, undoubtedly because of greater noise at the higher frequencies. Figure 37 suggests correlation between electron density and oxygen for waves of the order of 1000 km. Correlation at still smaller wavelengths may be obscured by noise, though indicated in Table IIIa.

One may use the crude phase shifts from the CCF calculations and the mean square fluctuations of the parameters to describe transfer functions between the responses of the parameters for further use in modeling. This is described next.

5. Theoretical Modeling

The presence of waves is clearly shown in Figures 11 to 16. More than one wave is present as shown by the spectra of Figures 20,21,22,24 and 26. The waves that dominate depend on the filter, since the spectrum decreases with decreasing wavelength as shown in Figures 21 and 25 and as required by the various spectral exponents listed in Table IIIb. The lowest frequency components passed by the filter dominate. Two dominant peaks may be observed in Figure 24 for the 0.006 Hz cutoff filter. The first peak is at a wavelength of 1193 km, whereas the second is at 962 km. These two peaks would beat against each other to produce a beat pattern. One may interpret the envelope variation in Figure 23 as arising from such a beat pattern. Of course, we must be careful in interpreting these fluctuations and spectra, since we are dealing with a finite data sample that is just a snapshot of the nitrogen distribution at one altitude in this case. This distribution is the result of stochastic sources and a number of geophysical processes that are at work and may not actually result from the beating of two waves.

It is important to know whether the waves are traveling or stationary, or both. If traveling, they are transporting energy and momentum from their sources. If standing waves, they may be stationary spherical modes due to one source (Mayr et al, 1982), or they may originate from interference of waves from near duplicate stochastic sources in both auroral zones, such as could arise from diffuse aurora. This type of auroral activity may produce the same effects in both hemispheres (Lui et al, 1982; Akasofu, 1974). Standing waves would die out by dissipation simultaneously over a large region, much like plucking a violin string. It has been noted in Section 3.3, for example, that there is more activity in the level of the fluctuations in the entire northern hemisphere portion of the trajectory than the southern hemisphere, with the exception of the southern auroral zone. It may be that these waves are primarily due to one source and both stationary and traveling waves are present. Analysis of simultaneous ground measurements of ionization and satellite measurements of in situ neutral and ionization data may aid in understanding better these wave systems.

In the absence of such ground measurements, and with the limitations of in situ measurements, we can only test for traveling waves. To determine whether the waves are pure traveling waves we assume a plane parallel model and a plane wave of some horizontal wavelength and temporal frequency. The assumption of a plane parallel model is a crude approximation for propagation over a sphere. It still may be useful, since, as shown by Francis (1972), the waves tend to follow the curvature due to rotation of the direction of

gravitational acceleration as the wave propagates. One seeks the values of wave parameters that provide the closest duplication of the ratios of the responses of nitrogen density, electron density and ion temperature fluctuations to that of oxygen; that is, the transfer functions between these various geophysical parameters. In this way we can obtain the wave properties not directly observable from the spatial distribution, such as the temporal frequency and direction of propagation. The experimental transfer functions are given by a magnitude and phase angle. The magnitude is obtained from the ratio of the root mean square fluctuations of the geophysical parameters (Figures 11 through 16), and the phase angle is estimated from the cross correlation function (Figures 32 through 37). Such transfer functions are determined for each filter. We give here two examples, that for 0.003 Hz filter and for the 0.006 Hz filter, to be consistent with the previous material. Table IV lists these transfer functions.

TABLE IV

TRANSFER FUNCTIONS		RELATIVE TO OXYGEN					
FILTER CUTOFF FREQ Hz	DOMINANT WAVELNTH Km	NITROGEN AMPL	NITROGEN PHASE	ION TEMP AMPL	ION TEMP PHASE	DENSITY FLUCTUATIONS ELEC DENS AMPL	DENSITY FLUCTUATIONS ELEC DENS PHASE
0.003	1930+	2.13	11°*	1.14	-169°	12.8	?
0.006	995	2.10	21°	1.62	-138° to -159°	9.4	21°

* positive angles represent leading phase angles, whereas negative angles are lagging phase angles.
+ based on periodicity in cross correlation function in Figures 32 and 33.

There is, of course, a question of the meaning of these transfer functions, since the amplitudes of the fluctuations vary over the time span of the data. One can see in Figures 11 through 16 that, although the amplitude of the fluctuations vary and there are differences in their variation, the fluctuations of all the parameters behave somewhat in the same way. Therefore, the ratio of the rms fluctuations may be useful within some limits for the purpose here. Similarly, the cross correlation function may be an acceptable indicator of the phase shift, since there is some confirmation with phase relationships observable in Figures 11 to 16, though perhaps only partly so for the electron density.

In any event, adoption of these magnitudes and phase shifts may be the best one can do with the data.

The model employed assumes two species, one major in density, the other minor. Then all minor species do not seriously affect the major species, and one may have any number of minor species. Each is treated in turn as the second species together with the major constituent. It is assumed that a gravity wave is moving through the main atmosphere and drags each of the minor species by collisions. This is a reasonable model for ionization and oxygen. The nitrogen density is smaller than the oxygen density (Figure 1) throughout the entire data span. Though nitrogen is not necessarily truly minor throughout, the approximation is still useful considering the coarseness of the transfer functions in Table IV.

The model must also incorporate the earth's magnetic field to determine the response of the ionization. It is assumed that charged particles are constrained to move only along the magnetic field. Figure 4 shows the plot of the orbit in geomagnetic coordinates. The times along the abscissas in Figures 11 to 16, 18,23,26 and 27 are shown there. A major portion of the orbit for the times in the above figures (not the full time span shown in Figure 4) is at geomagnetic latitudes of magnitude greater than 30^{o}, so that the magnitude of the dip angle exceeds 49^{o} for most of the orbit. The average of the magnitude of the dip angle is 60^{o} over the entire time span. Since the model employs a plane stratified geometry, it is not possibl to vary the dip angle very readily as could be done ith a spherical model. Therefore, constant dip angles are used. The transfer functions for a value of 60^{o} were compared with those for smaller dip angles. Since it was found that variations due to the dip angle over a range of values were mostly secondary, the choice of a single angle for a given set of calculations is useful. However, it makes a difference whether propagation is towards the equator or away from the equator. The calculations for zero dip angle yields results that are like propagation away from the equator with non-zero dip angles. The closest approximation to the values in Table IV were found for propagation towards the equator. Results for electron density are presented for dip angles of 20^{o} and 60^{o}.

Since collisions between species is of importance, one must have adequate esti ates of the collision frequencies. The value of the collision frequency between nitrogen and oxygen, 0.372 sec^{-1}, had been obtained from the hard sphere model (Chapman and Cowling, 19) for a mean temperature of $830^{o}K$ (as determined from the ion temperature), a total density of 10^{9} particles/cm^{3}, and collision diameters of 0.18 nm and 0.19 nm for oxygen and nitrogen, respectively. Then, computations were made with this collision frequency and

values differing by factors of two above and below to compensate for differences in temperature and inadequacies of the hard sphere model. Ion-neutral collision frequencies are based on an expression given by Stubbe (1968) for O^+, the principal ion, and atomic oxygen. The average ion temperature, 830°K, and a neutral density of 10^9 particles per cm^3 were employed and gave a nominal value of $1.75 sec^{-1}$. Again values differing by factors of two were employed to compensate for inexact temperatures and inadequacies in the collision frequency estimates.

5.1 Formulation

The theory of coupling of species in the atmosphere to gravity waves moving through the entire atmosphere has been developed for two species (Gross and Eun, 1976 and 1978; Del Genio et al, 1978 and 1979), though Mayr et al (1978) has modeled the problem for a number of constituents on the computer. In Gross and Eun, the second species is taken as minor relative to the first, with the advantages as explained above for multiple minor species. The theory of Del Genio et al is more general; it is also for two constituents, but they may be of equal importance. The formulation for nitrogen and oxygen densities used here are based on the theory of Gross and Eun. Neither of the above references treat ionization in an oxygen dominated atmosphere. There have been treatments of ionization density based on the continuity and momentum equations (Hooke, 1968), but none incorporate the ion and electron temperatures as fluctuating parameters. A formulation for ionization driven by a gravity wave in the neutral medium, with a superposed magnetic field and incorporating the ion and electron temperature fluctuations, has been developed and used here. The details will not be given here for brevity. Only the expression for the transfer function will be given. Though the theory is not restricted to isothermal conditions, this assumption was made for simplicity. The vertical temperature gradient is not known, and probably not important here. It would represent a refinement in the calculations. The formulation also neglects viscosity, but this may be important. It also ignores possible reflections from below (Francis, 1974).

The ratio, T_N, of the nitrogen density response to that of the oxygen density, for a plane wave $\exp(-i\omega t+ik_x x+ik_z z)$, may be shown to be given by equation (1):

$$T_N=1+\frac{(M-1)\gamma}{\gamma-w^2-i\gamma K_z}\left[1-w\frac{wK_z^2+iK_z(M-\frac{w_{an}}{w_{an}-iw})+K_x^2+K_zM(w_{an}-iw)}{K_z^2+iK_z(M-\frac{w_{an}}{w_{an}-iw})+K_x^2-iw\frac{\gamma-1}{\gamma}M(w_{an}-iw)}\right] \quad (1)$$

Here, M=ratio of the particle masses of nitrogen to oxygen (=28/16); w is the temporal frequency, ω, relative to the buoyancy frequency N, that is, $w=\omega/N$; K_x and K_z are the wave numbers k_x and k_z in the horizontal and vertical directions, respectively, normalized to the scale height of the main neutral constituent, H_o, so that $K_x=k_xH_o$ and $K_z=k_zH_o$; γ is the ratio of specific heats of atomic oxygen (=5/3); w_{an} is the colision frequency between oxygen and nitrogen, ν_n, relative to the buoyancy frequency. The model assumes an isothermal atmosphere, so that the buoyancy frequency is given by

$$N=\sqrt{\gamma-1}\,g/a_n \qquad (2)$$

where g is the acceleration of gravity (9.05m/sec at 260 km altitude) and a_n is the velocity of sound. If ω and K_x, or w and K_x, are real, k_z, or K_z, will be complex in general. K_z is related to w and K_x by the dispersion relationship for an isothermal atmosphere:

$$K_z=\pm 1/w\left[\frac{\gamma-1}{\gamma^2}w^4-(K_x^2+1/4)w^2+K_x^2\right]^{1/2}-i/2 \qquad (3)$$

The plus sign is for upward phase propagation and the minus sign for downward propagation for time harmonic variation $\exp(-i\omega t)$. It is assumed in these calculations that the source is below the observation point, so that phase propagates downwards, or energy propagates upwards.

The ratio of the electron density fluctuations, R_i, and the ion temperature fluctuations, τ_i, to that of oxygen is given by solving the matrix equation (4):

$$\begin{bmatrix} a_{11} & a_{12} & 0 \\ a_{21} & a_{22} & a_{23} \\ 0 & a_{32} & a_{33} \end{bmatrix} \begin{bmatrix} R_i \\ V_i \\ \tau_i \end{bmatrix} = \begin{bmatrix} 0 \\ S_2 \\ S_3 \end{bmatrix} \qquad (4)$$

where

$$a_{11}=i\sqrt{\gamma-1}w/\gamma,$$

$$a_{12}=(iK_z+1/H_i)S_b-iK_xC_b,$$

$$a_{21}=i(1+\alpha)K_xC_b+[1-(1+\alpha)(iK_z+1/H_i)]S_b,$$

$$a_{22}=\sqrt{\gamma-1}w_{in},$$

$$a_{23}=(1+\alpha)[iK_xC_b-(iK_z+1/H_i)S_b],$$

$$a_{32}=iK_xC_b-iK_zS_b,$$

$$a_{33}=3/2\frac{\sqrt{\gamma-1}}{\gamma}w_{in},$$

and

$$S_2=\frac{\gamma w_{in}}{\gamma-w^2-i\gamma K_z}[K_x/w\ (1-w^2)C_b-iw(iK_z-\frac{\gamma-1}{\gamma})S_b], \qquad (5)$$

$$S_3=3/2\frac{\sqrt{\gamma-1}}{\gamma}w_{in}\frac{-w^2(\gamma-1)+i\gamma K_z}{\gamma-w^2-i\gamma K_z}. \qquad (6)$$

In (4) V_i is the ratio of ion velocity along the field line to the acoustic velocity of the principal neutral constituent; w, K_x, K_z and γ have been defined; C_b and S_b are short hand for $\cos\theta_b$ and $\sin\theta_b$, where θ_b is the dip angle, positive in the northern hemisphere and negative in the southern hemisphere; w_{in} is the ion-neutral collision frequency, ν_{in}, relative to the buoyancy frequency, N. The ratio of electron to ion temperatures is α. It is assumed that the relative electron and ion temperature fluctuations are also in the same ratio. Electron temperature enters effectively only through the electron pressure, since collisions between electrons and ions are neglible at 260 km altitude. Since coupling of neutrals to the electrons is primarily by means of the ions at this altitude, the assumption appears reasonable. The value of α that was chosen is based on the mean electron and ion temperatures (Figures 2). A value of 2 was adopted based on their averages. The quantity H_i in equation (4) is the ratio of the ion density scale height to the scale height of oxygen. Assuming a beta Chapman layer at 260 km altitude, one can show that $H_i=4/3$. (In this regard it should be noted that the satellite was in sunshine for over 70% of the data.) Other values of H_i are also possible, though it not expected that significantly different results would be obtained.

The coordinate system assumes that x is positive northward, so that K_x is positive for northward propagation and negative for southward propagation.

5.2 Results of Model Calculations

The ratio of the response of nitrogen to that for oxygen using equation (1), and the ratios of the response of the electron density R_i and ion temperature τ_i to that of oxygen, on inverting the matrix equation (4), were calculated as a function of frequency for a given temperature T_o, nitrogen-oxygen collision frequency ν_n, ion-neutral collision frequency ν_{in}, dip angle θ_b and horizontal wavelength λ_x. These ratios will be referred to as transfer functions. The purpose of the calculations was to find those parameters which come closest to matching the values in Table IV. The normalized vertical wavenumber for each value of frequency is obtained from (3). Several values of both nitrogen-oxygen and ion-neutral collision frequencies were used. Values for the nitrogen-oxygen collision frequency were $0.093sec^{-1}$, $0.186sec^{-1}$, $0.372sec^{-1}$ and $0.75sec^{-1}$. Values for the ion-neutral collision frequency were $0.44sec^{-1}$, $0.87sec^{-1}$, $1.75sec^{-1}$ and $3.5sec^{-1}$. Dip angles from 0^o to $\pm 80^o$ were employed.

It was quickly found that waves traveling towards the poles did not provide suitable phase shifts or amplitudes as given in Table IV. Waves traveling towards the equator, however, did provide the phase shifts over certain ranges of the parameters. Emphasis in the calculations was therefore placed on waves of this type, particularly for a dip angle of 60^o, the mean magnitude. Temperatures other than 830^oK were also used; namely, 600^oK and 1200^oK.

An example of the calculated nitrogen to oxygen transfer function amplitude and phase shift, as given by equation (1), is shown in Figure 38 for a horizontal wavelength of 2000 km, collision frequency $\nu_n = .75sec^{-1}$ and $T_o = 830^oK$. This plot is against the actual temporal frequency in mHz. The left scale is the phase shift as given by the dotted curve. The right scale is for the amplitude as given by the solid line. The points of the phase curve matching the phase shifts of the fourth column of Table IV are indicated by the 3's for the 0.003 Hz filter ($11^o \pm 1^o$) and by the 6's for the 0.006 Hz filter ($21^o \pm 1^o$). The amplitudes for this case exceed somewhat the values given in the third column of Table IV. Similar examples for the electron density and ion temperature transfer functions are shown in Figures 39 and 40 for a horizontal wavelength of 1000 km, ion-neutral collision frequency $\nu_{in} = .87sec^{-1}$ and dip angle $\theta_b = 60^o$. The 3's and 6's shown there are at the points of the spectra where the phase angles in columns 6 and 8 of Table IV are obtained. Since the phase shift for the electron density fluctuations after passing through the 0.003 Hz

filter is uncertain, no 3's are shown in Figure 39. A small phase shift is expected which would be smaller than the value indicated by the 6's in the figure, so that the frequency would be some value less than the frequency at the 6's. The amplitudes of the ion temperature transfer function in Figure 40 are nearly unity in all cases, different from the values in column 5 of Table IV. The magnitudes of the electron density transfer function significantly exceeds unity. That shown in Figure 39 near the 6's is about 17, a value greater than the values in column 7 of table IV.

The resonance like peak in the electron density transfer function is due to a complex pole in the transfer function arising from coupling between gravity waves and a sort of ion diffusion wave. This type of resonance was described by Gross and Eun (1978) for helium.

Figures 41 and 42 contain summaries of the calculations for a temperature of 830°K. These are typical of results for the other temperatures used in the calculations. Frequency in millihertz is plotted vs horizontal wavelength in each figure. The horizontal wavelength here is assumed to be the true wavelength, so that it takes values less than or equal to the maximum on-track wavelength in Table IV, where we have rounded off the 1930 km and 995 km there to 2000 km and 1000 km, respectively. If the true wavelength is less than these values, the satellite track must be at an angle to the wave normal. The ratio of the true to the observed wavelength is then the cosine of the angle between the track and the wave normal. Horizontal wavelengths from 500 to 2000 km were considered adequate for the purposes, and the plot only extends over this range.

Figures 41 and 42 contain contours of frequency vs horizontal wavelength for the phase angles in Table IV. Thus, Figure 41 shows four contours with different nitrogen-oxygen collision frequencies ν_n, as indicated, to obtain a nitrogen to oxygen transfer function phase shift of 11° as required in Table IV for fluctuations from the 0.003 Hz filter. Figure 42 shows a similar set of contours for a nitrogen to oxygen transfer function phase shift of 21°, as required in Table IV for the 0.006 Hz filter. The dashed line in Figure 41 is for the ion temperature transfer function phase angle of -169° given in Table IV for the 0.003 Hz filter. The frequency for this parameter is almost independent of dip angle and ion-neutral collision frequency. It is labelled 'all T_i' for this reason. If the dominant wave system in the output of the 0.003 Hz filter were a plane traveling wave driven by the neutrals, in which the observed on-track wavelength were about 2000 km, as required by the 0.003 fluctuations, spectra and correlation functions, the ion temperature contour would intersect the nitrogen-oxygen contours at some point. Since there is no intersection, it would appear from the figure that a simple plane wave cannot

explain the data. An intersection would require more than a tenfold increase in ν_n, which is unreasonable. Further decrease of wavelength would not help as well. Reasonable tolerances for the phase shift values of Table IV do not help either.

Figure 42 also contains an ion temperature contour as in Figure 41. It also contains some electron density contours for ion-neutral collision frequencies of 0.44sec^{-1}, 0.87sec^{-1} and 1.75sec^{-1} for dip angles of 20° and 60°. The electron density response contains a complication not evident in the ion temperature response. As horizontal wavelength is increased a root of the denominator of the transfer function may pass close to a complex pole of the determinant of the system. Depending on which side of the pole is passed, one may obtain a leading or lagging transfer function phase shift. Lower wavelengths are found to yield leading phase shifts. Since the desired phase shift for the 0.006 Hz filter is 21° leading, one finds that the 0.87sec^{-1} collision frequency and 60° dip angle contour must end between 1500 and 2000 km, since the phase angles are lagging for $\lambda_x =$ 2000 km. The contour for $\theta_b=60^{\circ}$ and $\nu_{in}=0.44\text{sec}^{-1}$ is lagging for wavelengths somewhat greater than 500 km, and is not shown for that reason. All contours for $\theta_b=20^{\circ}$ provide leading phase angles.

Note again that the ion temperature and the electron density contours in Figure 42 do not intersect the nitrogen-oxygen contours. More than a reasonable increase in nitrogen-oxygen collision frequency would be required than is acceptable to achieve this intersection. Thus, it would appear that a simple plane wave model does not explain the on-track wave for the 0.006 filter; that is, for a wave of about 1000 km based on fluctuations, spectra and correlation functions. Decreasing horizontal wavelength below 500 km also does not help, as can be seen.

In all the cases shown in Figures 41 and 42 and for similar computations at other temperatures, one finds that, if the phase shifts of Table IV are satisfied, the amplitudes of Table IV are not satisfied, the calculated values being too large. It is not inconceivable, though, that one might make a comparison for amplitudes, discarding the phase angles as too inaccurate. As can be seen from Figure 38, a given amplitude may be achieved for both a frequency that is higher and a frequency that is lower than that for the frequency based on the phase shift. On being consistent with amplitude for all parameters, one comes to the same conclusion as for phase shifts; that is, a plane traveling wave cannot provide the values in Table IV. In fact, the ion temperature amplitude is almost always very close to unity, whereas the values in Table IV are larger. Graphs for amplitudes similar to Figures 41 and 42 will not be given here.

The plasma transfer functions in Figures 41 and 42 assume that the true wave is traveling in the north-south direction, south in the northern hemisphere and north in the southern hemisphere. It is possible that the wave normal has an east-west component. In this case K_x in equations (4) and (5) is the north-south component of the true wavenumber vector. K_x in equation (3), however, is replaced by the true normalized horizontal wave number. In this case the wavelength along the north-south direction is greater than the true wavelength. Computations were made for this case, as well, for horizontal wave number vectors from 0^o to as much as 76^o off the north-south direction. The results of these calculations are not significantly different from those obtained for waves traveling in the north-south direction. No traveling wave solution is found as above. The results will not be given here.

6. Discussion

Figures 11 to 16,18,23,26 and 27 illustrate the oscillatory content of the fluctuations of the various parameters for data passed through various high pass filters with cut-off frequencies from 0.0015 Hz to 0.013 Hz. In each of these examples the period of the oscillations is nearly constant. There appear to be many such periods, or wavelengths, as indicated by the spectra of Figure 25 and the outstanding waves listed in Table IIIa.

Yet, one would not expect such near constancy in the period of the fluctuations over the large distance travelled by the satellite during the 4,125 seconds of time of Figures 11 to 16. For one, motion is over a sphere and in both hemispheres. Also, the sources for these waves may be in both auroral zones and not necessarily coherent. As the satellite path enters a localized source region and moves away, the angle of the path relative to the wave normal of the waves emanating from the sources changes. For a source of fixed horizontal wavelength, the change in this angle with satellite position would change the apparent periodicity, or, equivalently, the apparent horizontal wavelength, which is not observed. The apparent constancy of the oscillations may imply an extended rather than a localized source region, which appears to be in the northern auroral region, based on the discussion of fluctuations in Section 3.3. However, sources appear present in both auroral regions with the southern hotter. Both could be generating waves that interfere to produce the observed pattern. These sources could have similar spatial and temporal structures, though not completely coherent. Diffuse aurora is known to have some symmetry in both hemispheres and is of the appropriate scale size to excite large scale waves (Lui et al, 1982; Akasofu, 1974).

The fluctuations represent spatial waves along the path of the satellite with wavelengths from about 4000 km to about 400 km. Figures 11 to 16 demonstrate the correlations between the fluctuations of all four parameters that were studied for two different dominant wavelengths. These wavelengths were on the order of 2000 km in Figures 11 to 13 and 1000 km in Figures 14 to 16. Similar fluctuations and correlations may be shown for other wavelengths by using different filters. The extent of the correlation is well brought out in the plots of the cross correlation functions in Figures 32 to 36 for the data passed through the same two filters as for Figures 11 through 16. Correlation of nitrogen and oxygen is strong as shown in Figures 32 and 33, and the fluctuations appear nearly in phase, confirming the relationship shown in Figures 11 and 14. Anti-correlation of ion temperature and oxygen density, apparent in Figures 12 and 15, is clear in Figures 34 and 35; however, the degree of correlation is not as strong as that of oxygen and

nitrogen densities. It is interesting that the ion temperature is somewhat better correlated with the nitrogen density than the oxygen density. This correlation could possibly relate in some way to the chemistry and thermodynaamics of the region, if not unique to this orbit. It should be investigated for other orbits and their data.

Figures 13 for the 0.003 Hz filter and Figure 16 for the 0.006 Hz filter, to a lesser extent, suggest that the electron density behaves differently in the two hemispheres, since the phase of the fluctuations changes on passing from one region to the other. This difference may arise from the orientation of the magnetic field. For example, at low temporal frequencies and for horizontal wavelengths in the range of 500 km to 2000 km, the phase shift of the electron density transfer function is small and leading if the wave is traveling toward the equator, but large and lagging if traveling away from the equator. These characteristics appear to be like the phase shifts observed in Figures 13 and 16.

Nevertheless, the data do not appear to be in accordance with a pure traveling wave, as described in Section 5. However, there is no doubt that the constituents, both neutral and ionized, including temperature, are coupled with spatial characteristics over a wide range of scale sizes down to hundreds of kilometers over global regions. The use of 15 second data samples precludes study of coupling for still smaller scale sizes. Gross et al (1980) have looked at these smaller scales using 1.5 second AE-C data samples and also found correlation between parameters.

Since the plane wave model of Section 5. did not account for the characteristics of the data, one may expect that the model is too simple. Perhaps, viscosity and other factors that were neglected are important. Beating effects, over and above noise, make the analysis difficult, as well. Also, the transfer functions of Table IV may be of questionable accuracy, directly affecting the modeling analysis. A mixed wave system of stationary and traveling waves is possible, which could arise from both a single or two sources, one for each hemisphere. In the latter case the sources need not be truly coherent, though of similar spatial and temporal characteristics. Traveling components most certainly exist, as is known from observations of large scale TID's by ground instrumentation. But ground instrumentation may not recognize a stationary structure. More than one facility may be required, distributed in some way in two dimensions on the ground. Also, analysis of data of many orbits appear to indicate that these waves with large scale lengths are quite common in the global structure, yet such waves are not commonly observed on the ground (Georges, 1968). Experiments are needed to study these matters further.

It is difficult to analyze a system of stationary and traveling waves with just satellite measurements, no less in situ data. Ground measurements are needed to augment the satellite measurements by providing temporal and possibly directional information. The satellite provides the spatial distribution. The ground measurements should be made at the time of a satellite pass over the ground station. Because of the difficulty of finding coordinated measurements in the past, one must arrange for such experiments in advance, if a suitable satellite is in orbit, and for enough time to insure decent and useful measurements. (Such an opportunity exists with the Dynamic Explorer 2 satellite.) Further modeling efforts are desirable, particularly for propagation over a sphere with a superposed dipolar magnetic field, such as has been started by Mayr et al (1982).

An interesting question concerns the large number of waves that appear to make up the distribution, as indicated by the number of wavelengths in Table IIIa. Nothing like this has been observed with TID's measured from the ground. Such large numbers of waves are seen for other orbits. Of course, a number of waves may be present for part of the data span. Also, some of these waves may be viewed as the Fourier decomposition of a structure, or wave packet, in the distribution sampled by the satellite and not as individual waves; that is, this number of waves may be merely an indication of the spatial complexity of the distribution resulting from complex source regions. Nevertheless, each wave has its own identity in a linear system, as long as linearity applies. There is no guarantee that any or all are propagating, stationary or a mixture.

An important find is the power law decrease of spectra, with each parameter having its own index, though that of nitrogen and oxygen are close. Since the wavelength range is only 16.5:1 here, the fall off may not be logarithmically linear over a larger range of wavelengths. This type of behavior was also observed for shorter wavelengths using AE-C 1.5 second data samples (Gross et al, 1980) for an additional 10:1 wavelength range. Thus, it appears that this type of spectrum occurs for wavelengths ranging from thousands of kilometers to tens of kilometers, but not necessarily with a constant spectral index over the entire range. Differences in the fall off rate may arise from the transfer functions between major and minor species responses. The fall off rate itself may arise from the nature of the source and propagation in the intervening medium between source and observation point. The relationship to turbulence is of interest, and these matters deserve further research. Perhaps, the Van Zandt (1982) thesis for a universal spectrum for buoyancy waves is very revelant.

This study provides a measure of the rms fluction level for the four parameters which depend on the wavelength of

the disturbancee. Values are given in Table I and II. If temporal frequencies are known (even for standing waves), the flux of energy and momentum may be deduced. Such determinations can only obtained from more comprehensive, coordinated measurements of satellite and ground facilities. The methods used here permit a study of the magnitude of fluctuations and their spectral properties under both quiet and disturbed conditions, as well.

Finally, this study of AE-C data from orbit 5133 on January 20, 1975 is not a unique set of data. Less complete studies were made of data from many other orbits of that satellite and of data from the AE-E satellite. The results shown are typical. Similar fluctuations are observed, spectra are similar with peaks at particular on-track wavelengths and with a decreasing power law fall off.

REFERENCES

Akasofu, S. I., "A Study of Auroral Displays Photographed from the DMSP-2 Satellite and from the Alaska Meridian Chain of Stations," Space Sci. Rev. 16, 617-725, 1974.

Akasofu, S.I. and S. Chapman, Solar-Terrestrial Physics, Oxford, at the Clarendon Press, pp. 552-560.

Anderson, D. N., A. D. Richmond, B. Balsley, R. G. Roble, M. A. Biondi and D. P. Sipler, "In-situ Generated Gravity Waves as a Possible Seeding Mechanism for Equatorial Spread-F," Geophys. Res. Lett. 7, 789-792, 1982.

Baxter, R. G. and P. C. Kendall, "A Theoretical Technique for Evaluating the Time-Dependent Effects of General Electrodynamic Drifts in the F2 layer of the Ionosphere," Proc. Roy. Soc. A 304, 171-185, 1968.

Bertin, F., J. Testud, L. Kersky and P. R. Rees, "The Meteorological Jet Stream as a Source of Medium Scale Gravity Waves in the Thermosphere; An Experimental Study," J. Atmos. Terr. Phys. 40, 1161-1183, 1978.

Brace, L. H., R. F. Theis and A. Dalgarno, "The Cylindrical Electrostatic Probes for Atmosphere Explorer-C,-D, and -E," Radio Science 8, 341-348, 1973.

Chandra, S. and N. W. Spencer, "Exospheric Temperature Inferred from the Aeros-A Neutral Composition Measurement," J. Geophys. Res. 80, 3615-3621, 1975.

Chandra, S. and N. W. Spencer, "Thermospheric Storms and Related Ionospheric Effects," J. Geophys. Res. 81, 5018-5026, 1976.

Chapman, S. and T. G. Cowling, The Mathematical Theory of Non-Uniform Gases, Cambridge Univ. Press, 1939, pp. 53-62.

Davis, M. J. and A. V. daRosa, "Traveling Ionospheric Disturbances Originating in the Auroral Oval During Polar Substorms," J. Geophys. Res. 74, 5721-5735, 1969.

Davis, T. N. and M. Suguira, "Auroral Electrojet Activity Index AE and its Universal Time Variations," J. Geophys. Res. 71, 785-801, 1966.

Del Genio, A. D., G. Schubert and J. M. Strauss, "Characteristics of Acoustic-Gravity Wave in a Diffusively Separated Atmosphere," J. Geophys. Res. 84, 1865-1871, 1979.

Del Genio, A. D., J. M. Strauss and G. Schubert, "Effects of Wave-Induced Diffusion on Thermosphere Acoustic-Gravity Waves," Geophys. Res. Lett. 5, 265-267, 1978

Dyson, P. L., J. P. McClure and W. B. Hanson, "In-situ Measurements of the Spectral Characteristics of F Region Ionospheric Irregularities," J. Geophys. Res. 79, 1497-1502, 1974.

Dyson, P. L., C. P. Newston and L. H. Brace, "In-situ Measurements of Neutral and Electron Density Wave Structure from the Explorer 32 Satellite," J. Geophys. Res. 75, 3200-3210, 1970.

Forsythe, G. E., M. A. Malcolm and C. B. Moler, Computer Methods for Mathematical Computations, Prentice Hall, Englewoods Cliffs, N.J., 1977, pp. 70-79.

Francis, S. H., "Propagation of Internal Acoustic-Gravity Waves Around a Spherical Earth," J. Geophys. Res. 77, 4221-4226, 1972.

Francis, S. H., "A Theory of Medium-Scale Traveling Ionospheric Disturbances," J. Geophys. Res. 79, 5245-5260, 1974.

Georges, T. M., "HF Doppler Studies of Traveling Ionospheric Disturbances," J. Atmos. Terr. Phys. 30, 735-746, 1968.

Gross, S. H. and H. Eun, "Traveling Neutral Disturbances," Geophys. Res. Lett. 3, 257-260, 1976.

Gross, S. H. and H. Eun, "Traveling Neutral Disturbances and Minor Constituent Particle Mass," J. Atm. Terr. Phys., 40, 183-193, 1978.

Gross, S. H., C. A. Reber, F. Huang, "Large Scale Waves in the Ionosphere Observed by the AE Satellites," AGARD Meeting, 27th Symposium of the Electromagnetic Wave Propagation Panel, 28-31 October 1980, Pozzuoli, Italy.

Gross, S. H., C. A. Reber, F. Huang, "Large Scale Waves in the Ionosphere at Equatorial Latitudes, XXth General Assembly of URSI, August 11-18, 1981, Washington, D. C.

Hamming, R. W., Digital Filters, Prentice Hall, Englewood Cliffs, N.J., 1977, pp. 98-104.

Hanson, W. B. and R. J. Moffett, "Ionization Transport Effects in the Equatorial F Region," J. Geophys. Res. 71, 5559-72, 1966.

Hanson, W. B., D. R. Zuccaro, C. R. Lippincott and S. Sanatani, "The Retarding-Potential Analyzer on Atmosphere Explorer," Radio Science 8, 333-339, 1973.

Hines, C. O., "The Upper Atmosphere in Motion," Geophysical Monograph 18, American Geophysical Union, Washington, D.C., 1974.

Hoegy, W. R., P. Dyson, L. E. Wharton and N. Spencer, "Neutral Atmospheric Waves," GRL 6, 187-190, 1979.

Hooke, W. H., "Ionospheric Irregularities Produced by Internal Atmospheric Gravity Waves," J. Atmos. Terr. Phys. 30, 795-823, 1968.

Hunsucker, R. D., "Atmospheric Gravity Waves in the High Latitude Ionosphere: A Review," Rev. Geophys. Space Phys. 20, 293-315, 1982.

Jenkins, G. M. and D. G. Watts, Spectral Analysis and Its Application, Holden-Day, San Francisco, 1968, pp. 162-167.

Kelley, M. C., M. F. Larsen, C. LaHoz and J. P. McClure, "Gravity Wave Initiation of Equatorial Spread F: A Case Study," J. Geophys. Res. 86, 9087-9100, 1981.

Larsen, M. F., W. E. Swartz, R. F. Woodman, "Gravity Wave Generation by Thunderstorms Observed with a Vertically-Pointing 430 MHz Radar," Geophys. Res. Lett. 9, 571-574, 1982.

Lui, A. T. Y., C.-I Meng and S. Ismail, "Large Amplitude Undulations on the Equatorward Boundary of the Diffuse Aurora," J. Geophys. Res. 87, 2385-2400, 1982.

Mastrantonio, G., F. Einaudi, D. Fua and G. P. Lalas, "Generation of Gravity Waves by Jet Streams in the Atmosphere," J. Atmos. Sci. 33, 1730-1738, 1976.

Mayr, H. G., I. Harris, F. A. Herrero and F. Varosi, "Global Excitation and Propagation of Gravity Waves in a Dissipative Multi-Constituent Medium," Paper SA 42A-08, EOS 63, 1051, 1982.

Mayr, H. G., I. Harris and N. W. Spencer, "Some Properties of Upper Atmosphere Dynamics," Rev. Geophys. Space Phys. 16, 539-565, 1978.

Mayr, H. G. and H. Volland, "Magnetic Storm Effects in the Neutral Composition," Planet. Space Sci. 20, 379-393, 1972.

Mayr, G. H. and H. Volland, "Magnetic Storm Characteristics of the Thermosphere," J. Geophys. Res. 78, 2251-2264, 1973.

Mayr, H. G. and H. Volland, "Magnetic Storm Dynamics of the Thermosphere," J. Atmos. Terr. Phys. 36, 2025-2036, 1974.

McIlwain, C. E., "Coordinates for Mapping the Distribution of Magnetically Trapped Particles," J. Geophys. Res. 66, 3681-3691, 1961.

Potter, W. E., D. C. Kayser and K. Mauersberger, "Direct Measurements of Neutral Wave Characteristics in the Thermosphere," J. Geophys. Res. 81, 5002-5012, 1976.

Prölss, G. W., "Perturbation of the Low-Latitude Upper Atmosphere During Magnetic Storm Activity," J. Geophys. Res. 87, 5260-5266, 1982.

Prölss, G. W. and U. vonZahn, "Magnetic Storm Associated Changes in Neutral Composition of the Atmosphere at Mid-Latitudes Observed by the ESRO 4 Gas Analyzer," Space Research XIV, Akademie-Verlag, Berlin 1974, pp. 157-161, 1974a.

Prölss, G. W. and U. vonZahn, "ESRO 4 Gas Analyzer Results 2. Direct Measurements of Changes in the Neutral Composition During an Ionospheric Storm," J. Geophys. Res. 79, 2535-2539, 1974b.

Reber, C. A., A. E. Hedin, D. T. Pelz, N. E. Potter and L. H. Brace, "Phase and Amplitude Relationships of Wave Structure Observed in the Lower Thermosphere," J. Geophys. Res. 80, 4576-4580, 1975.

Richmond, A. D., "Thermopheric Heating in a Magnetic Storm: Dynamic Transport of Energy from High to Low Latitudes," J. Geophys. Res. 84, 5259-5266, 1979.

Richmond, A. D. and S. Matsushita, "Thermospheric Response to a Magnetic Substorm," J. Geophys. Res. 80, 2839-2850, 1975.

Roble, R. G., A. D. Richmond, W. L. Oliver and R. M. Harper, "Ionospheric Effects of the Gravity Wave Launched by the September 18, 1974 Sudden Commencement," J. Geophys. Res. 83, 999-1009, 1978.

Spencer, N. W., H. B. Niemann and G. R. Carignan, "The Neutral Atmosphere Temperature Instrument," Radio Science 8, 287-296, 1973.

Stubbe, P., "Frictional Forces and Collision Frequencies Between Moving Ions and Neutral Gases," J. Atmos. Terr. Phys. 30, 1965-1985, 1968.

Taeusch, D. R., G. R. Carignan and C. A. Reber, "Neutral Composition Variation Above 400 Kilometers During a Magnetic Storm," J. Geophys. Res. 76, 8318-8325, 1971.

Testud, J., P. Amayenc and M. Blanc, "Middle and Low Latitude Effects of Auroral Disturbances from Incoherent Scatter," J. Atmos. Terr. Phys. 37, 989-1009, 1975.

Thome, G., "Long-Period Waves Generated in the Polar Ionosphere During the Onset of Magnetic Storms," J. Geophys. Res. 73, 6319-6336, 1968.

Trinks, H., S. Chandra, N. W. Spencer and U. vonZahn, "A Two Satellite Study of the Neutral Atmosphere Response to a Major Geomagnetic Storm," J. Geophys. Res. 81, 5013-5017, 1976.

Trinks, H. and H. G. Mayr, "Large-Scale Neutral Composition Gravity Waves in the Thermosphere Observed by ESRO 4," J. Geophys. Res. 81, 4023-4026, 1976.

Ulryck, T. J. and T. N. Bishop, "Maximum Entropy Spectral Analysis and Autoregressive Decomposition," Rev. Geophys. Space Phys. 13, 183-200, 1975.

Van Zandt, T. E., "A Universal Spectrum of Buoyancy Waves in the Atmosphere," Geophys. Res. Lett. 9, 575-578, 1982.

Vickrey, J. F., R. R. Vondrak and S. J. Mathews, "Energy Deposition by Precipitating Particles and Joule Dissipation in the Auroral Ionosphere," J. Geophys. Res. 87, 5184-5196, 1982.

Wickwar, V. B., M. J. Baron and R. D. Sears, "Auroral Energy Input From Energetic Electrons and Joule Heating at Chatanika," J. Geophys. Res. 80, 4364-4367, 1975.

Yeh, K.C. and C. H. Liu, "Acoustic-Gravity Waves in the Upper Atmosphere," Rev. Geophys. Space Phys. 12, 193-216, 1974.

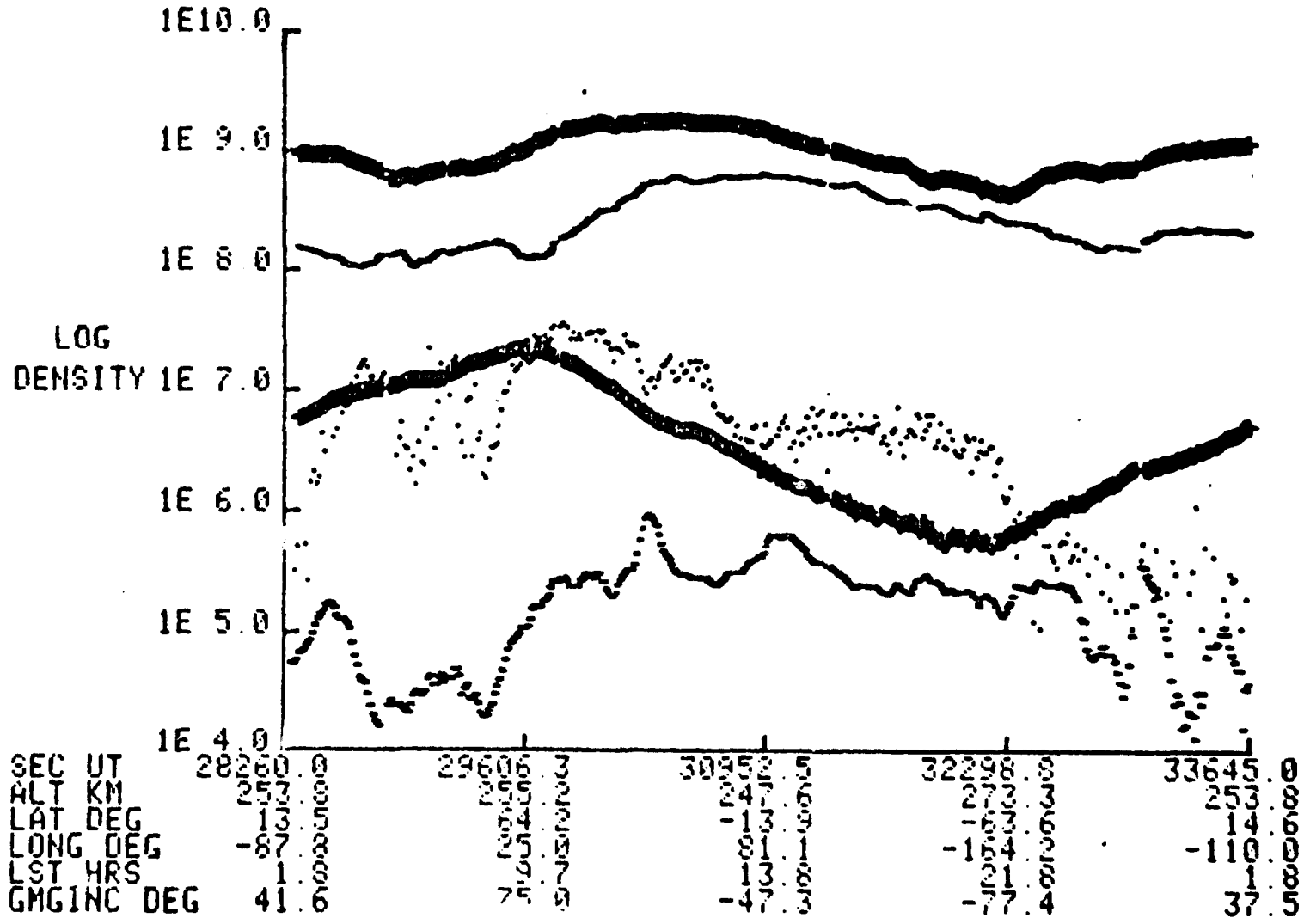

Fig. 1 Logarithm of oxygen, nitrogen, helium and electron densities in particles cm^{-3} vs. time in seconds UT. The coding for the curves are indicated. Oxygen is the uppermost curve. Next is nitrogen, then helium and lowest is the electron density. Atmosphere Explorer C UA data for orbit 5133, January 20, 1975. Other abscissa scales are altitude, latitude, longitude, local solar time, L shell radius and geomagnetic inclination.

Fig 2

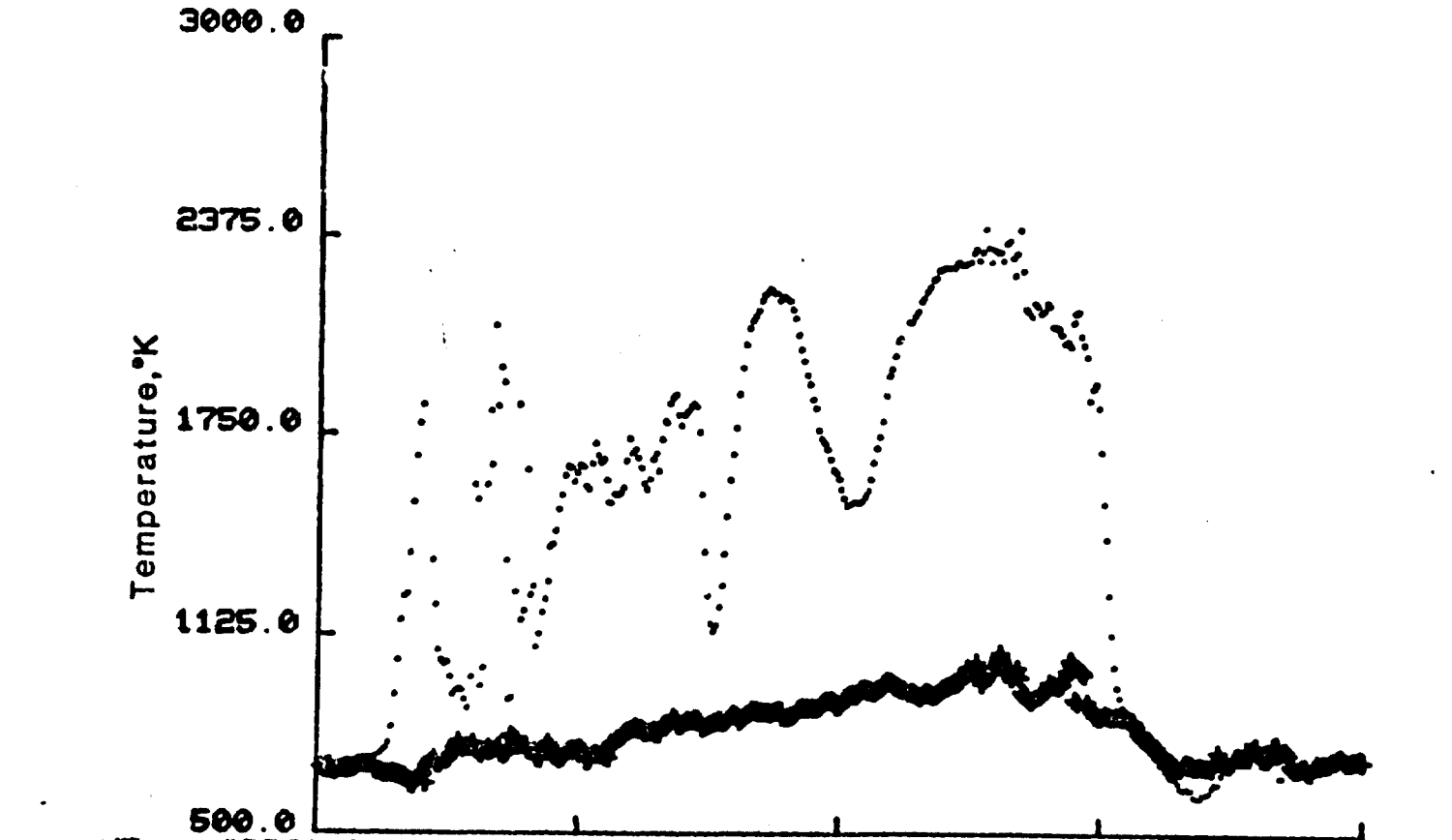

sec UT	28260.0	29606.3	30952.5	32298.8	33645.0
Alt km	253.8	255.2	247.6	273.3	253.8
Long deg	-87.8	25.0	81.1	-164.2	-110.0
LShell rad	1.3	4.3	1.2	5.5	1.2
GMgInc deg	41.6	75 0	-47.3	-77.4	37.5

Fig. 2 Electron and ion temperatures vs. time in seconds UT. The dotted curve is the electron temperature, the other curve the ion temperature. Atmosphere Explorer C UA data for orbit 5133, January 20, 1975.

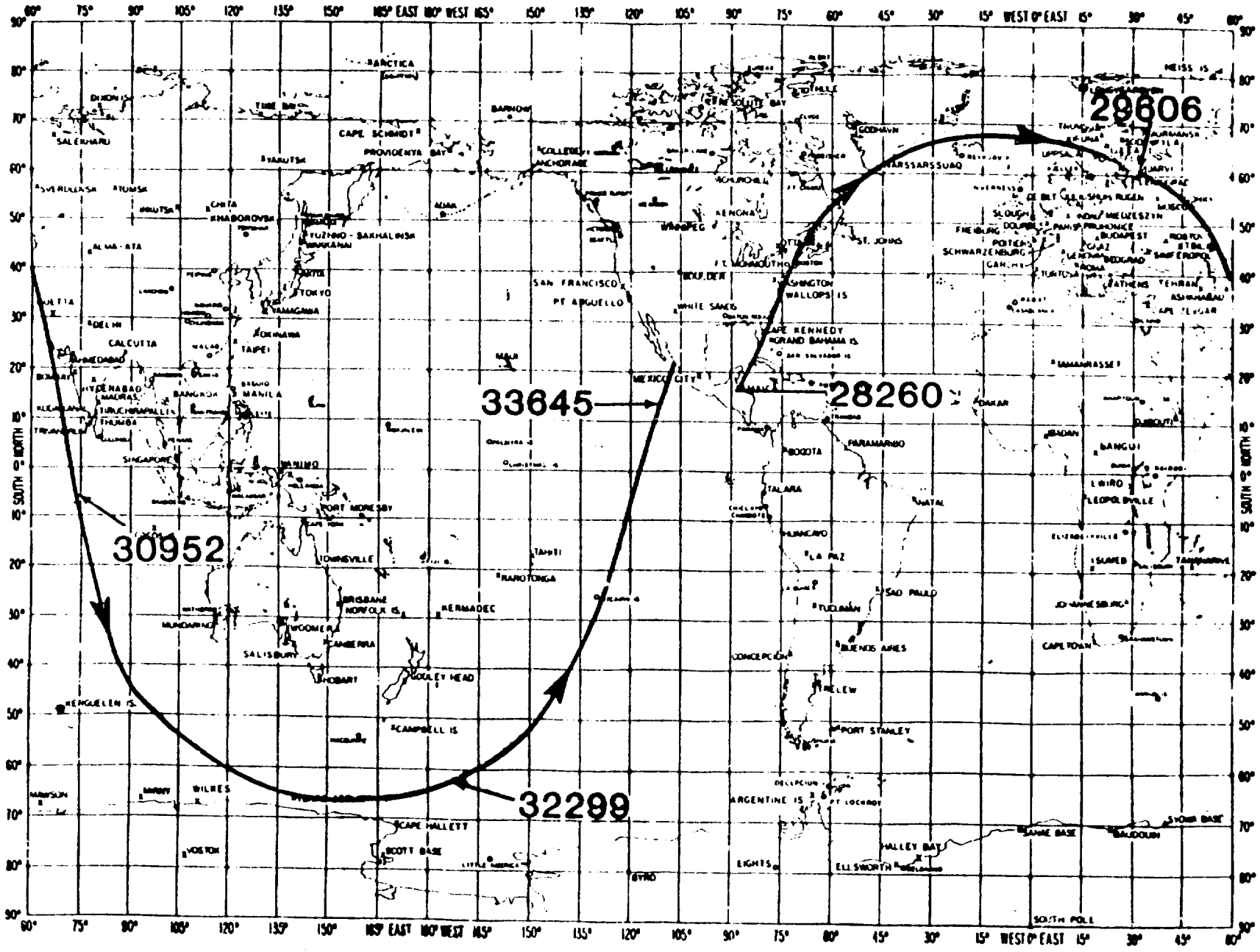

Fig. 3 Mercator plot of orbit 5133.

Fig 4

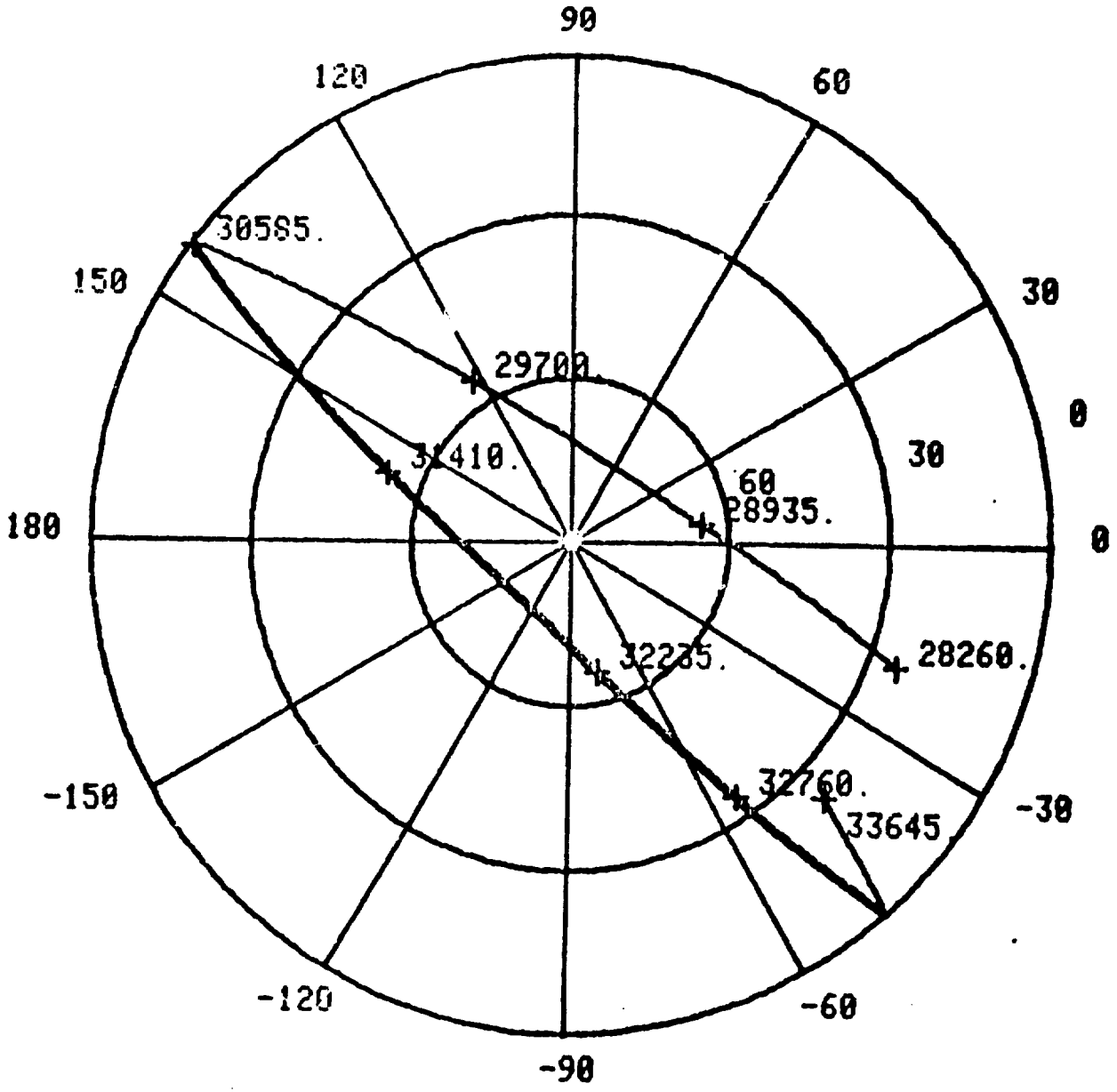

Fig. 4 Polar plot in geomagnetic coordinates of orbit 5133.

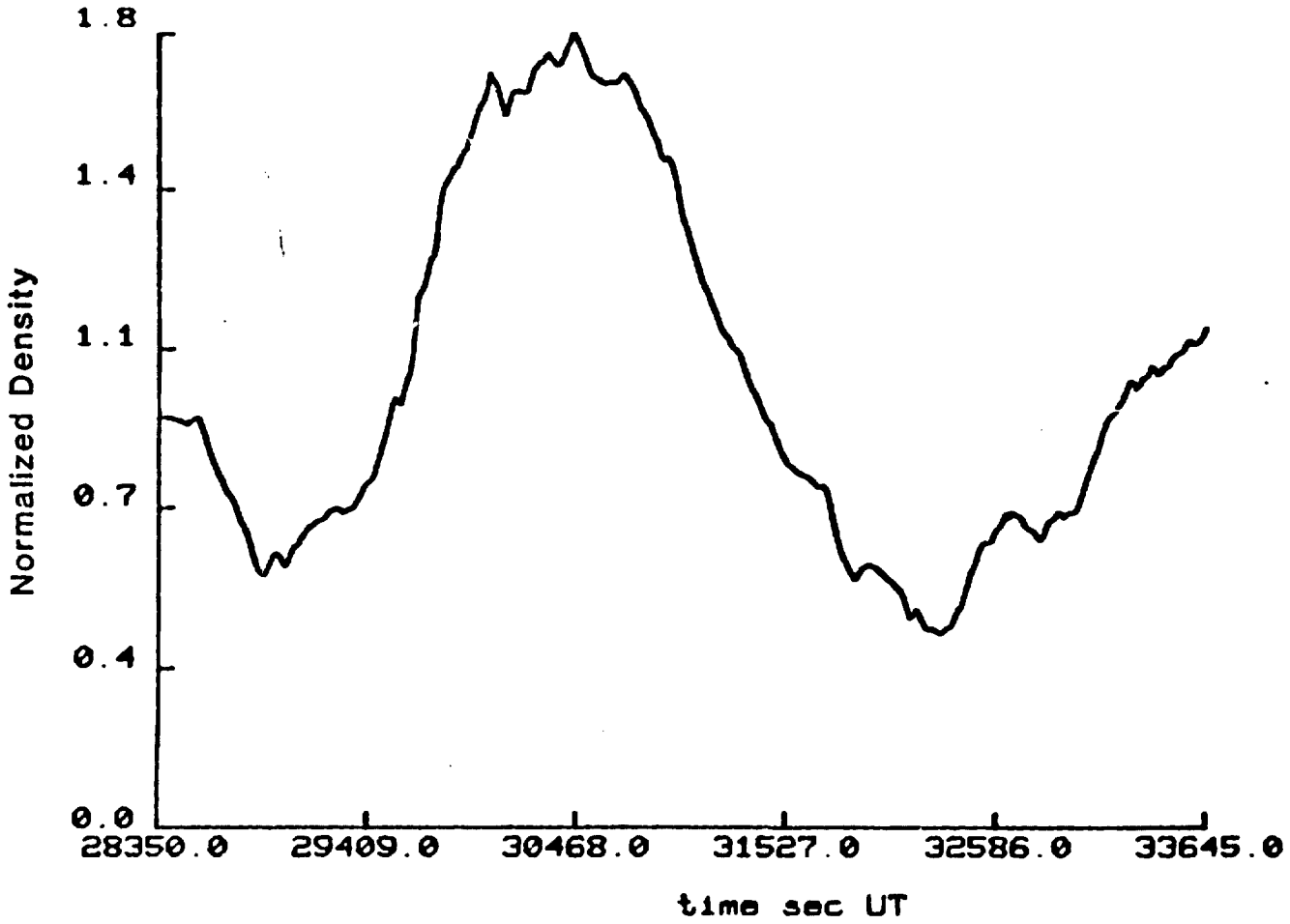

Fig. 5 Graph of normalized density of oxygen in Fig. 1 vs. time in seconds UT. Oxygen density is normalized to its average of 1.0268×10^9 particles cm^{-3}.

Fig

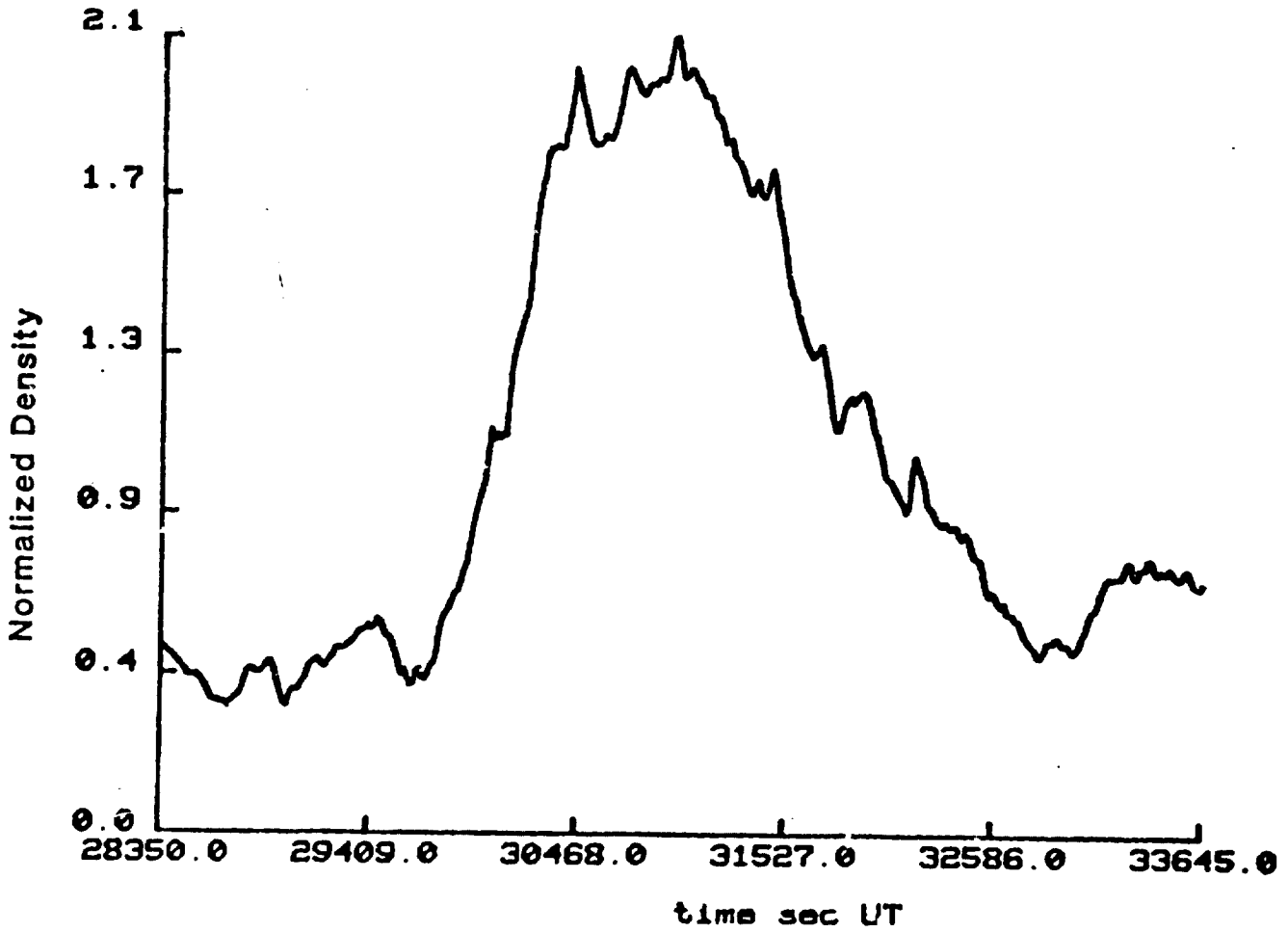

Fig. 6 Same as Fig. 5 but for nitrogen density. Average is 3.0496 x 10^8 particles cm^{-3}.

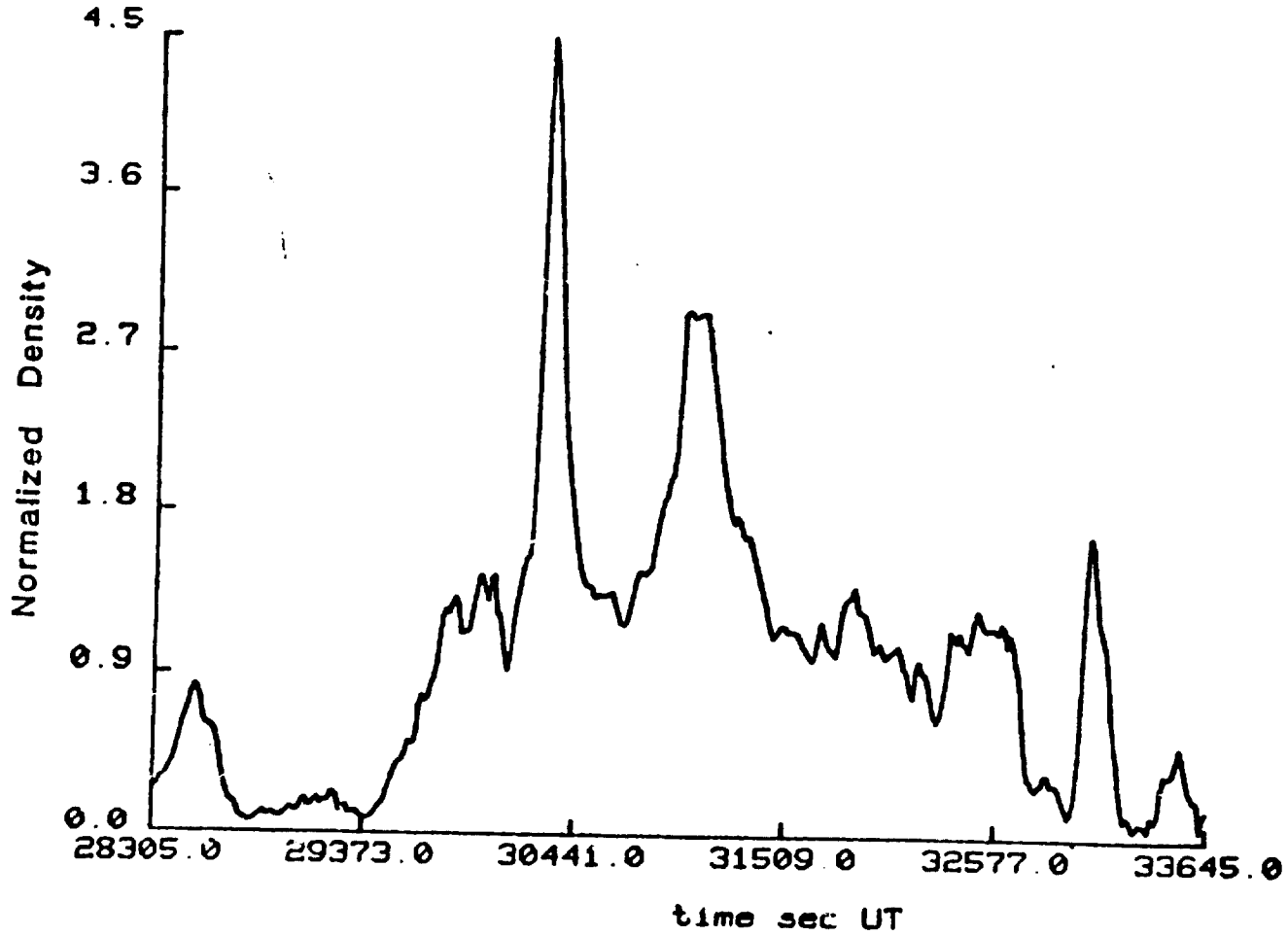

Fig. 7 Same as Fig. 5 but for electron density. Average is 2.0947 x 10^5 electrons cm^{-3}.

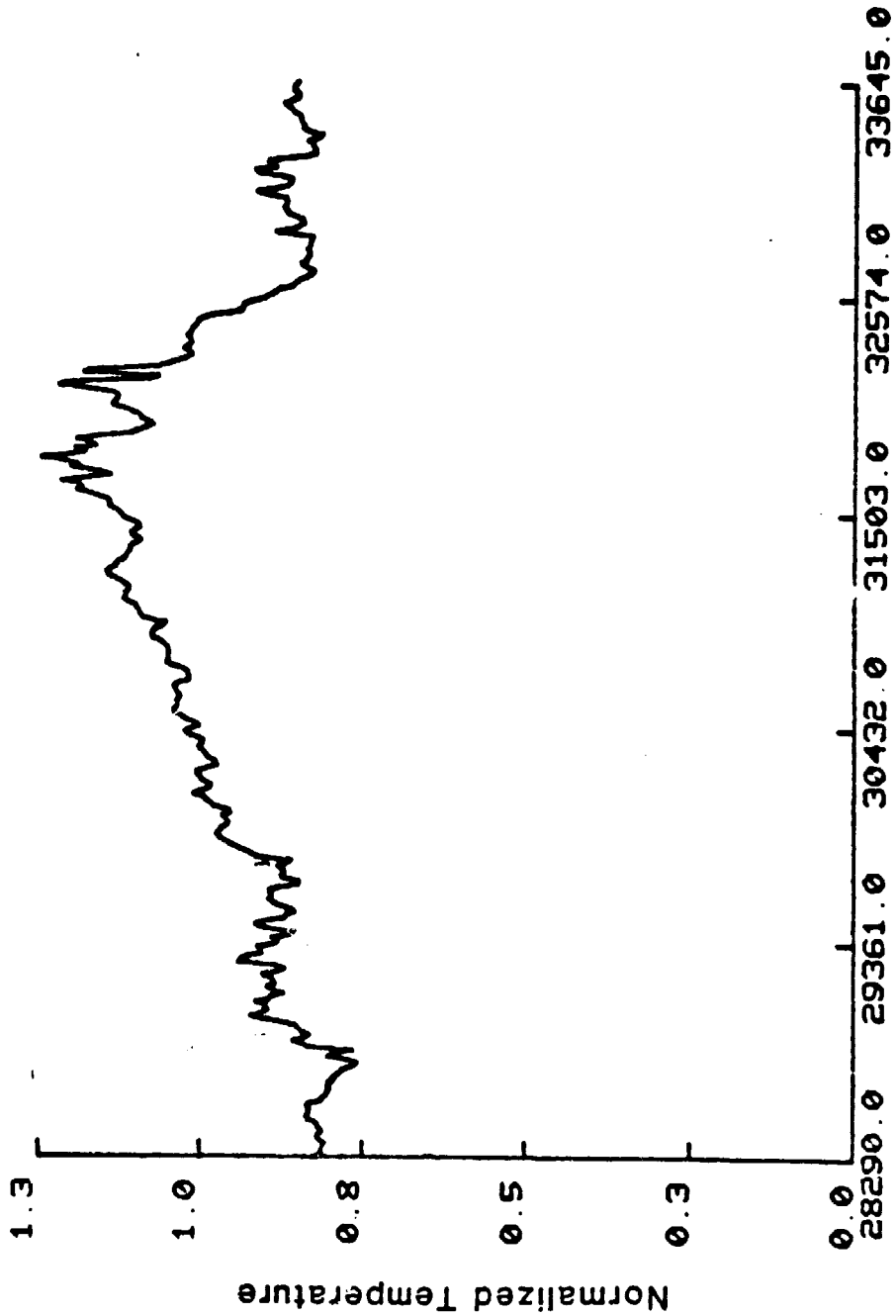

Fig. 8 Same as Fig. 5 but for ion temperature. Average is 932.47°K.

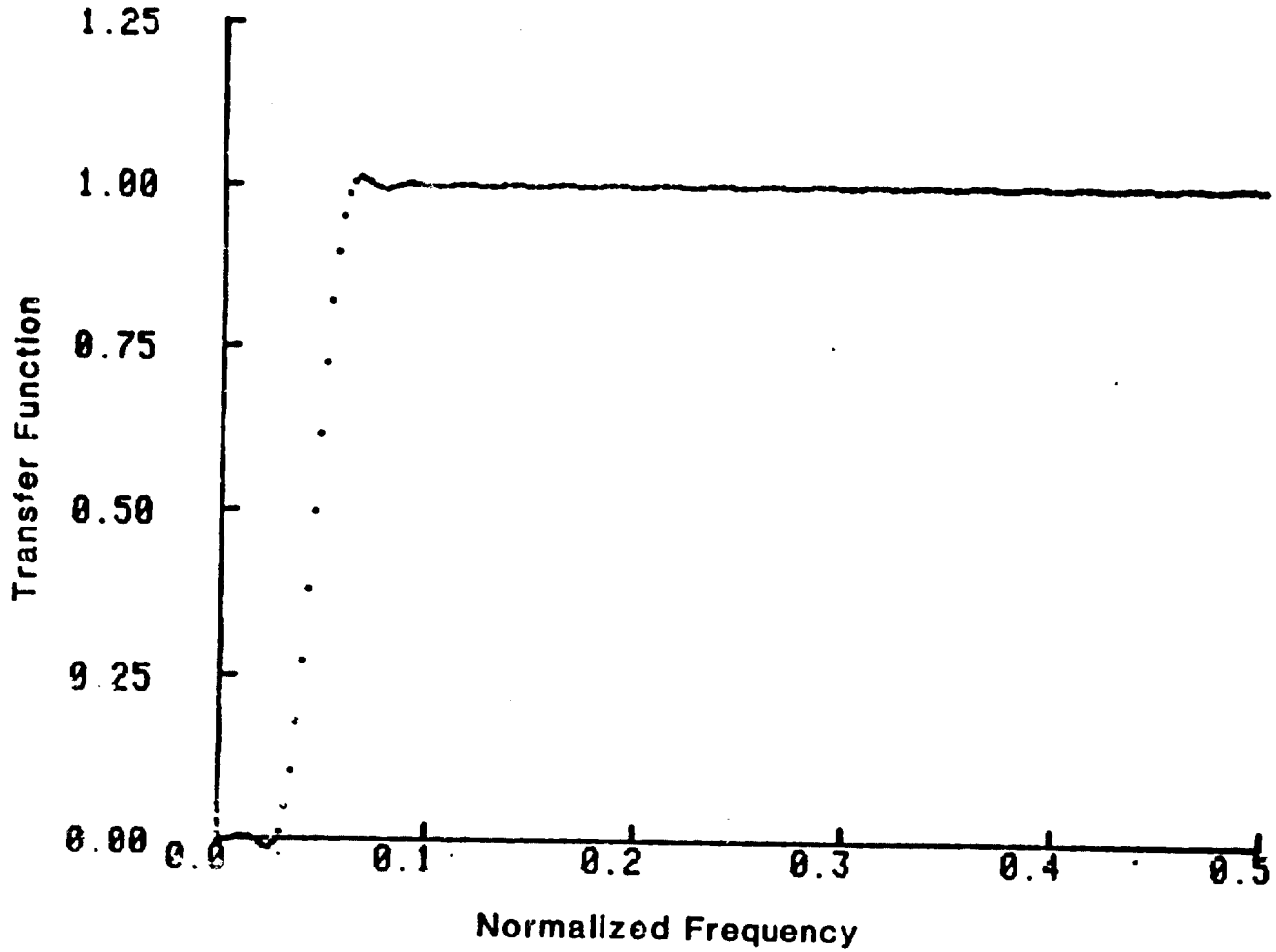

Fig. 9 High pass filter transfer function vs. normalized frequency. 0.5 is the Nyquist frequency. Actual frequency for 15 second data samples is obtained by dividing the normalized frequency by 15. Filter order is 40 and the cutoff frequency is 0.003 Hz.

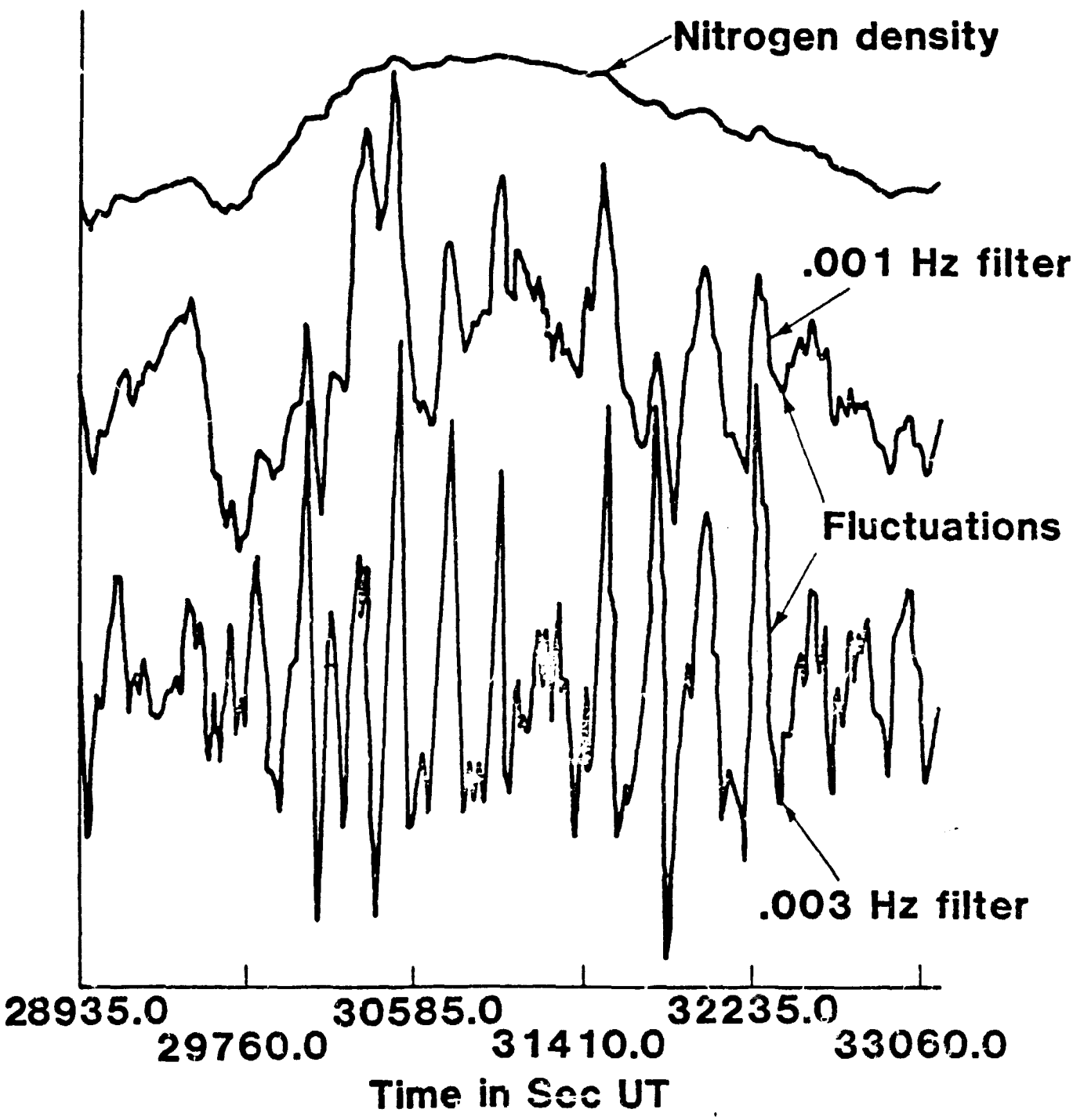

Fig. 10 Plot of nitrogen density as in Fig. 1 and normalized nitrogen density fluctuations at the output of high-pass filters of order equal to 40 and cutoffs of 0.001 Hz and 0.003 Hz vs. time in seconds UT.

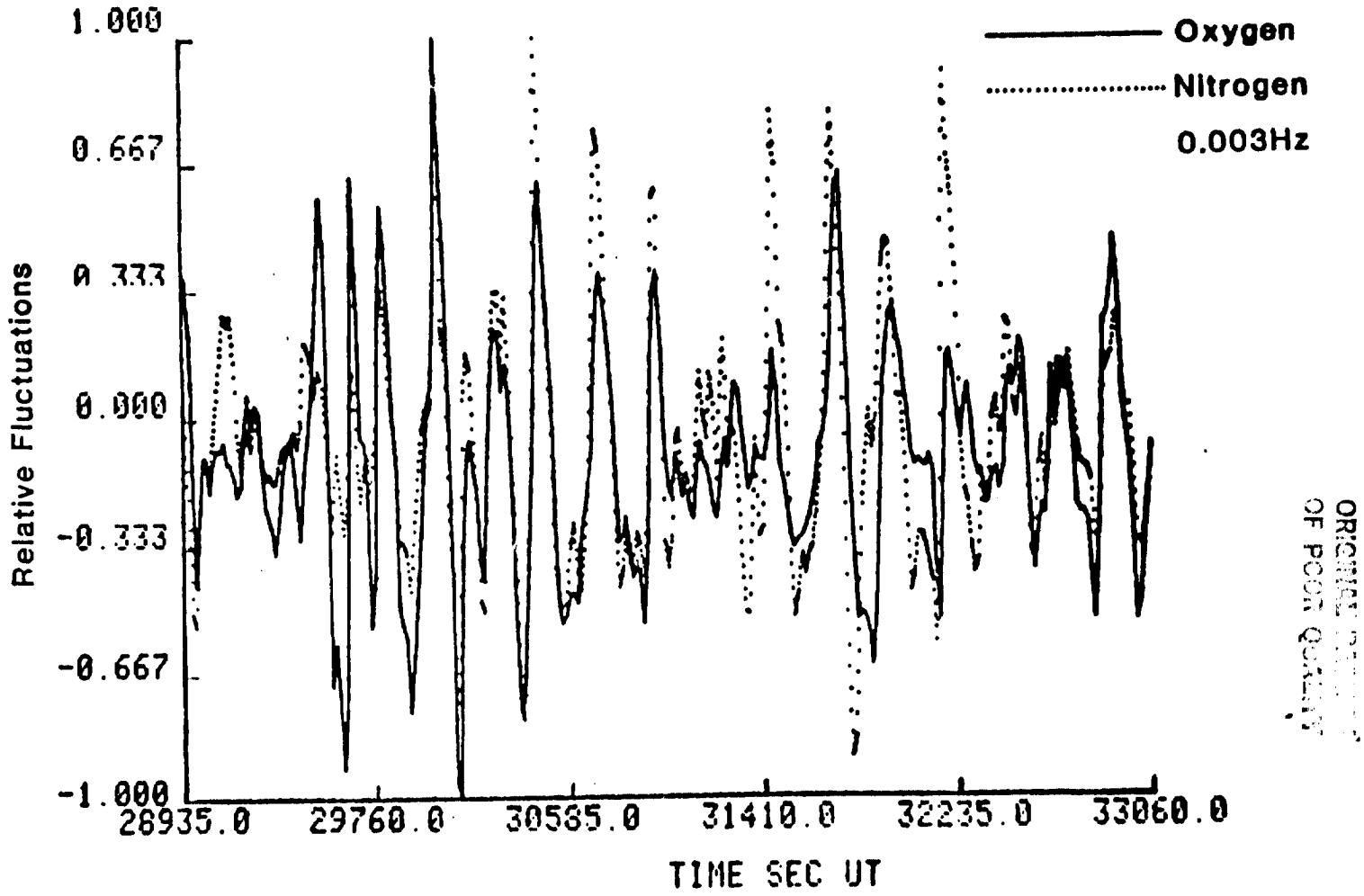

Fig. 11 Graph of fluctuations from a 0.003 Hz high-pass filter of order = 40 of oxygen and nitrogen vs. time in seconds UT. The solid curve is for oxygen, whereas the dotted curve is for nitrogen. Both of the fluctuations have been normalized to take values in the range -1 to 1.

F. 8 12

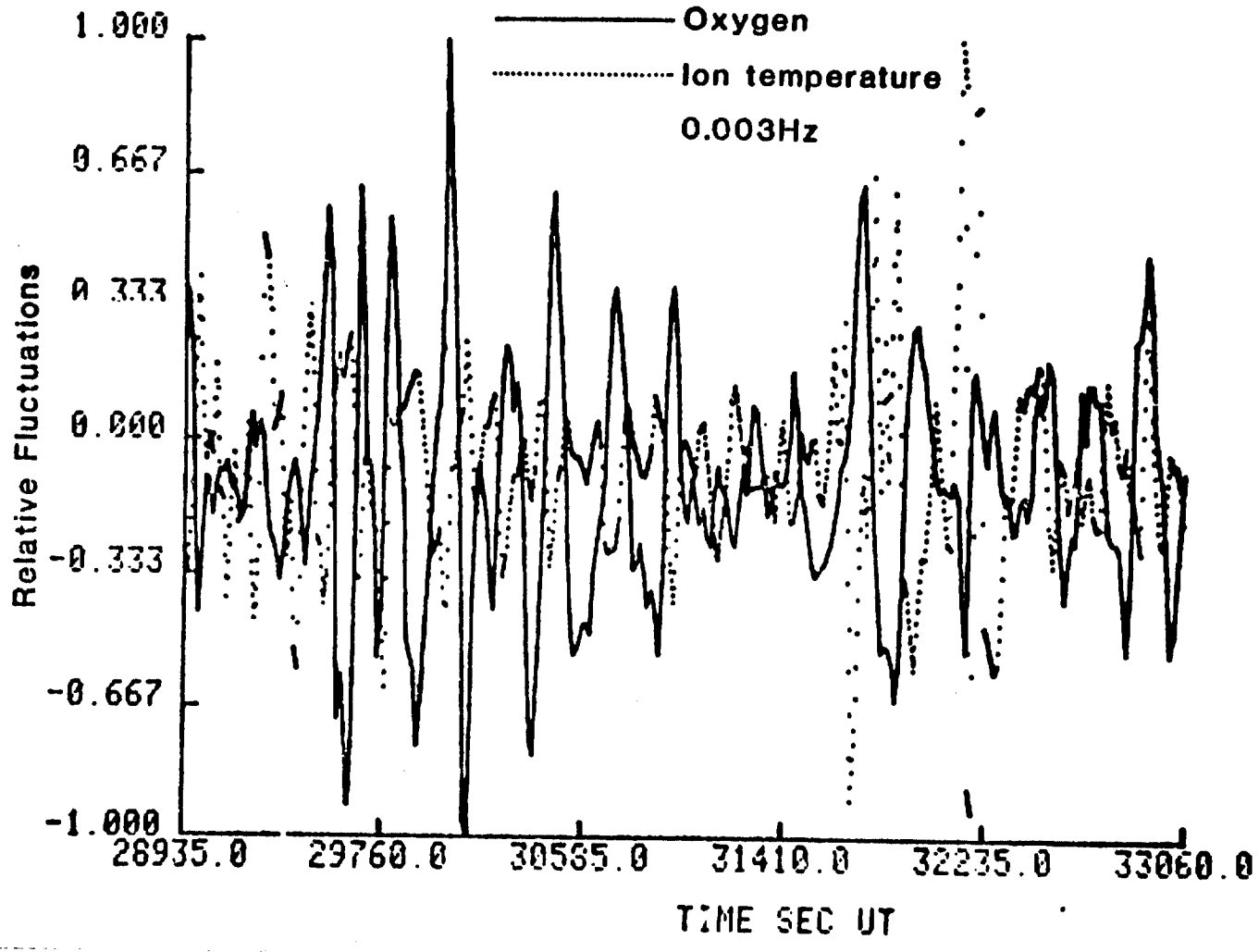

Fig. 12 The same as Fig. 11, but the dotted curve is for the ion temperature fluctuations.

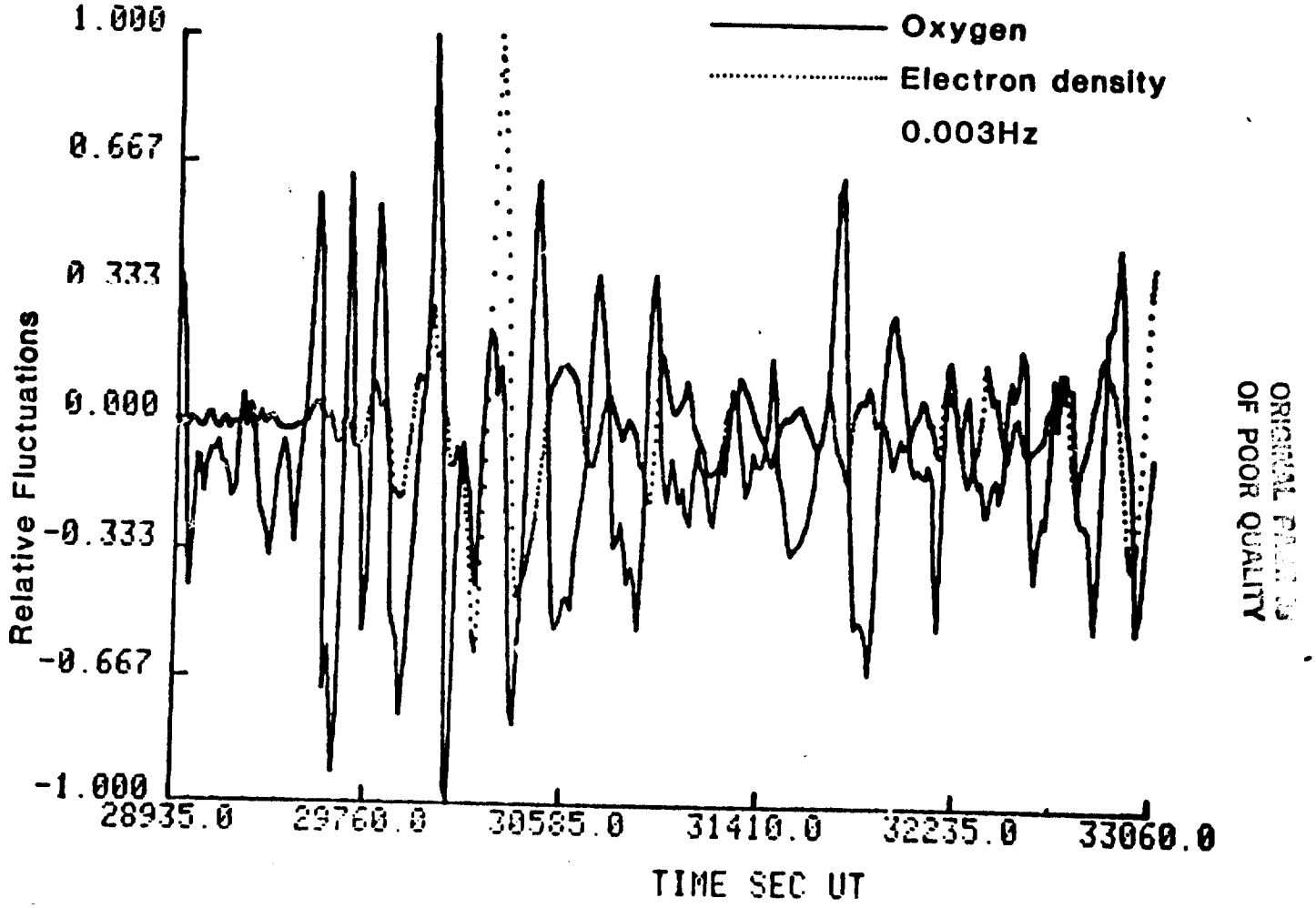

Fig. 13 The same as Fig. 11, but the dotted curve is for the electron density fluctuations.

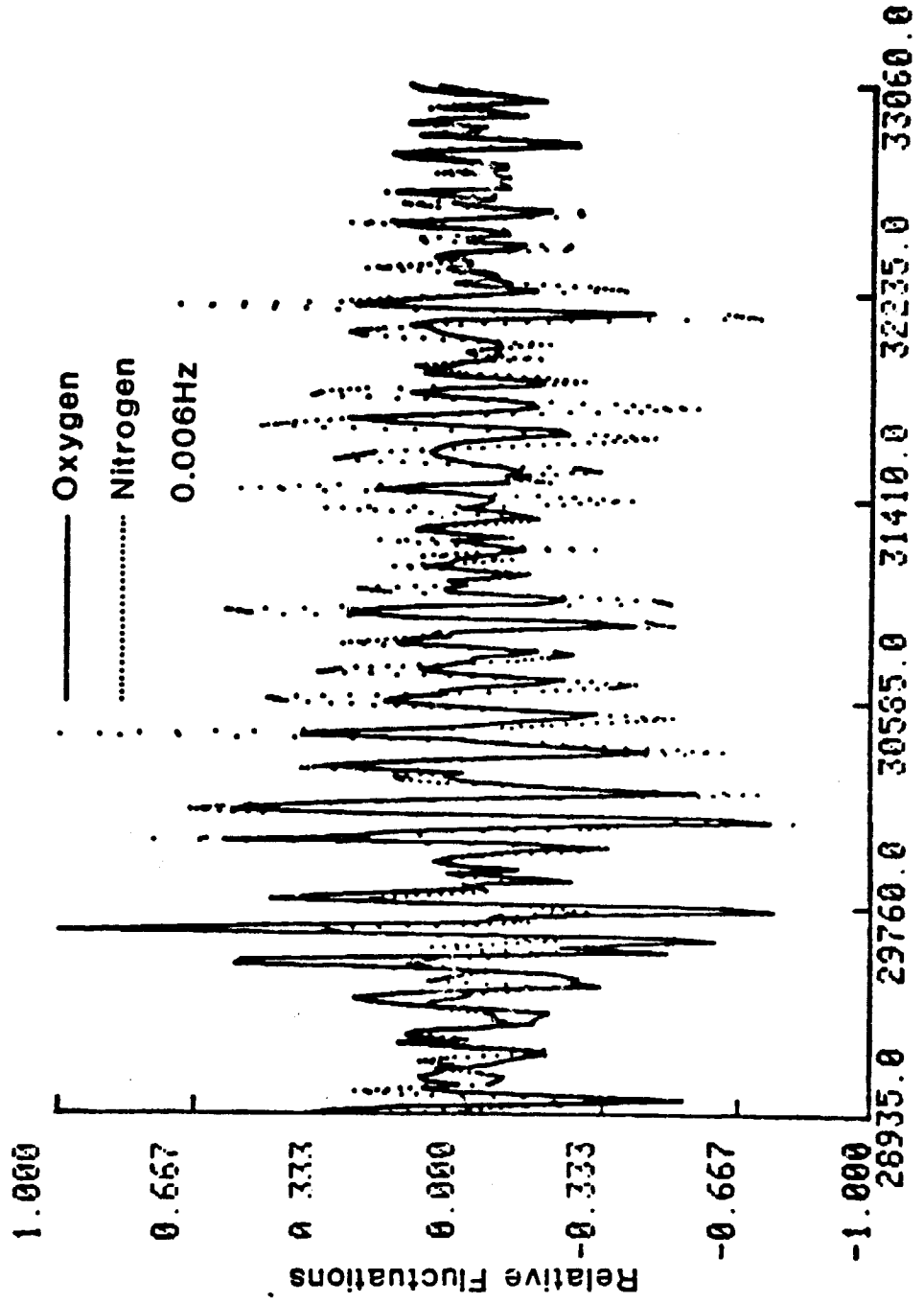

Fig. 14 The same as Fig. 11, except the cutoff of the high-pass filter is 0.006 Hz.

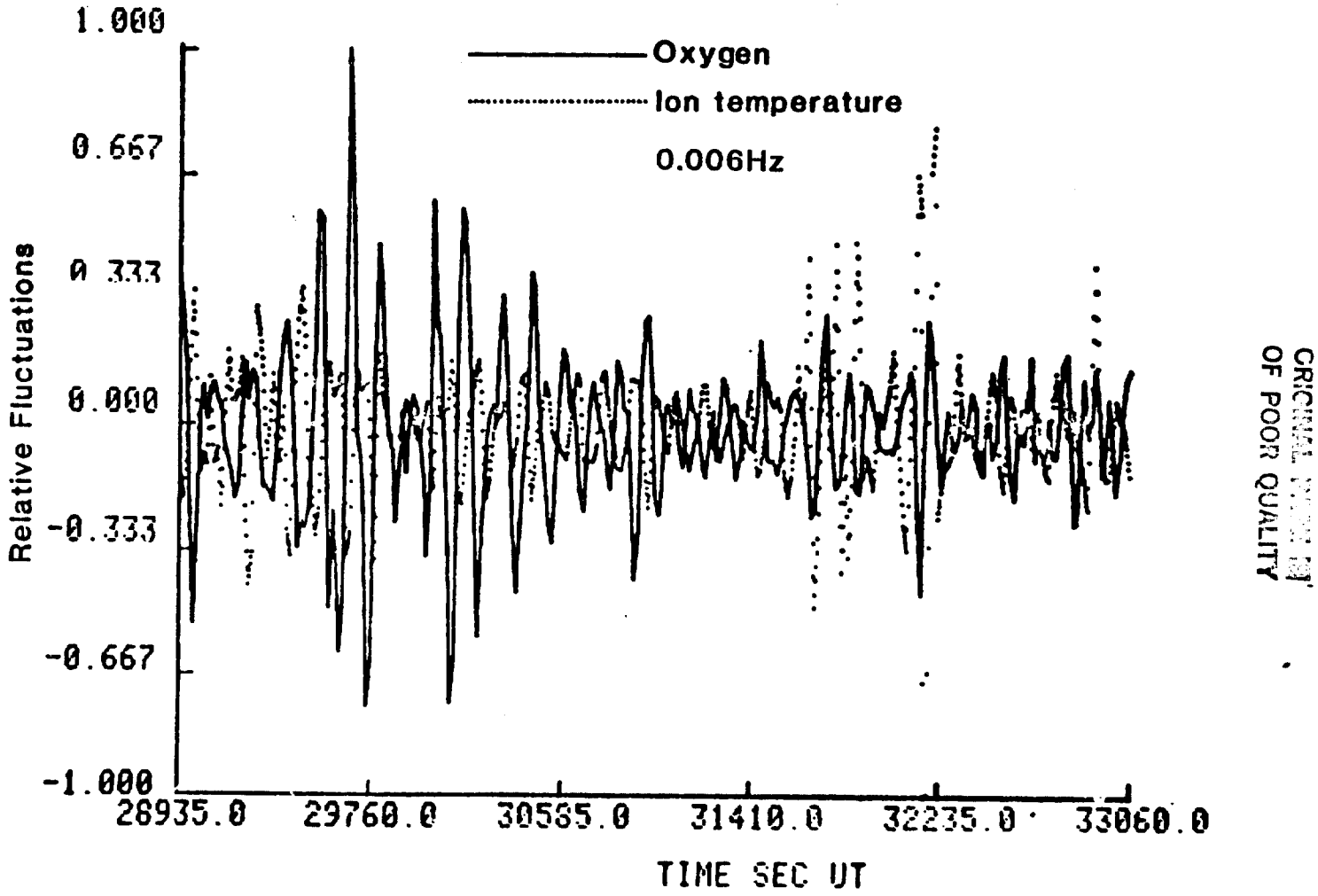

Fig. 15 The same as Fig. 14, but the dotted curve is for the ion temperature fluctuations.

Fig. 16

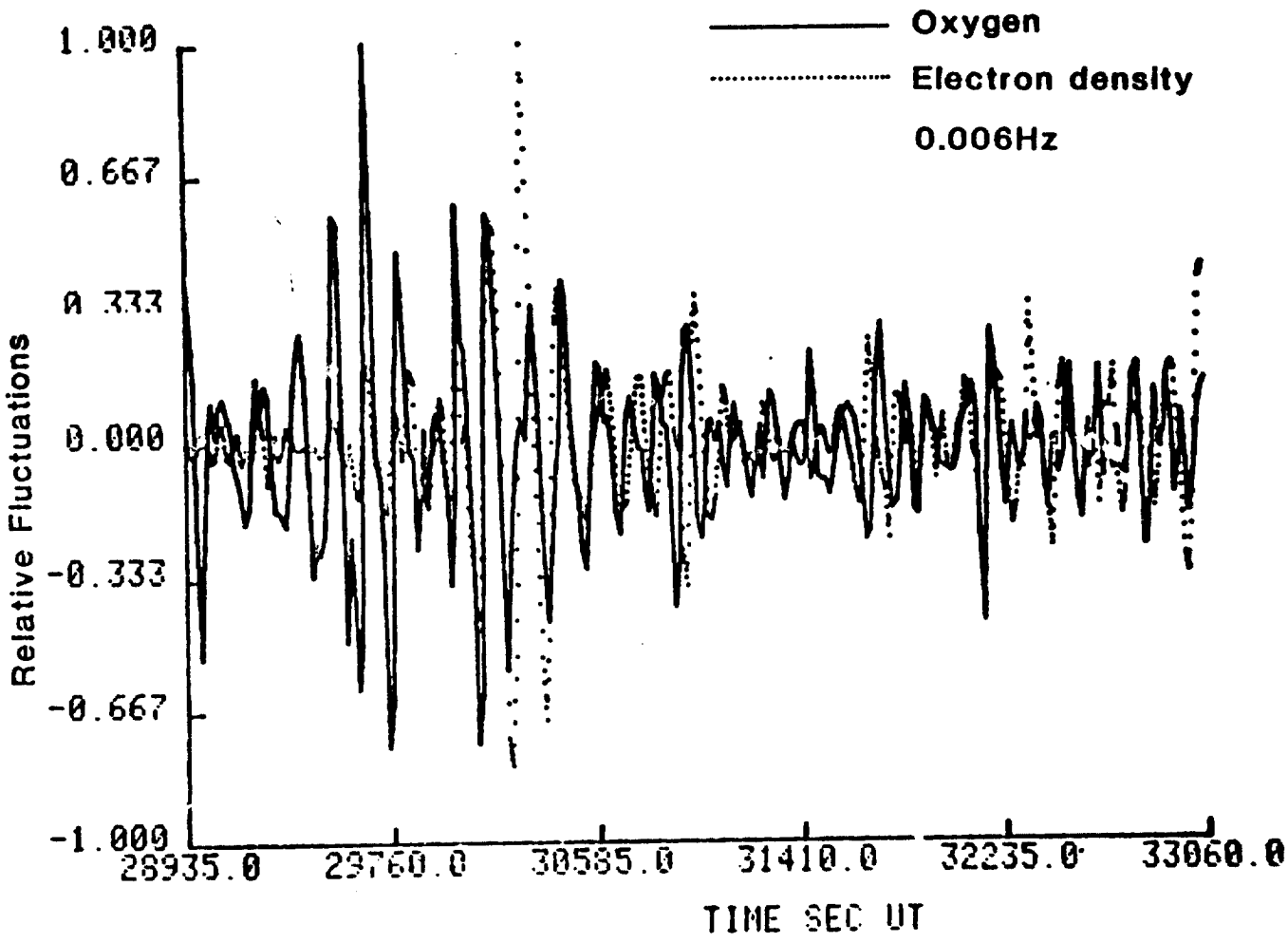

Fig. 16 The same as Fig. 14, but the dotted curve is for the electron density fluctuations.

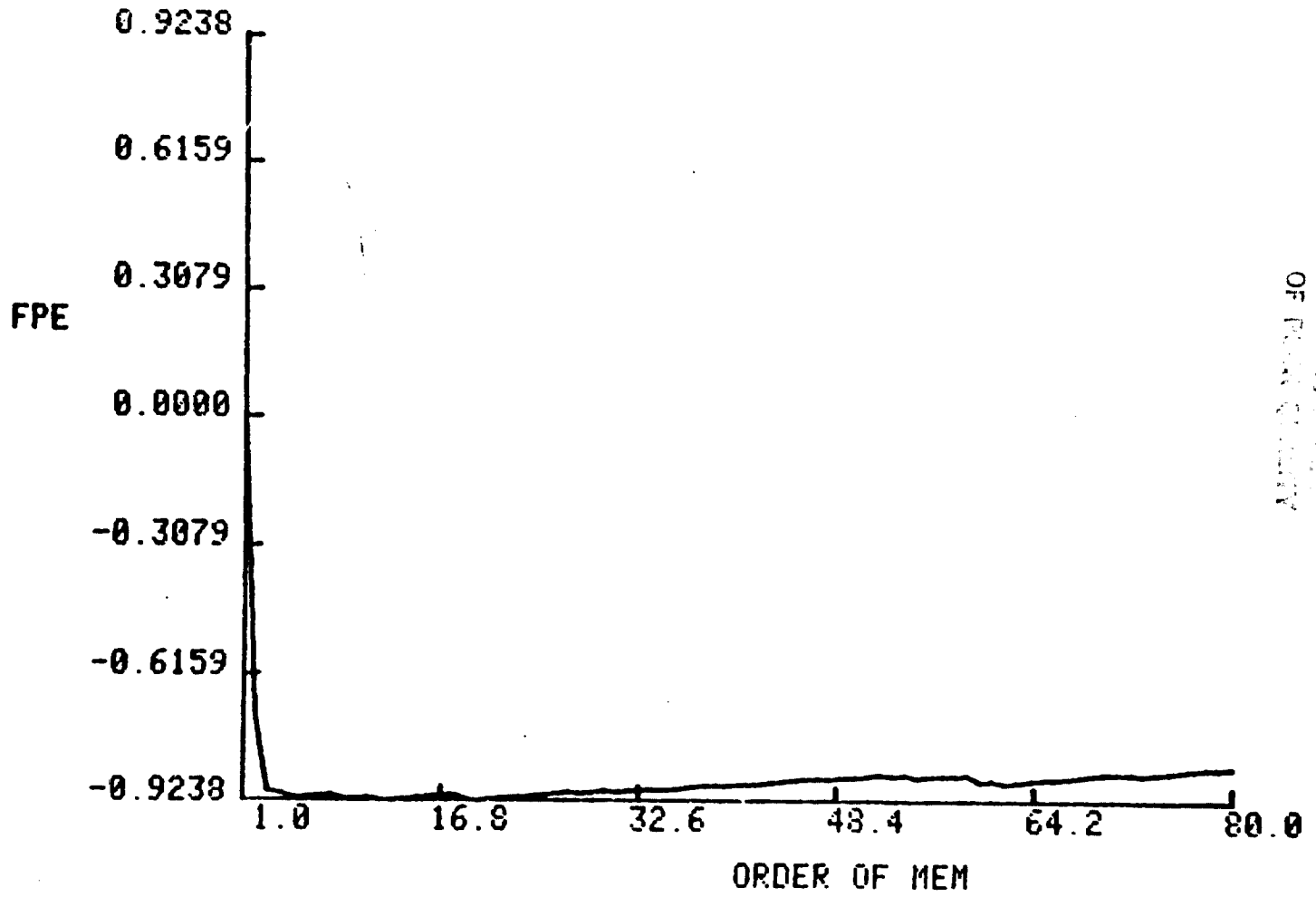

Fig. 17 Final Prediction Error (fpe) vs. MEM order for nitrogen density fluctuations from a high-pass filter of order = 40 and cutoff frequency of 0.0015 Hz.

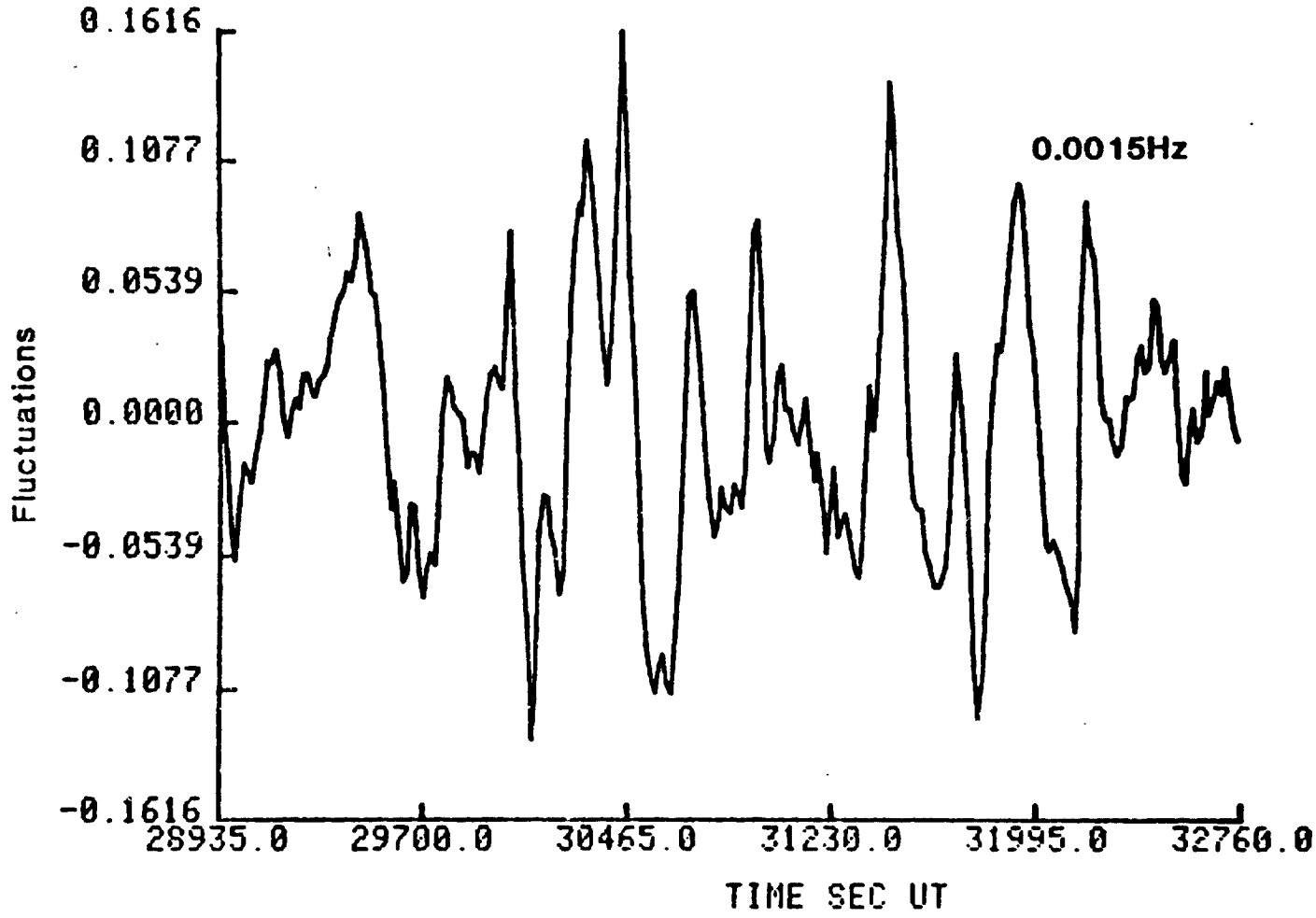

Fig. 18. Fluctuations of nitrogen density vs. time at the output of a high-pass filter of order = 40 and cutoff frequency of 0.0015 Hz.

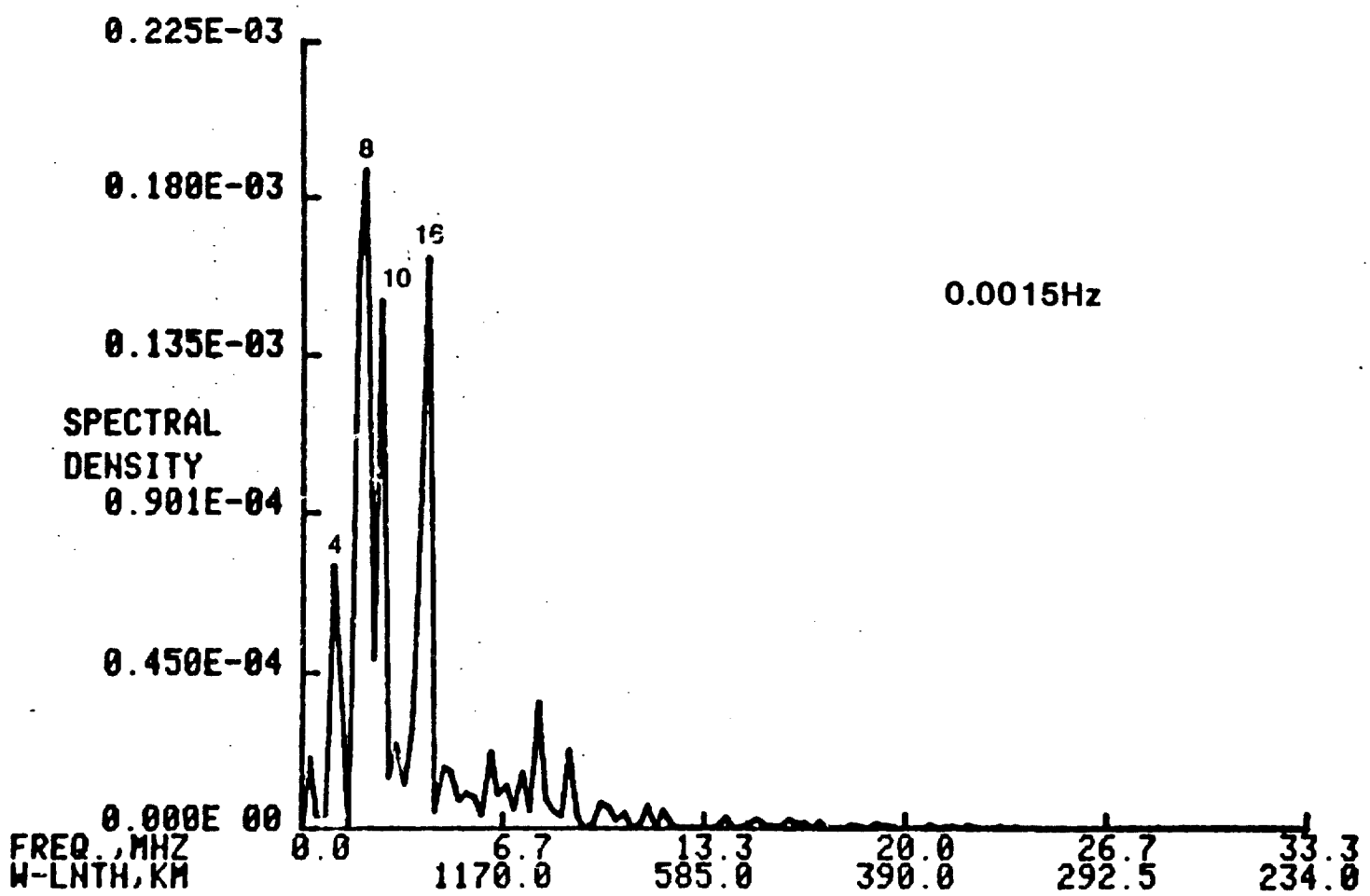

Fig. 19 fft power spectrum of the nitrogen density fluctuations from a high-pass filter of order = 40 and cutoff frequency of 0.0015 Hz. The abscissa scales are frequency in millihertz (mHz) and equivalent wavelength in kilometers. The numbers above the spectral peaks are the harmonic numbers where the fundamental frequency has a period equal to that of 256 data samples of 15 seconds sampling rate; namely, 3825 seconds. The last frequency on the abscissa scale, 33.3 mHz, is the Nyquist frequency for 15 seconds samples. The wavelengths are obtained by dividing the satellite velocity, 7.8 km/sec, by the

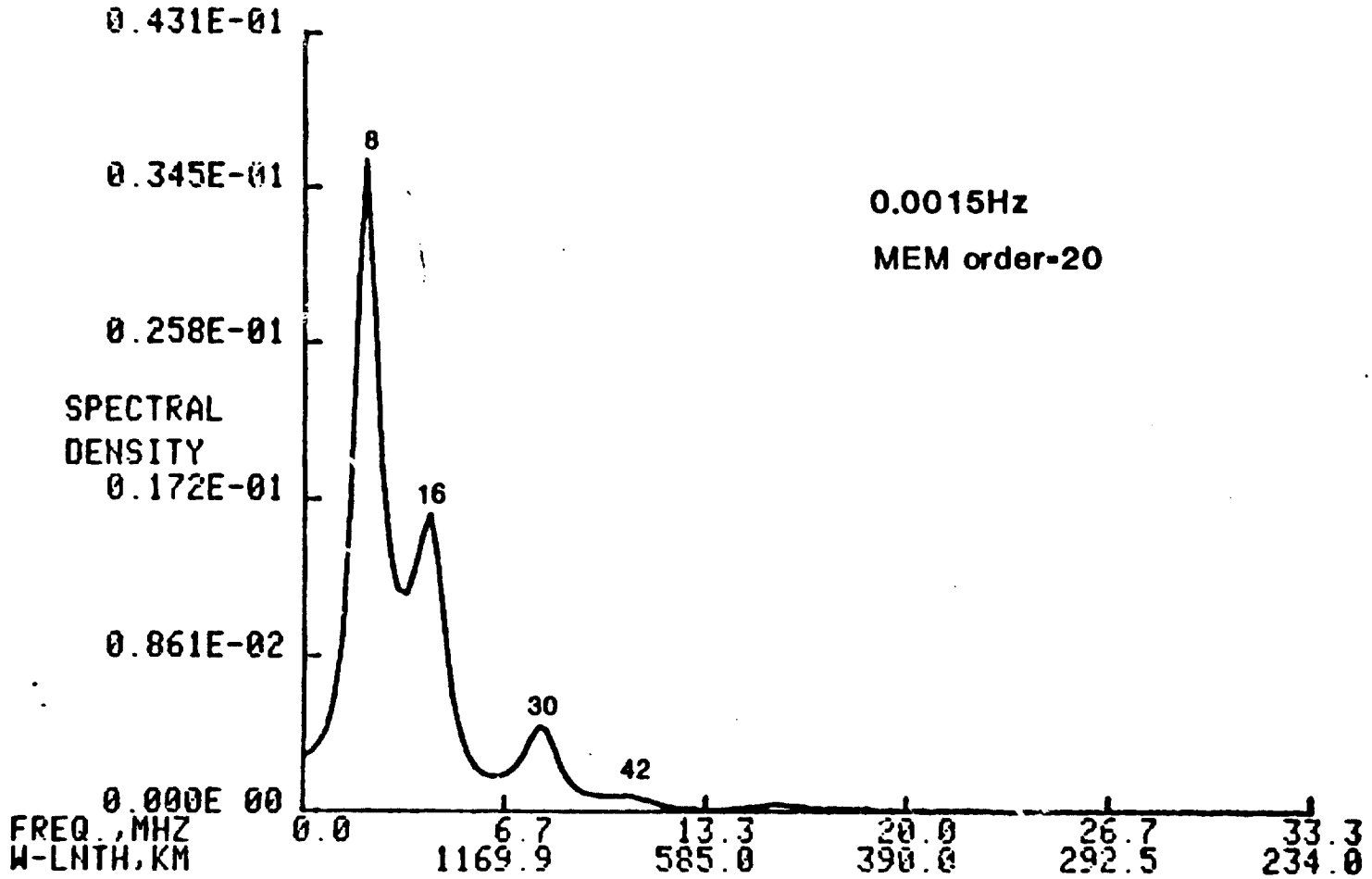

Fig. 20 Maximum Entropy Method (MEM) power spectrum of the nitrogen density fluctuations from a high-pass filter of order = 40 and cutoff frequency of 0.0015 Hz. The order of the MEM is 20. The scales and numbers above the peaks of the spectrum are as explained for Figure 19.

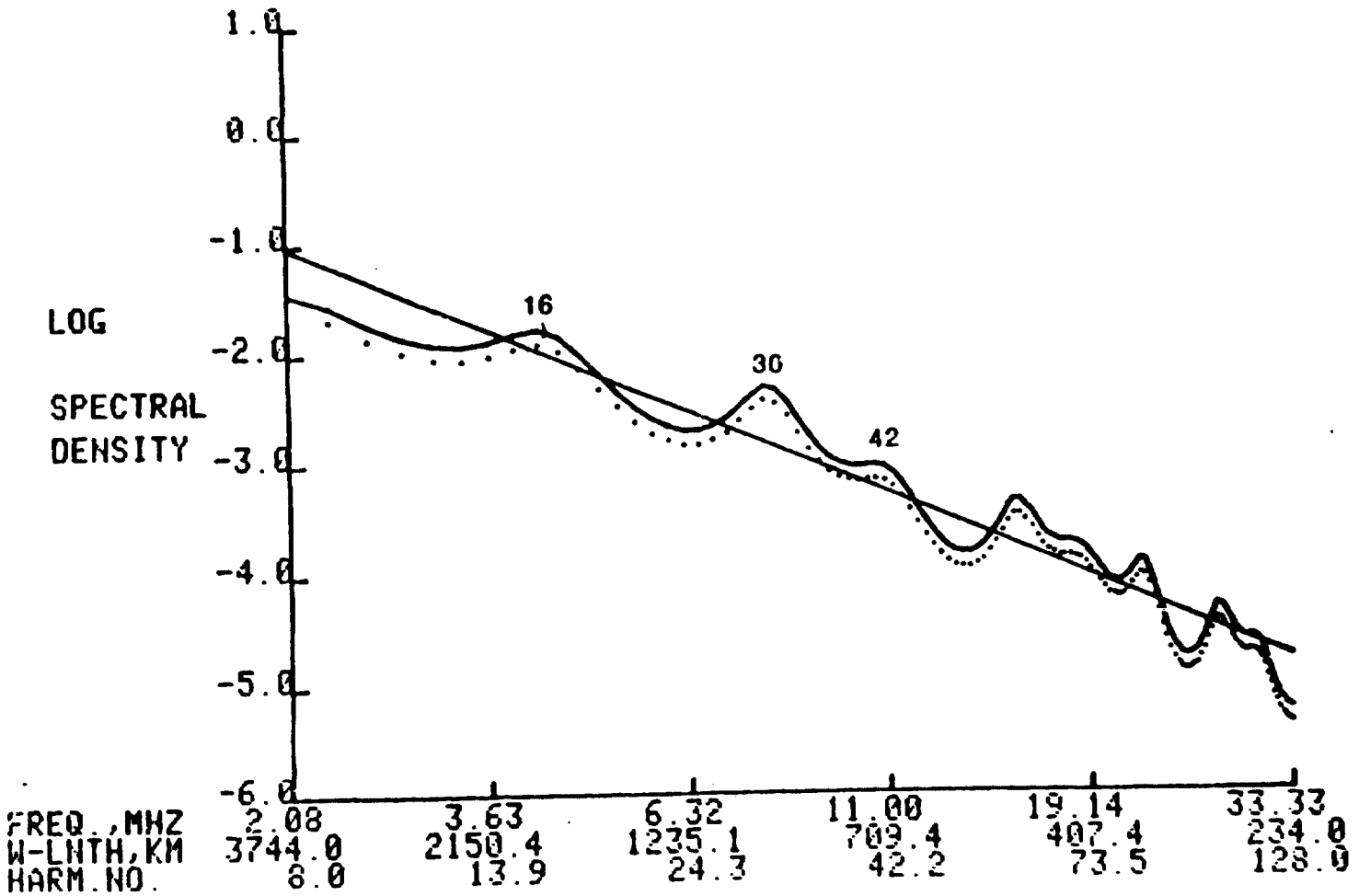

Fig. 21 The spectrum of Fig. 20 plotted on log-log scales. The straight line is a least square straight line fit to the spectrum. It has a slope of -3.1, meaning a power law fit of the form $f^{-3.1}$, where f is the frequency. The abscissa scales are frequency in mHz, wavelength in km and harmonic number. The plot starts from harmonic number 8 and extends to the Nyquist frequency. Decimal harmonic numbers are the result of the artificial division of the plot into five segments. Each dot is for an integral harmonic number to facilitate location of peaks.

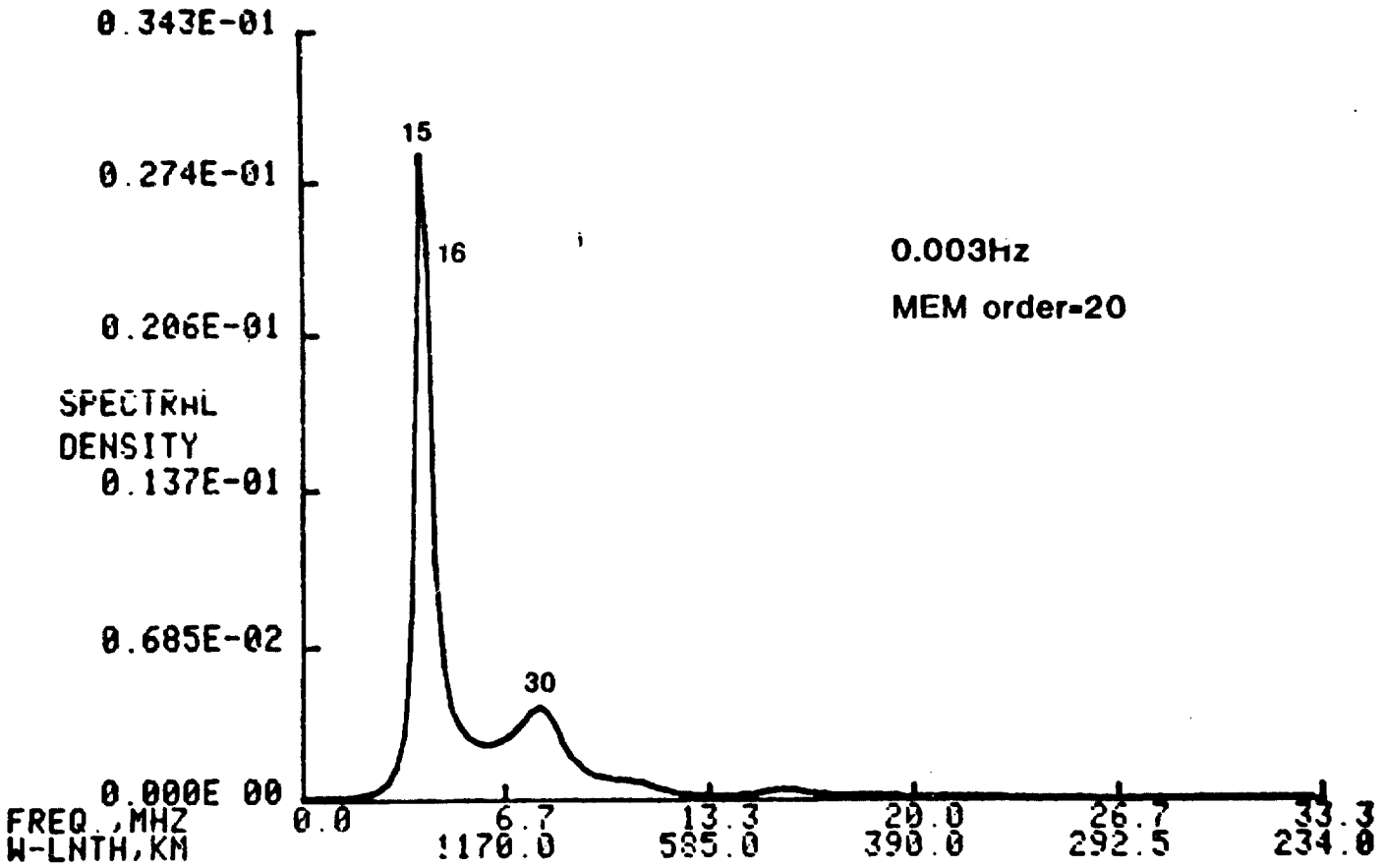

Fig. 22 Same as Fig. 20 but for a high-pass filter cutoff of 0.003 Hz.

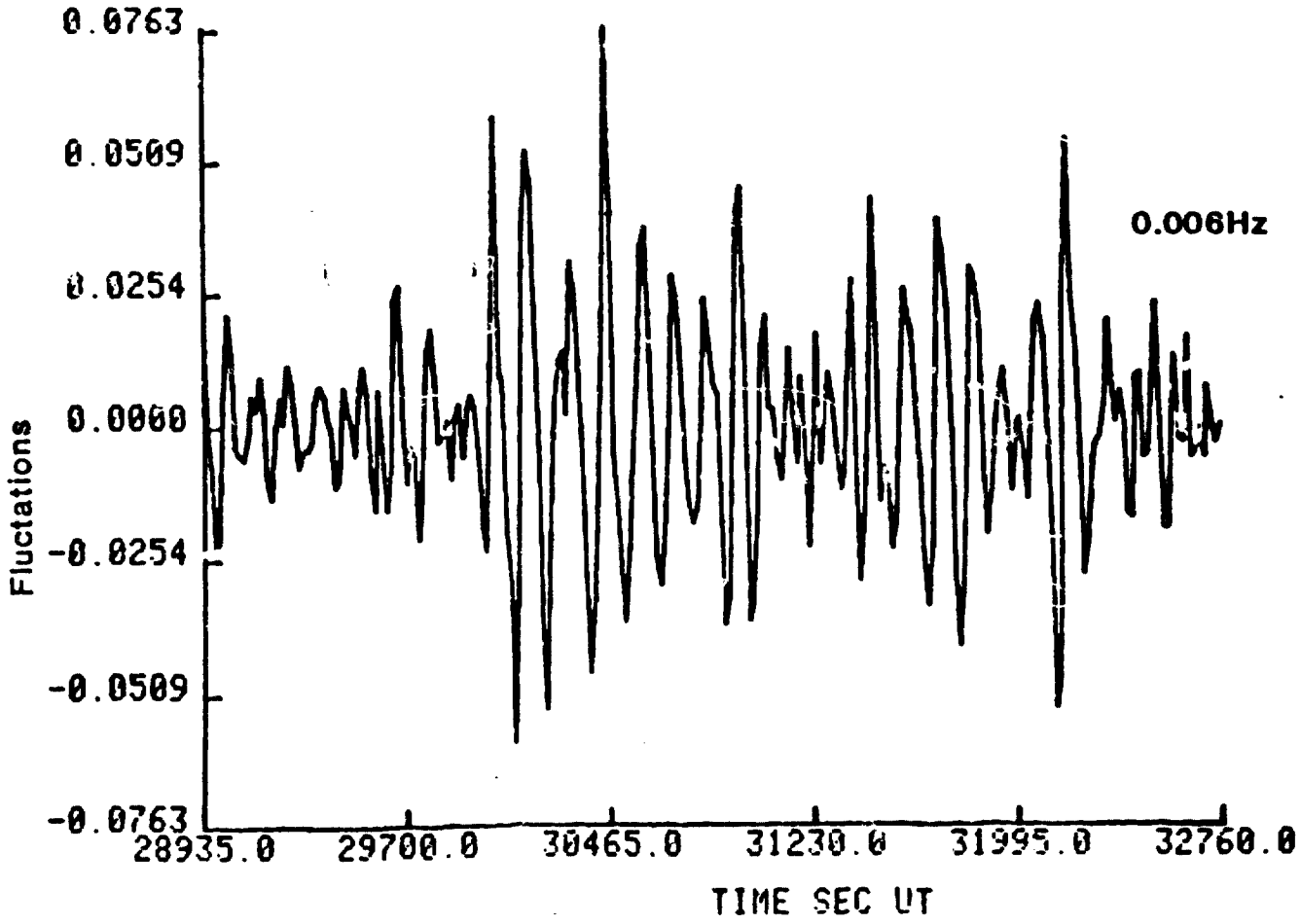

Fig. 23 Fluctuations of nitrogen density as in Fig. 18, but for a high-pass filter cutoff frequency of 0.006 Hz.

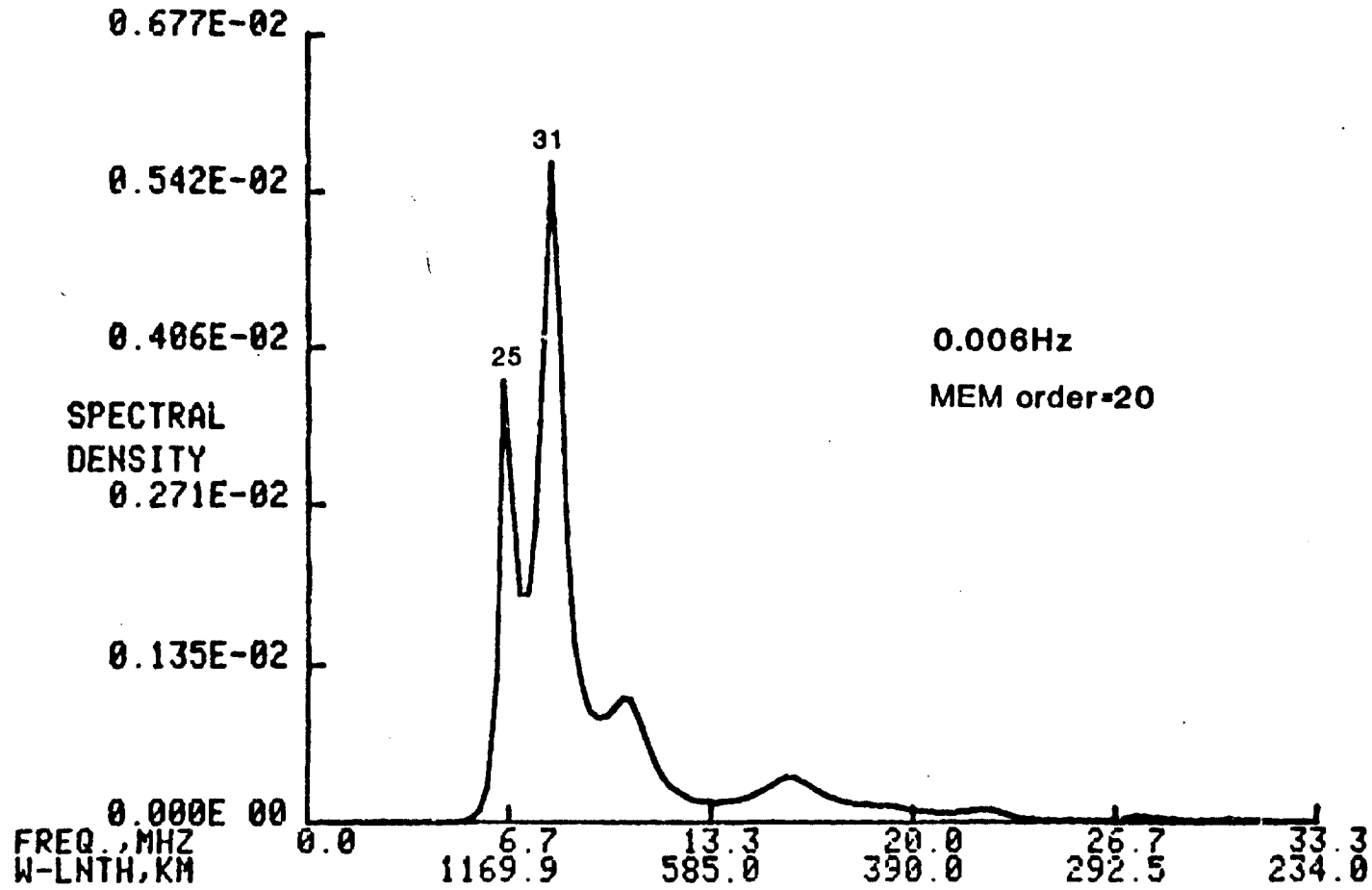

Fig. 24 Same as Fig. 20 but for a high-pass filter cutoff of 0.006 Hz.

Fig 25

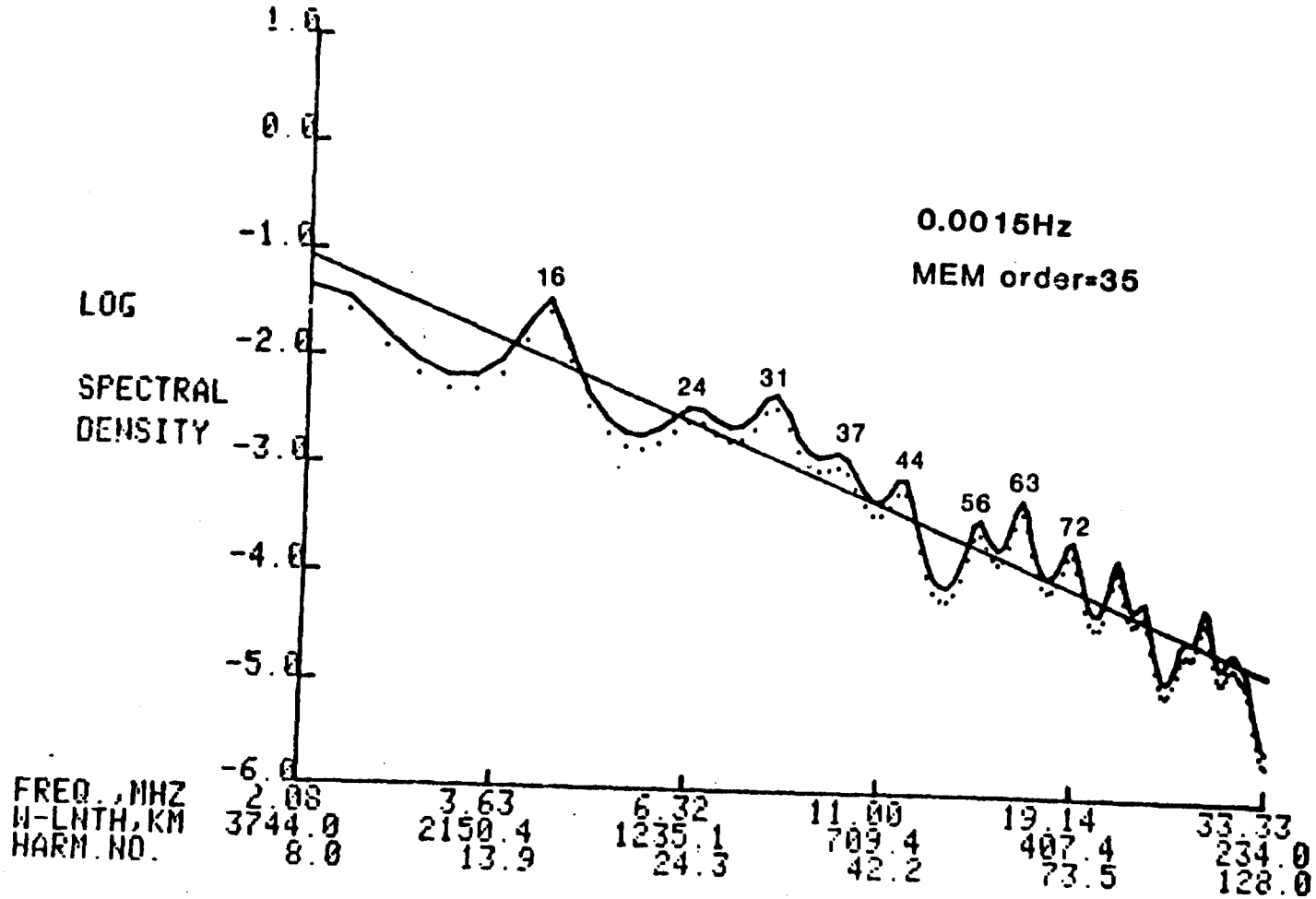

Fig. 25 Same as Fig. 21 but for the MEM order equal to 35. Peak frequencies are shown at harmonic numbers 8, 16, 24, 31, 37, 44-45, 56, 63, and 72.

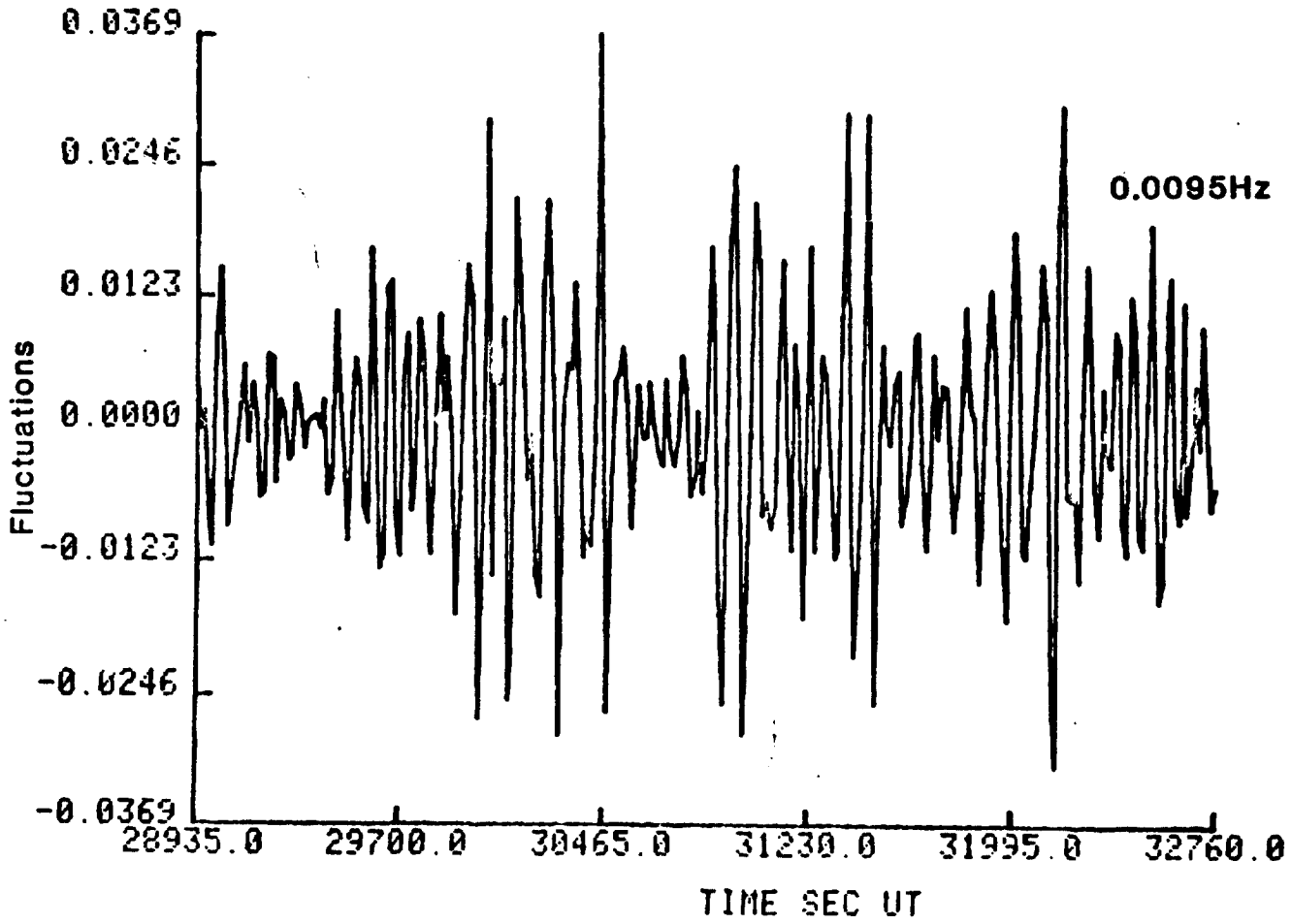

Fig. 26 Same as Fig. 18, but the high-pass filter cutoff is 0.0095 Hz.

Fig 27

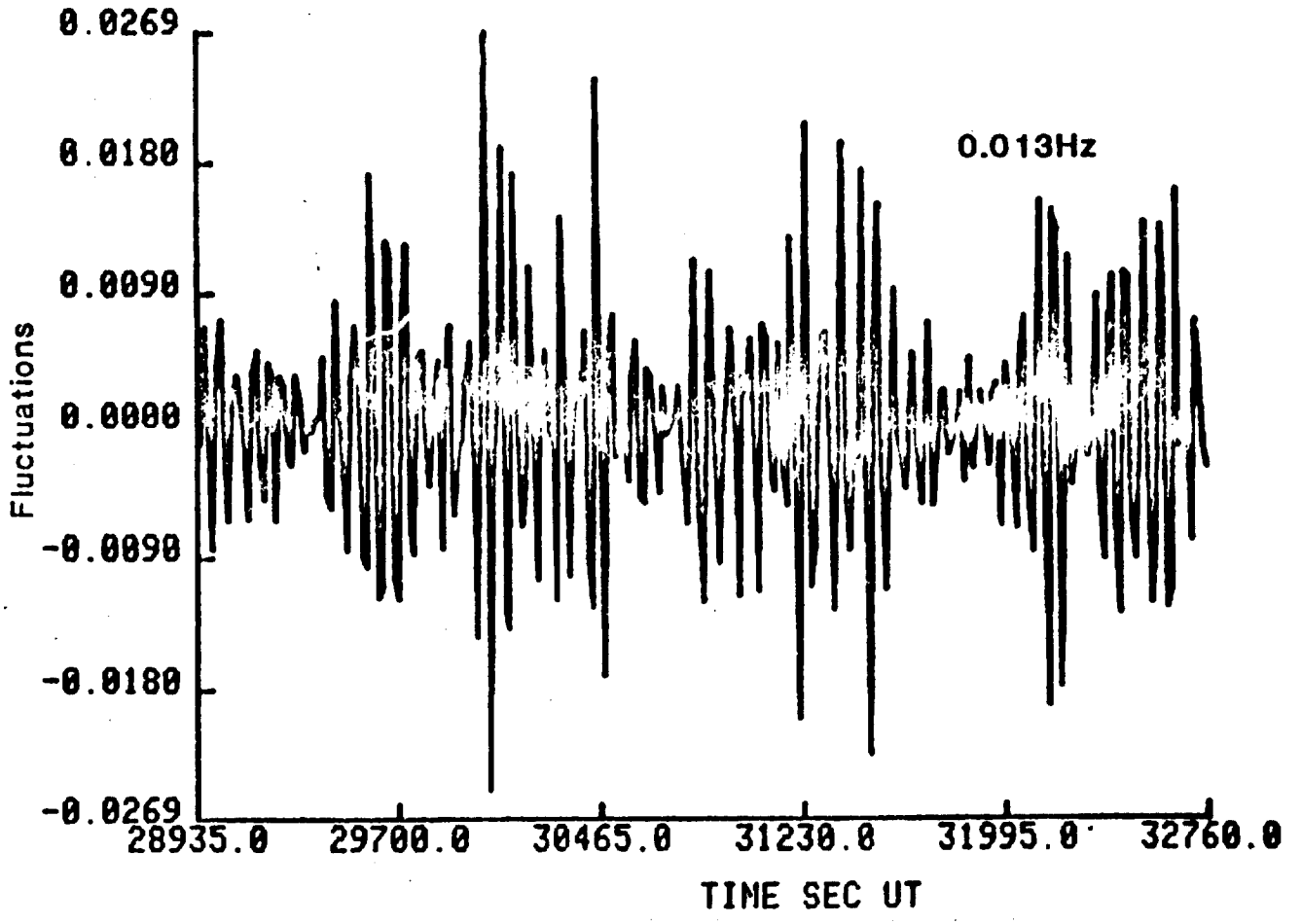

Fig. 27 The same as Fig. 18, but for a high-pass filter cutoff of 0.013 Hz.

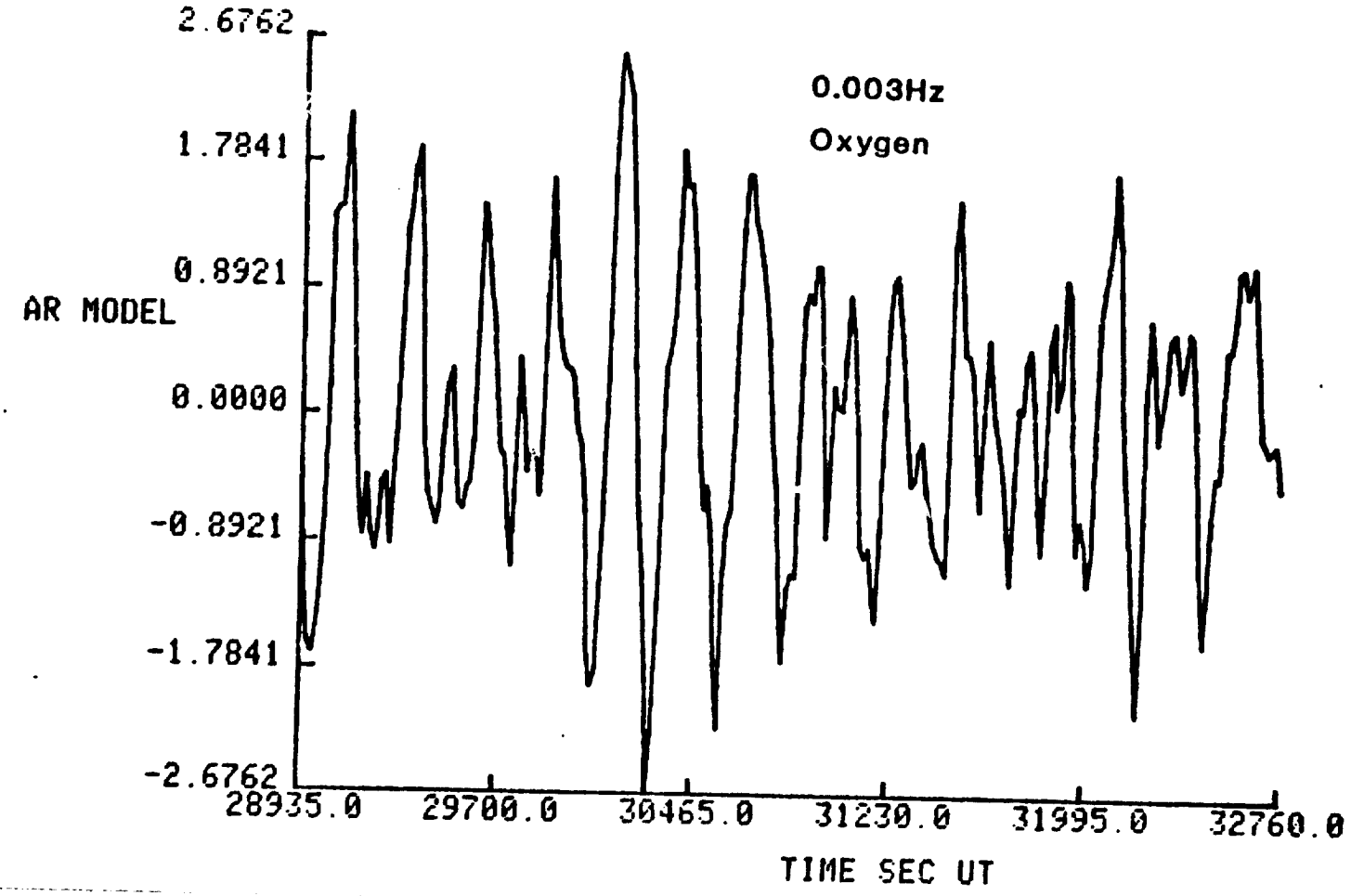

Fig. 28 Autoregressive model of order equal to 20 of the oxygen density fluctuations as expected from a high-pass filter with a cutoff frequency of 0.003 Hz.

Fig 29

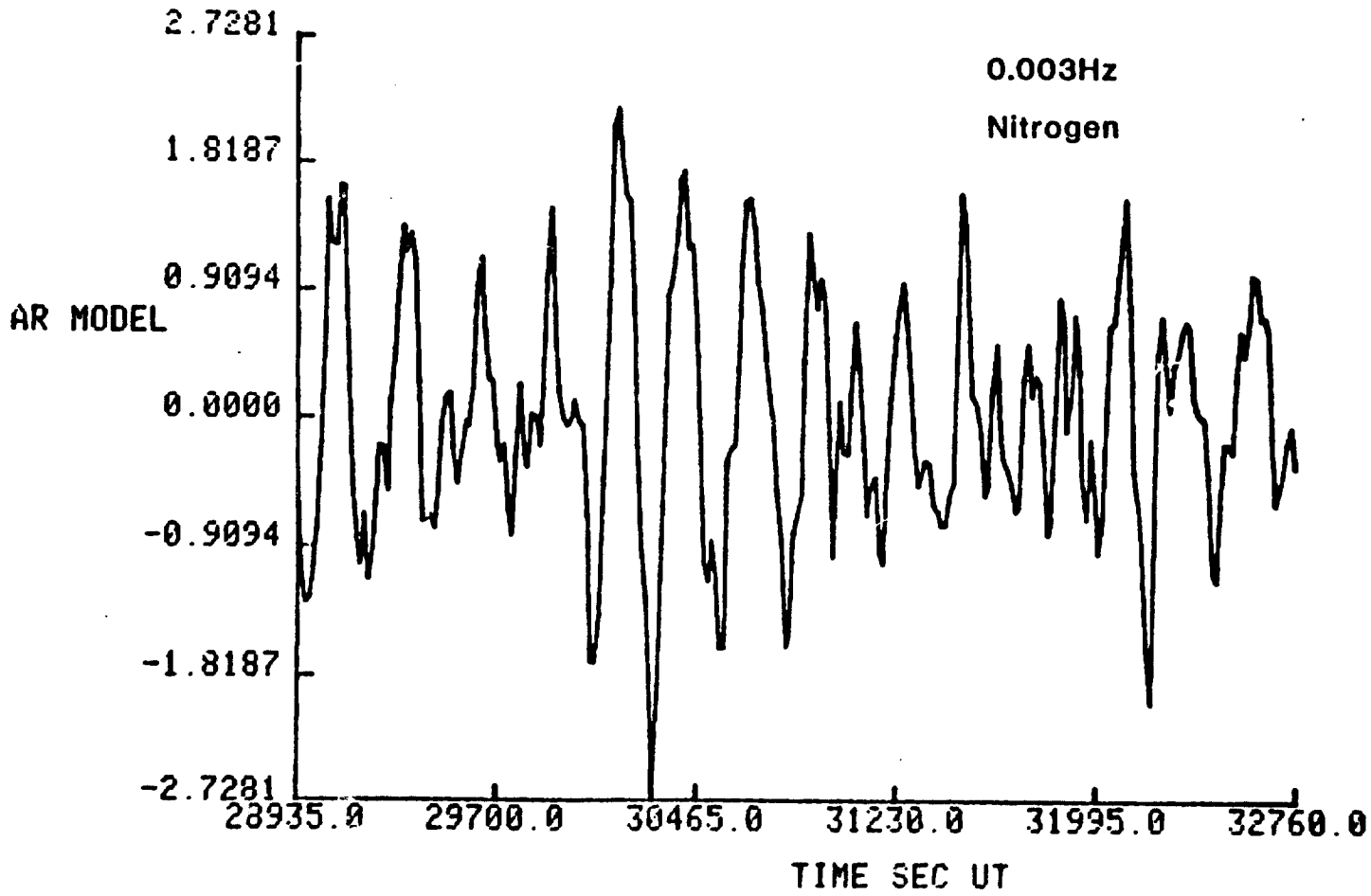

Fig. 29 The same as Fig. 28, but for the nitrogen density fluctuations.

Fig 30

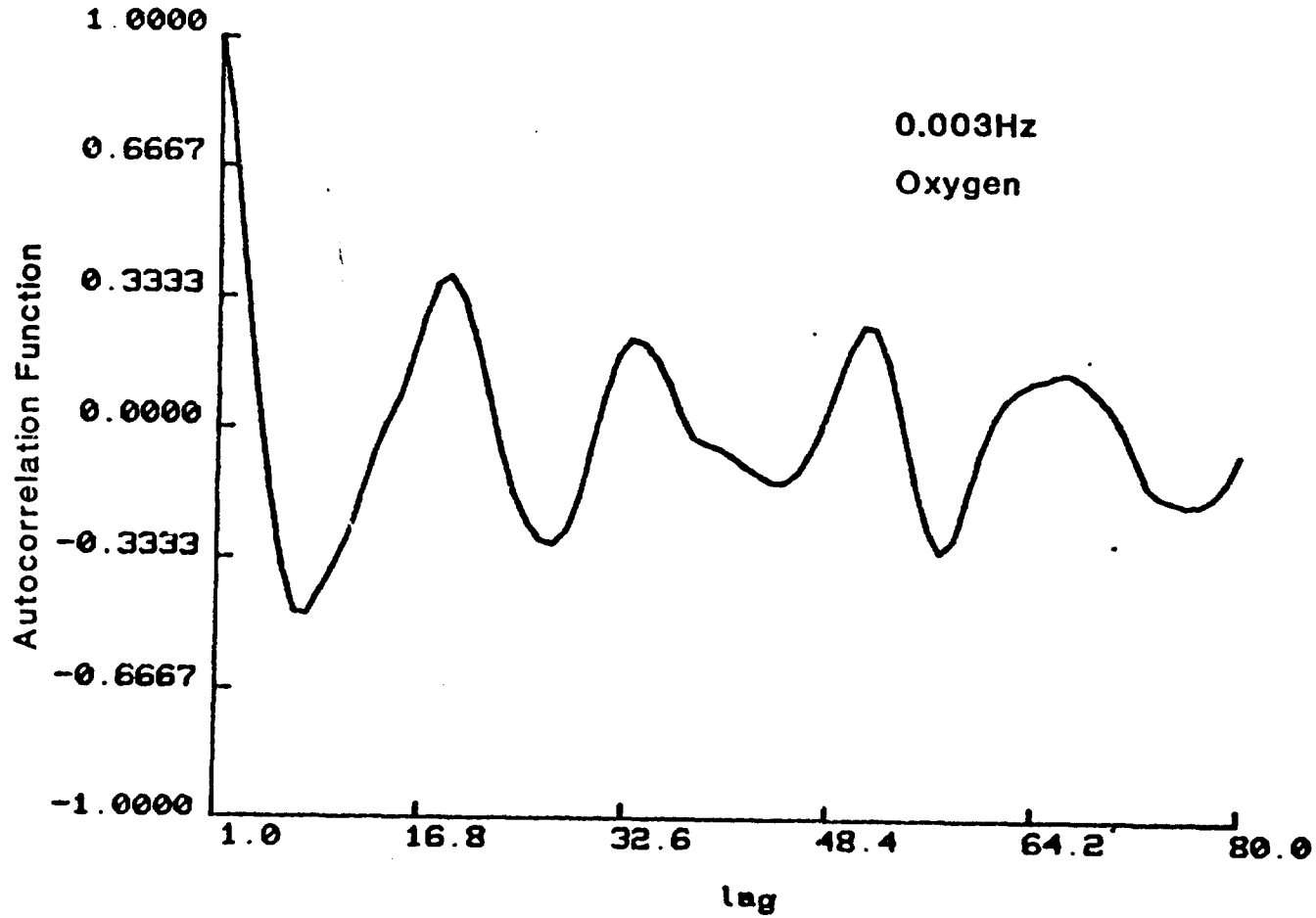

Fig. 30 Autocorrelation function of oxygen density fluctuations from a high-pass filter with a cutoff frequency of 0.003 Hz. The function is plotted vs. lag intervals where one interval is 15 seconds.

Fig 31

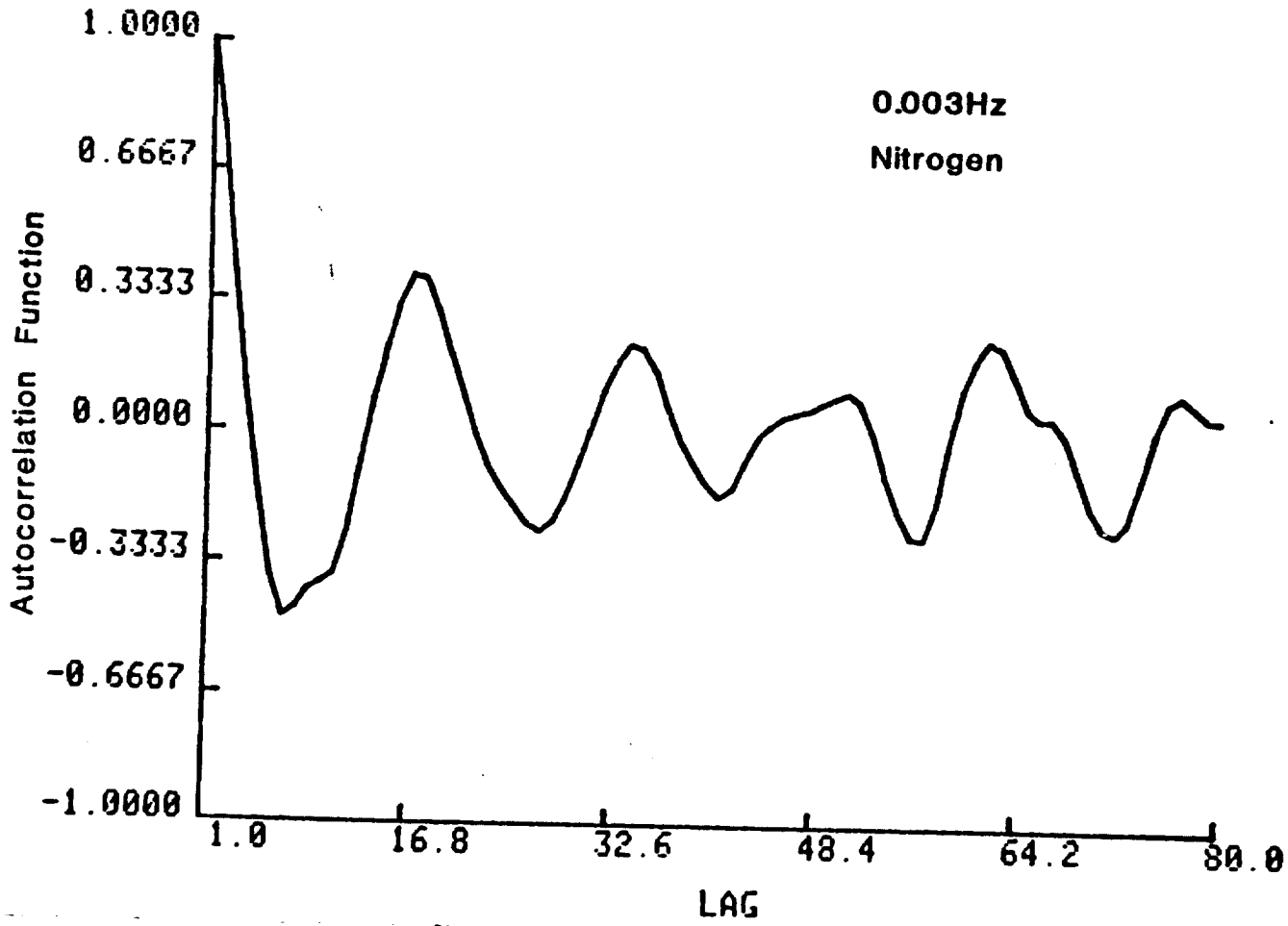

Fig. 31 The same as Fig. 30, but for nitrogen density fluctuations.

Fig 32

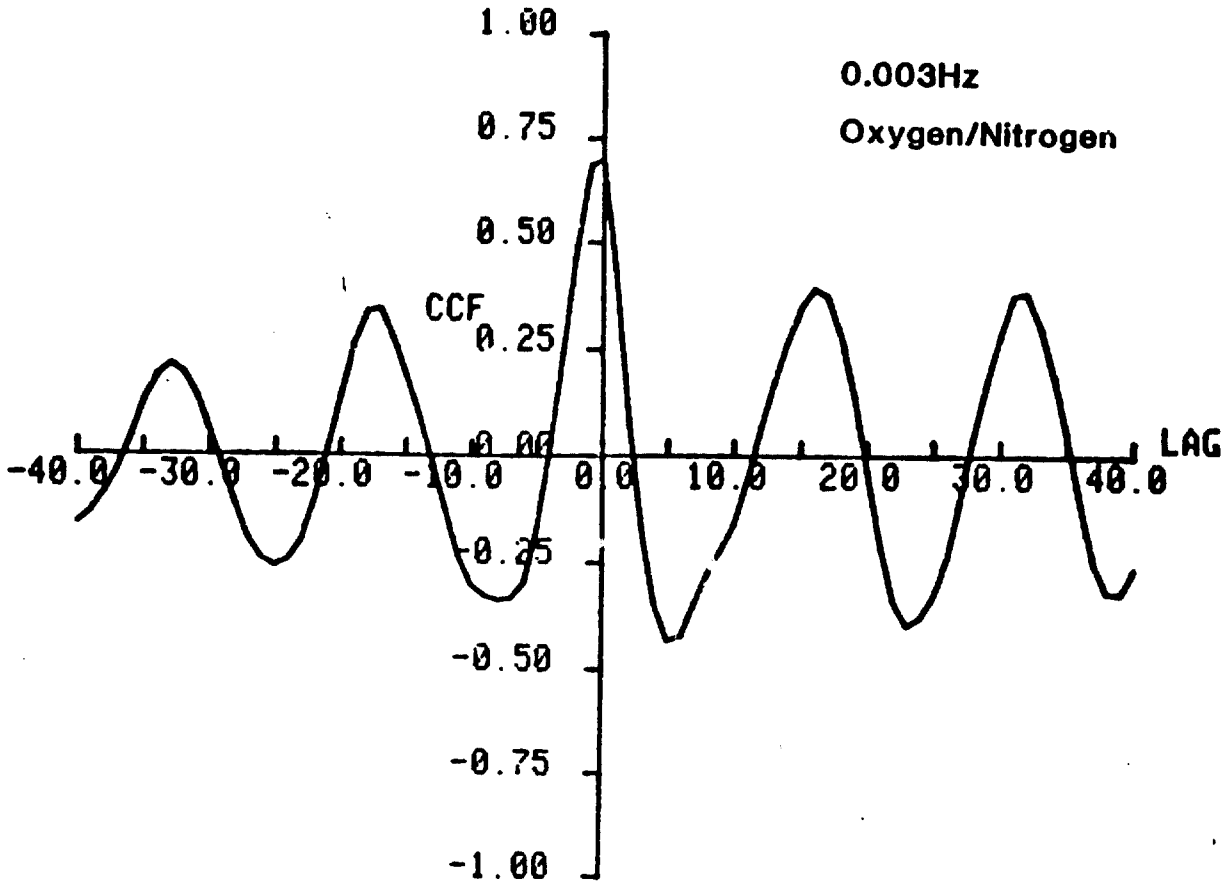

Fig. 32 Cross correlation function of oxygen and nitrogen fluctuations vs. lag intervals of 15 seconds each. Nitrogen is advanced relative to oxygen. Negative lags are for advances, positive for delays. The fluctuations are from a high-pass filter with a cutoff of 0.003 Hz.

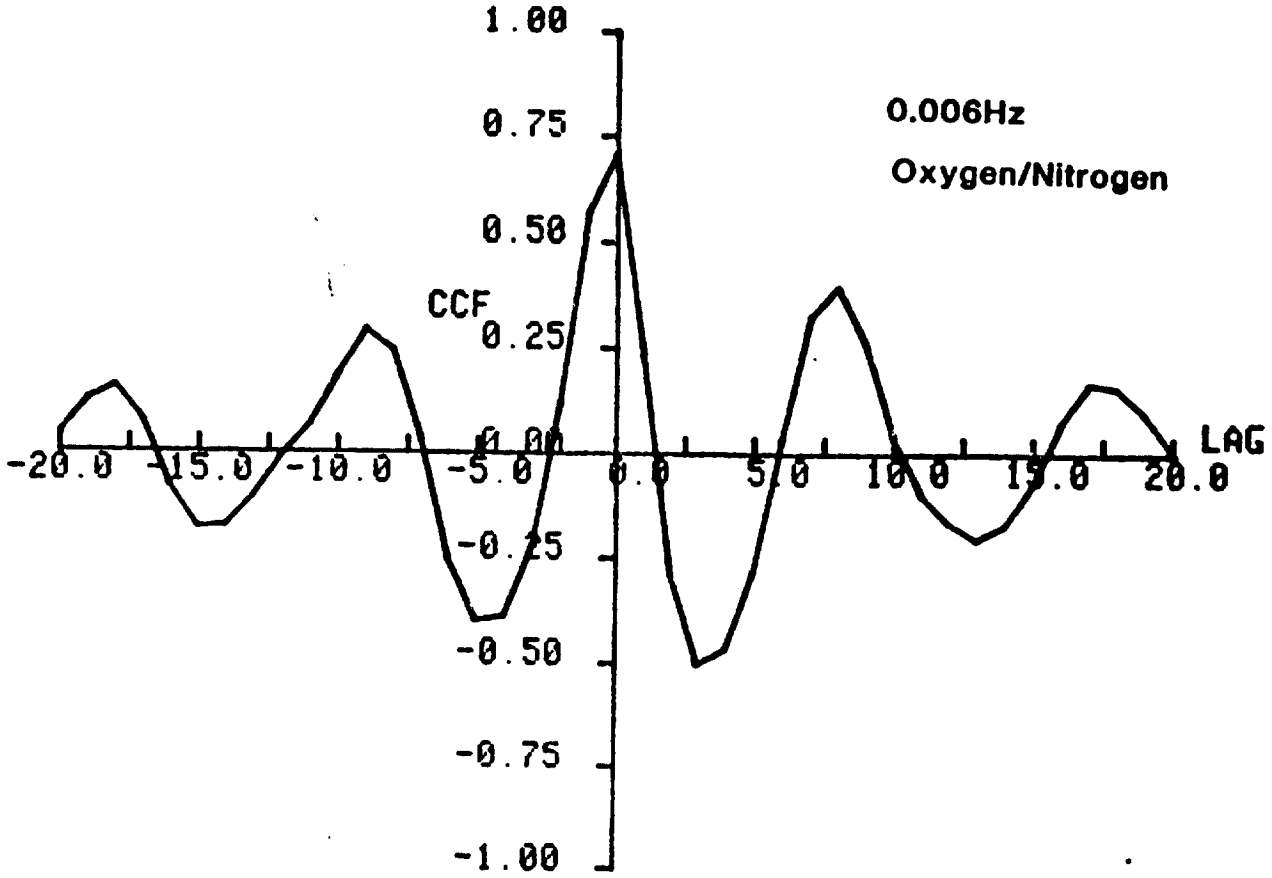

Fig. 33 The same as Fig. 32 with a high-pass filter with a cutoff of 0.006 Hz.

T2 24

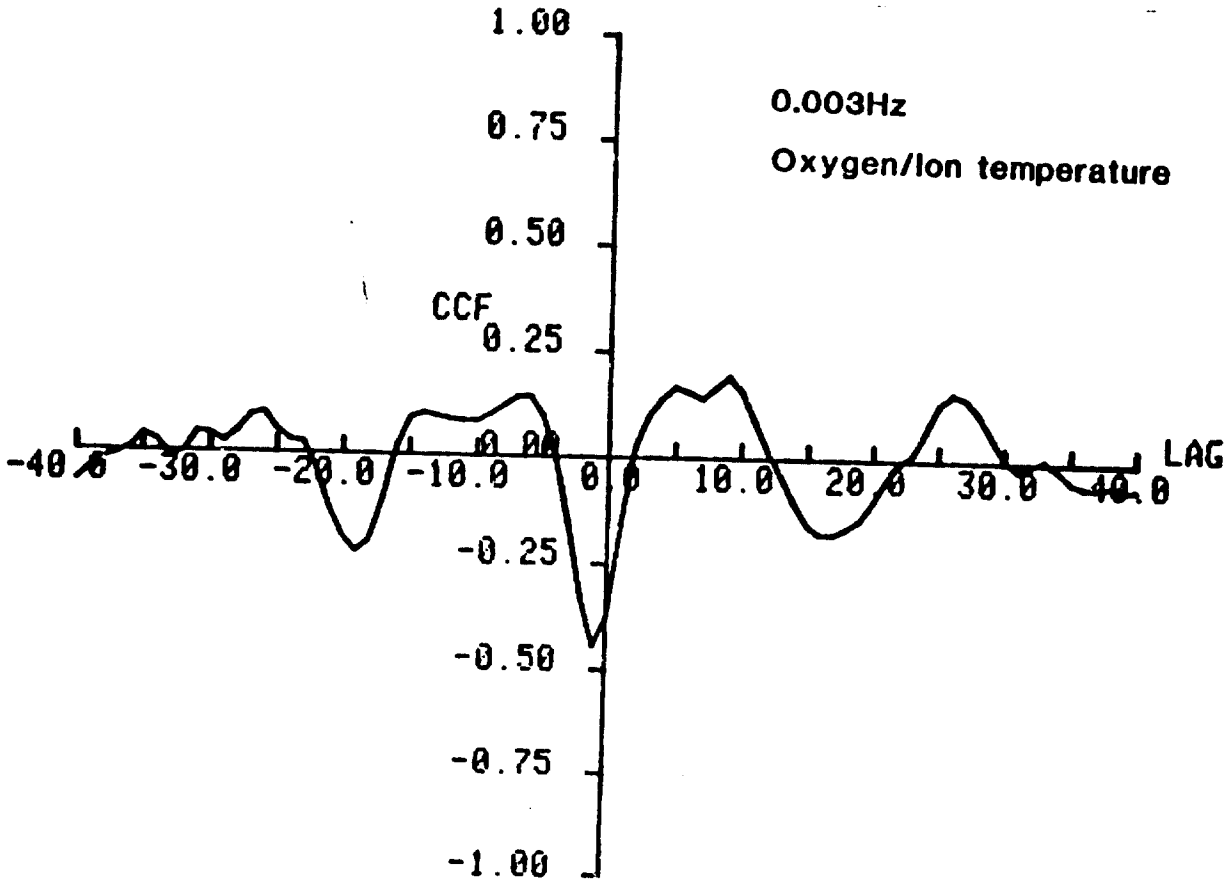

Fig. 34 The same as Fig. 32, but for oxygen density and ion temperature fluctuations.

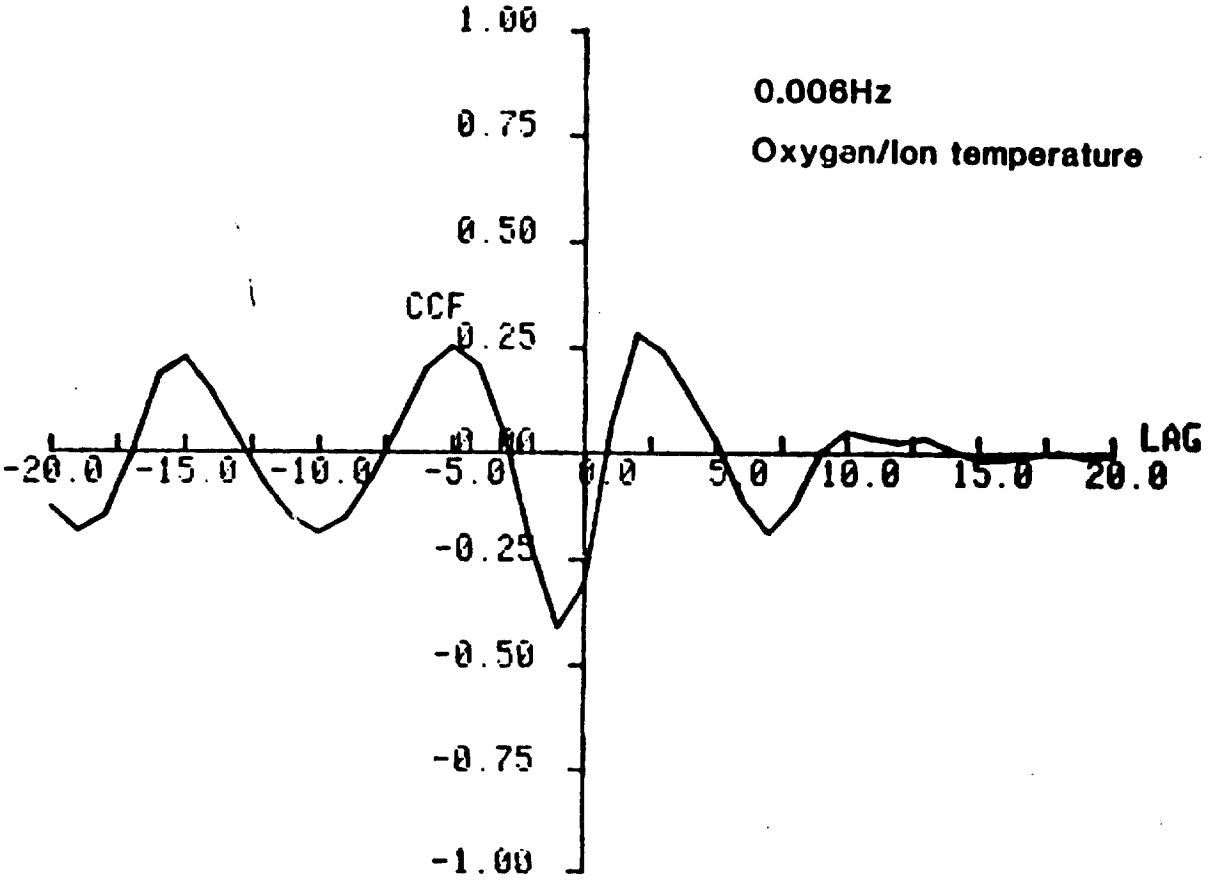

Fig. 35 The same as Fig. 34, but for a high-pass filter with a cutoff of 0.006 Hz.

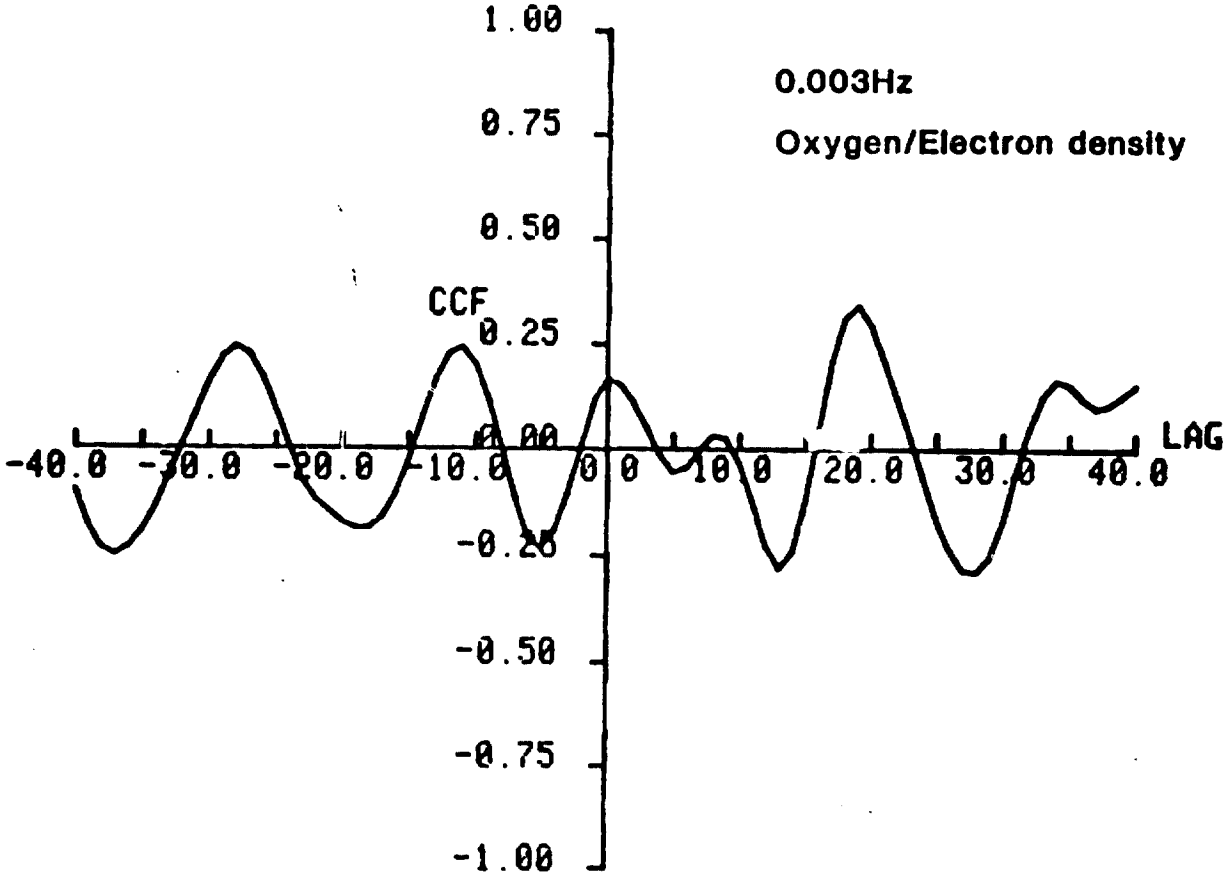

Fig. 36 The same as Fig. 32, but for oxygen density and electron density fluctuations.

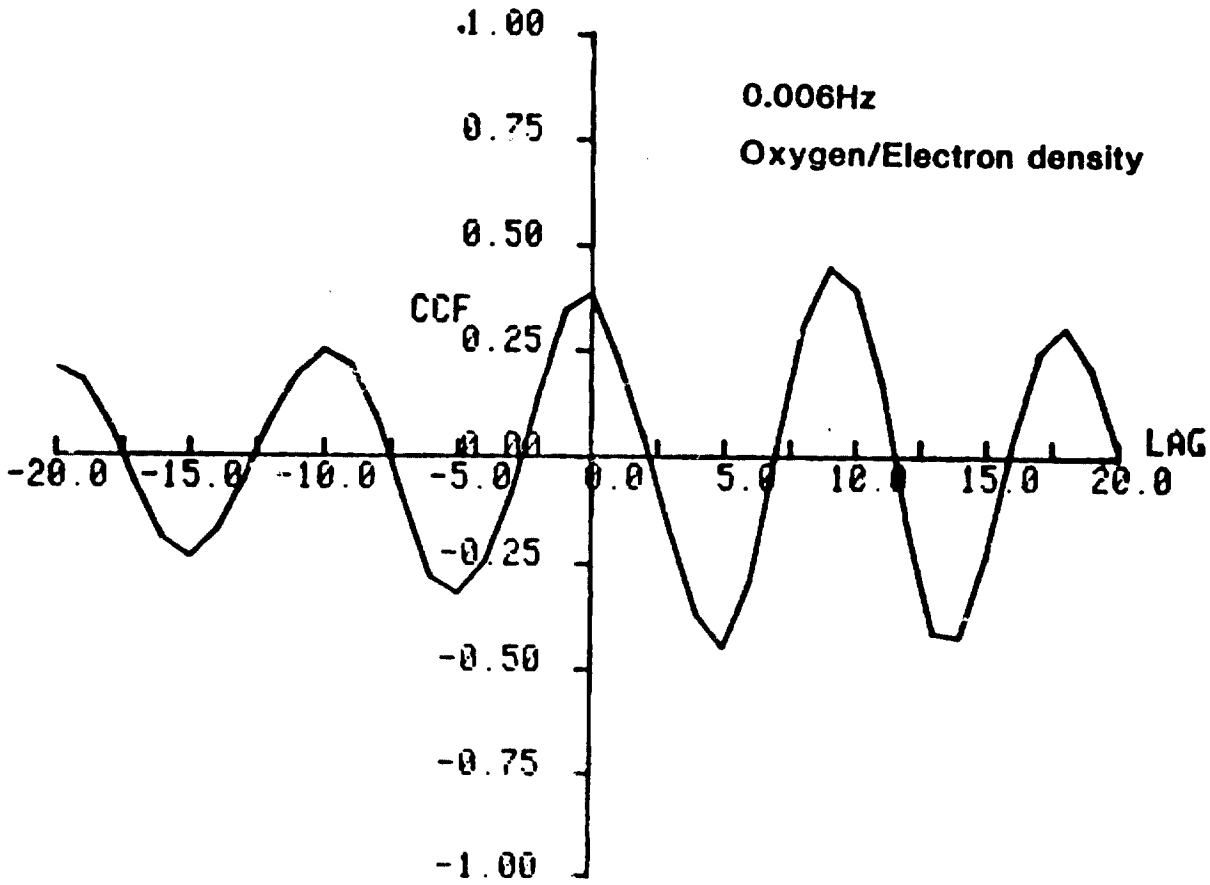

Fig. 37 The same as Fig. 36, but for a high-pass filter with a cutoff of 0.006 Hz.

Fig 38

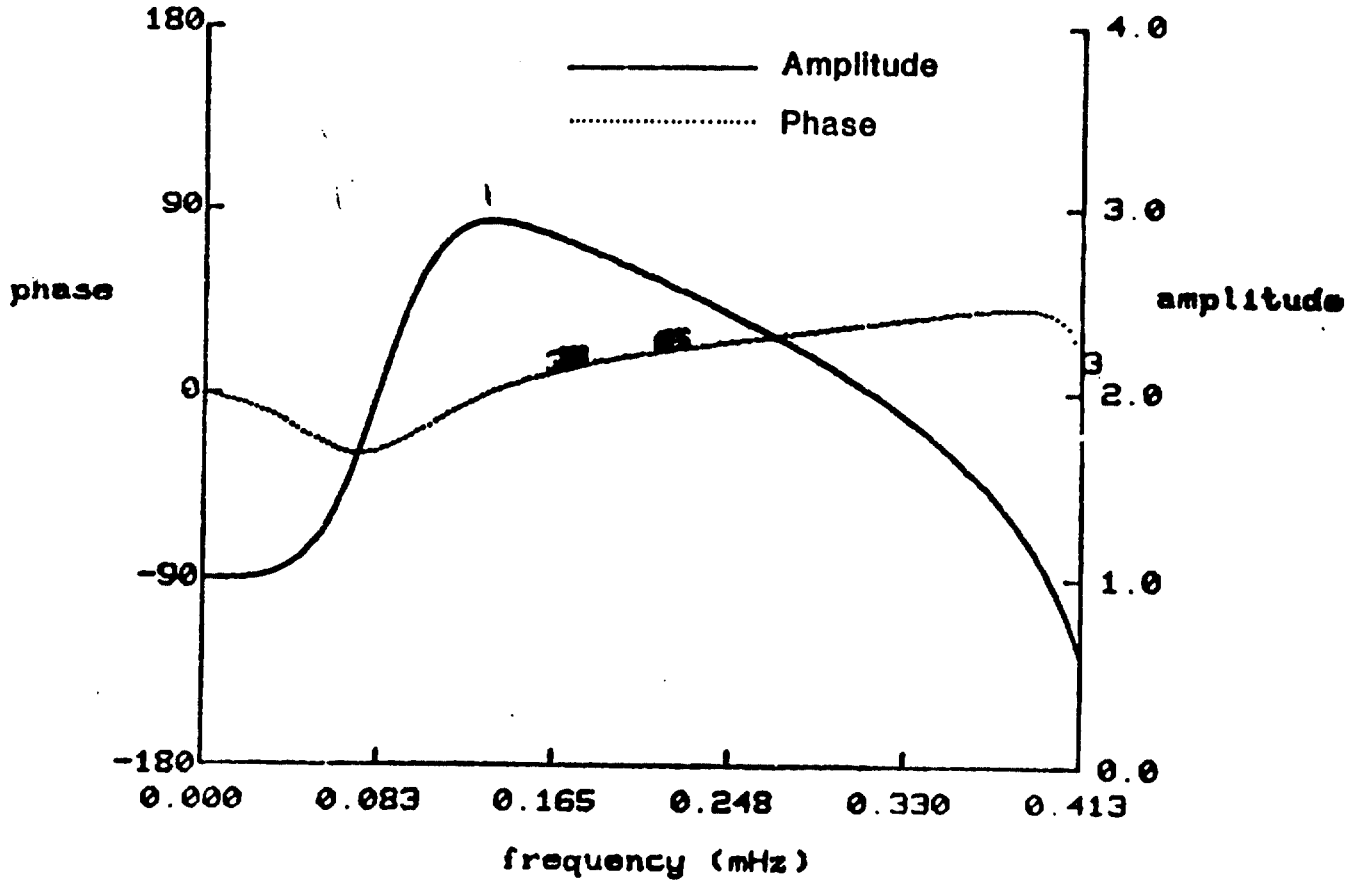

Fig. 38 Transfer function of the nitrogen density response relative to the oxygen density response as a function of frequency in mHz for a horizontal wavelength of 2000 km, a temperature of 830°K and a nitrogen-oxygen collision frequency of 0.75 sec^{-1}. The solid line is the amplitude as scaled on the right; the dotted line is the phase shift scaled on the left. The 3's and 6's on the phase shift curves are at the points where the phase shift take on the leading values 11° and 21°, respectively,

Fig 39

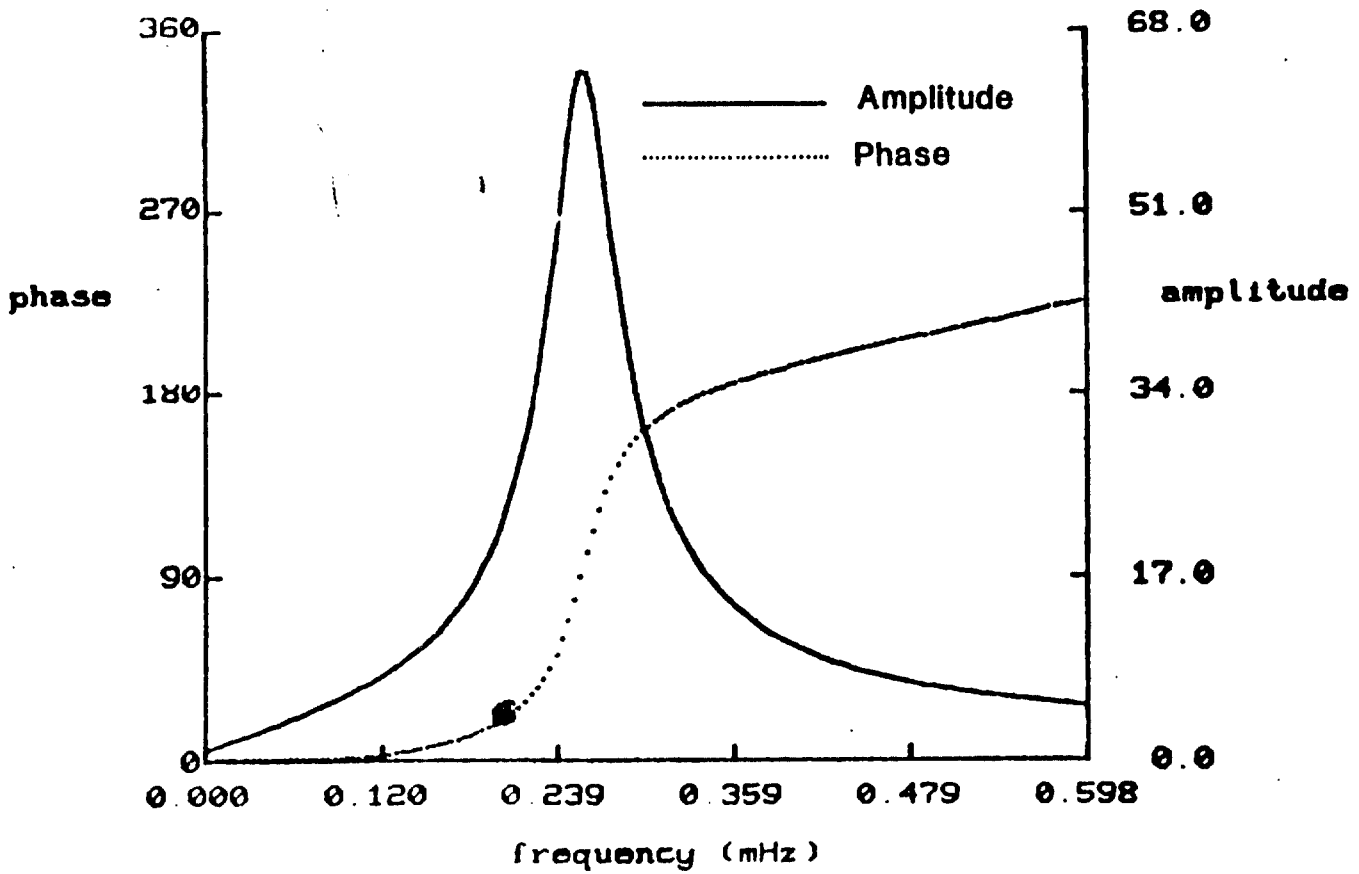

Fig. 39 Transfer function of the electron density response to the oxygen density response vs. frequency in mHz and for a horizontal wavelength of 1000 km, temperature of 830°K, ion-neutral collision frequency of 0.87 sec^{-1}. The dip angle is 60° and propagation is towards the equator. The ratio of electron temperature to ion temperature is 2.0. The solid line is the amplitude with the scale on the right. The dotted line is the phase shift with the scale on the left. The 6's are on the phase shift curve for the 21° leading angle of Table IV. See text.

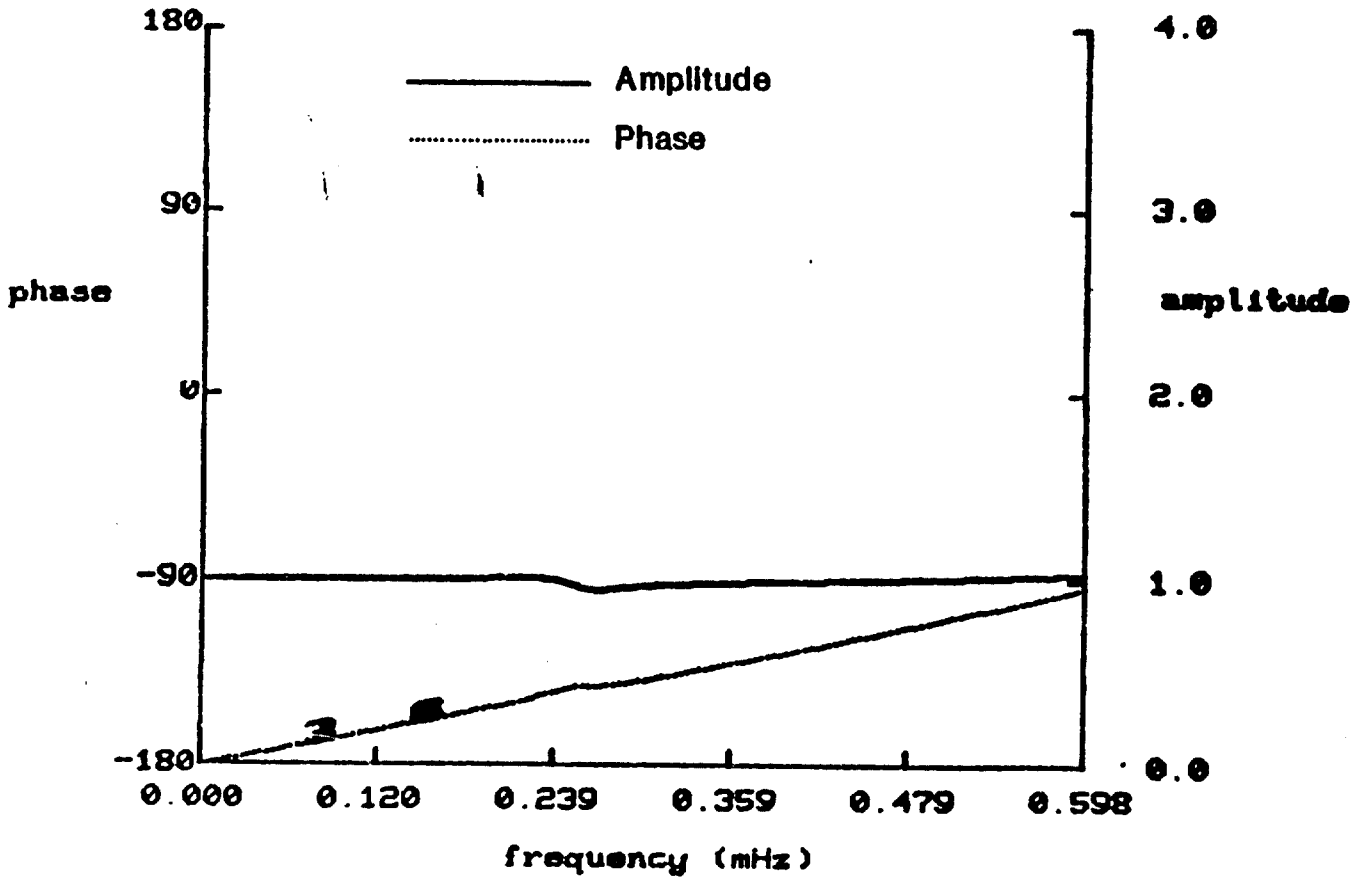

Fig. 40 The same as Fig. 39 but for the ion temperature transfer function. 3's and 6's on the phase shift curve are for the phase angles required in Table IV. See text.

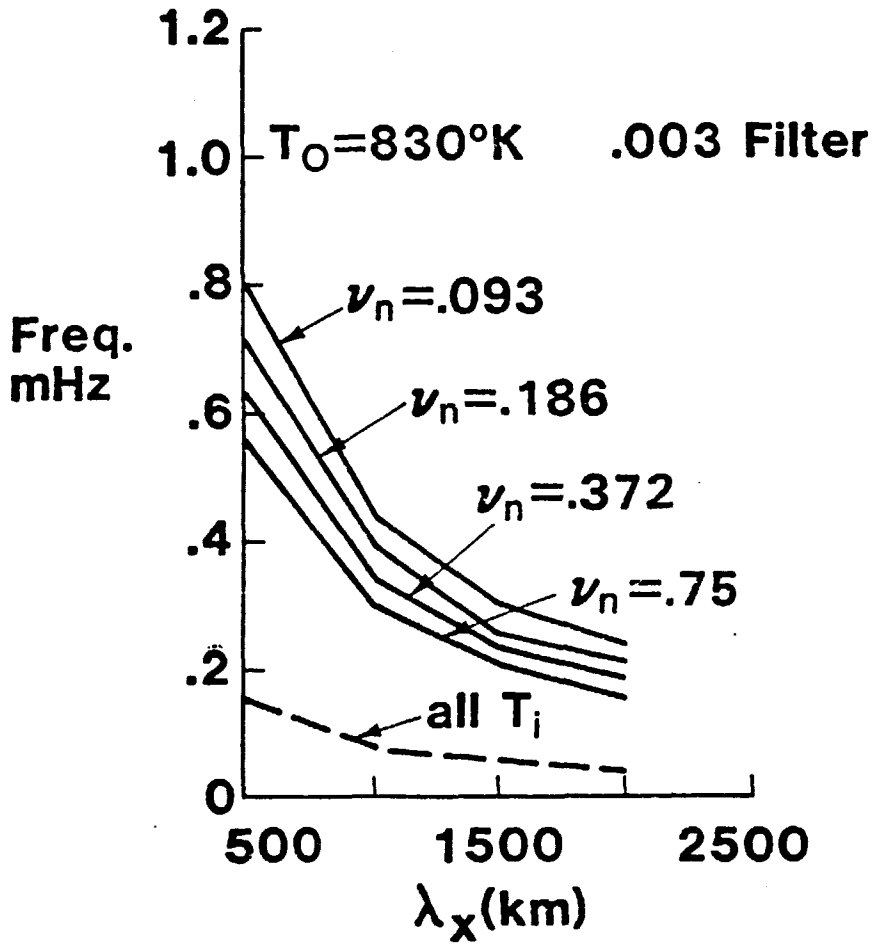

Fig. 41 Plot of theoretical frequency in mHz vs. horizontal wavelength in km to satisfy the phase shift requirements of Table IV for the 0.003 Hz high-pass filter. The temperature is 830°K. The solid lines are for the nitrogen transfer function phase shift for the different values of the nitrogen-oxygen collision frequency ν_n. All points for the ion temperature transfer function phase shift are on the dashed line. There are no electron density curves for this case.

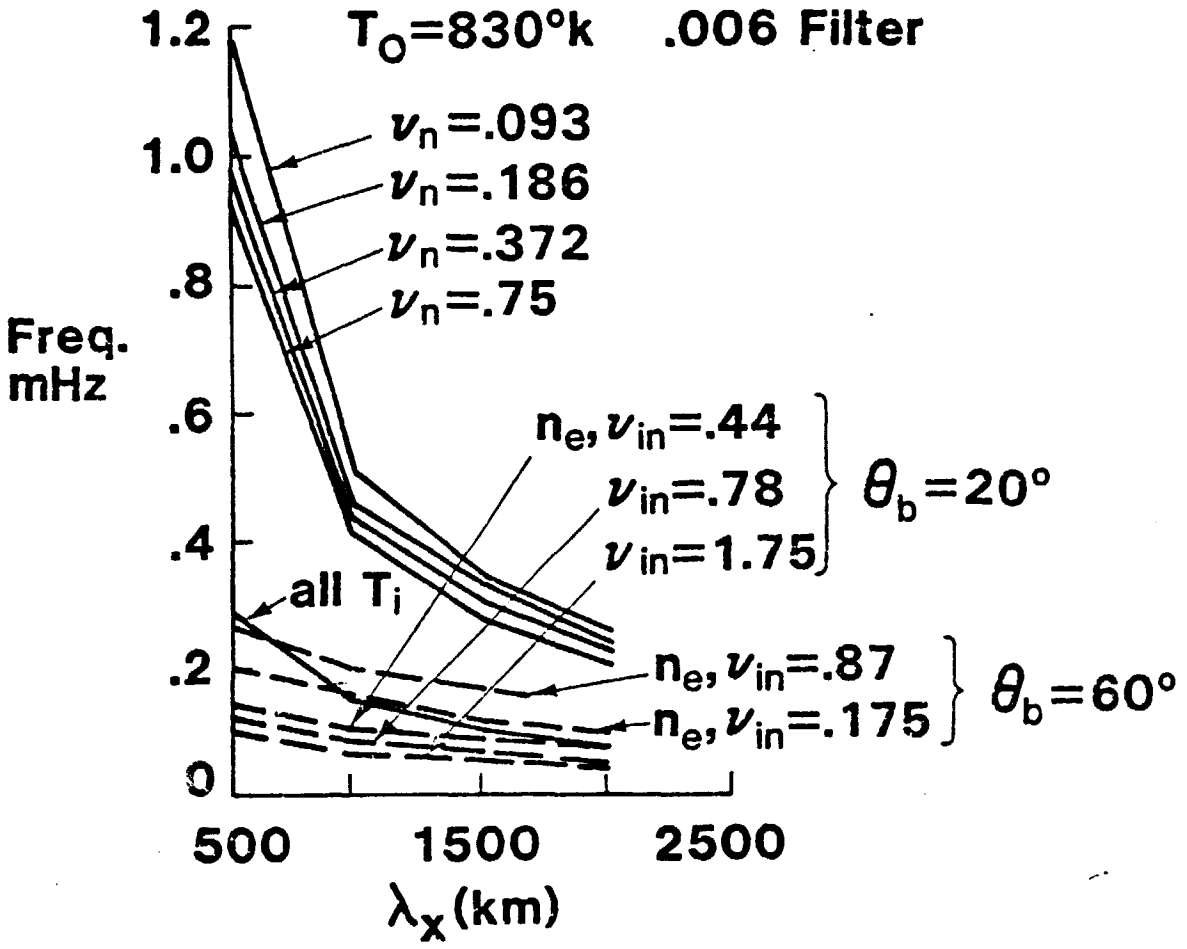

Fig. 42 The same as Fig. 41, except that the filter requirements are those for the 0.006 Hz cutoff frequency. Electron density contours for the transfer function phase shift are shown for dip angles of 20° and 60° for propagation towards the equator. Ion neutral collision frequency, ν_{in}, values associated with the curves are shown. These electron density contours are labeled.